Politecnico di Torino

Aerospace Engineering – Propulsion Systems
a.a. 2021/2022
Graduation Session October 2022

Methodology definition for lattice structure simulation: from lattice to equivalent solid's characteristics

Internal Supervisor:
Prof. Atzeni Eleonora
Prof. Biamino Sara
External Supervisor:
Ing. Zenatti Alessandro
Ing. Brasili Luca

Candidate:
Bolfo Federico

Abstract

Nowadays Engineering Industry is searching for new materials and manufacturing techniques to reduce weight and improve parts' mechanical characteristics. In this scenario, Additive Manufacturing represents a central role. This technique differs from the traditional one because a part is realized by overlapping layer by layer, adding material only where necessary. This feature permits the creation of reticulated structures called lattices.

Considering a structural analysis of lattice parts using FEM software requires many calculations power, and time, consequently elevating costs. These aspects are limitations in lattice structure applications.

The thesis work focuses on defining a methodology helpful for simplifying and speeding the structural analysis of lattice structure. In particular, an equivalent stiffness matrix is defined for a rhombic dodecahedron unit cell lattice structure made by SS316L with the L-PBF process and attributed to a full component, avoiding considering many nodes and elements during the analysis, saving time and money.

The thesis is composed of five chapters. The first one is dedicated to a brief introduction to the additive manufacturing and lattice world. The second one is divided into two subchapters: material research and state-of-the-art software approach to the lattice structure. Regarding material, the attention is put on metal ones, while the software approach is focused on the homogenization method. The third one represents the thesis' core and contains a step-by-step strategy to reach the goal. In particular, a material software characterization is done, and a short explanation of the unit cell is provided. Many analyses are run on lattice structures to extrapolate elastic moduli and then attributed to an equivalent solid. Both lattice and equivalent parts are successfully stressed similarly, and displacements are compared to verify their coincidence. This chapter conducts a dedicated study on equivalent solid shape, constraints, and loads application scheme. In the fourth chapter, conclusions are stated, and the equivalent stiffness matrix is reported for the specific lattice structure. Moreover, the methodology steps are listed to apply to any lattice component. In the fifth one, future developments are depicted, and suggestions are provided to improve the thesis results.

Table of Contents:

List of Figures:

VIII

List of Tables:

1. INTRODUCTION

1.1. Additive manufacturing

Today, Additive Manufacturing is a mode of production primarily used in many industrial fields (aerospace, medical, automotive, architecture, and many others). While today's 3D printers can realize parts with excellent performance, the performance was largely different when this technology was invented.

In 1980 the first Additive Manufacturing system was presented thanks to the impulse of the Cold War. Dr. Hideo Kodama is considered the inventor of this technology. He realized a prototyping machine starting from the knowledge of 3D scanning and the layering pattern from 3D topographical maps. Later, in 1984, Charles Hull created the material Stereolithography Apparatus (SLA), and in 1986 he built the first 3D printing company. The following year, he produced the first 3D printer [1].

After this, some inventors and researchers began to develop new methods and techniques for Additive Manufacturing, so the race to build the best machine and become a leader in the industry started.

Nowadays, Additive Manufacturing is an advanced manufacturing method used to realize parts for end-use, prototypes, and tools for a production line.

By ISO/ASTM, Additive Manufacturing is defined as a process of joining materials to make a part from 3D model data, usually layer upon layer, as opposed to subtractive manufacturing and formative manufacturing methodologies. The difference consists of producing parts that add materials only where necessary [25].

Furthermore, the design freedom and many different materials available make Additive Manufacturing able to realize lightweight and optimized components with high structural efficiency, reduce costs and make production more efficient.

1.2. AM techniques

In the actual scenario, metallic and plastic materials are largely used. In this working thesis, the attention is focused on metallic materials. This type of Additive Manufacturing is known as Metal Additive Manufacturing (MAM), and it has many advantages which push its development [58].

The central role is played by elevating mechanical performance provided by components. Although metal part realization isn't less expensive than traditional one, the possibility of creating a part with high characteristics is sufficient to invest in this technology. Regarding cost, it is important to underline that new factories aren't necessary, which significantly impacts saving money. Another aspect to consider is the time from design to the final product. Indeed, lead time is reduced because all phases of the production chain are in the same place (from

design to post-processing), while the machine time recovers a relevant role in total process time. The waste material is minimized thanks to the additive process, the great design freedom, and the availability of new printable materials [69].

The great interest in the Additive Manufacturing world permitted the development of different techniques to realize AM products.

Regarding ISO/ASTM 52900, there are seven significant techniques: Binder Jetting, Directed Energy Deposition, Material Extrusion, Material Jetting, Powder Bed Fusion, Sheet Lamination, and Vat Photopolymerization.

1.2.1. Binder Jetting

This process spreads powder material to realize a fine powder bed that constitutes the future part's layer. Successively a printhead deposits a liquid binding agent onto the powder to build the part respecting the CAD model. In the end, the building platform moves down, and the process restarts. The component is realized layer by layer by repeating this procedure, and if necessary, post-processing occurs [72].

1.2.2. Directed Energy Deposition

This technique consists of a nozzle that can move freely thanking a 4 or 5 axis arm and deposits powder on the upper surface of the part. After this phase, the material is melted by a power source, forming a layer. This procedure is repeated many times until the entire piece is built [72].

1.2.3. Material Extrusion

This method is based on a nozzle that can move horizontally and on a building platform able to translate up and down vertically. A layer is directly formed by depositing melted material where it is necessary. When a layer is realized, the platform moves down, and another layer is formed on the previous one because it is in a melted state, so they fuse. The process continues until the part is completely built [72].

1.2.4. Material Jetting

This process is the only one that can realize color parts because of its feature of providing many droplets as material to be fused permits this. The method consists of a building platform that moves vertically where the component is built layer by layer. There is a nozzle that provides the same time support and build material. During this phase, thermal and piezoelectric methods are used. Successively a cure process starts thanks to a UV light [72].

1.2.5. Sheet Lamination

This technique is based on a sheet or ribbon of metal bonding together by ultrasonic welding. The process is composed of different steps: material is placed on the cutting bed, and glue or adhesive sheets are taken together and in place. A cutting laser system permits the definition of

the final part's shape, and another layer is put above the previous one. It is possible to cut metal sheets before placing them [72].

1.2.6. Vat Photopolymerization

The method consists of a platform inserted into a resin vat. A UV light cures the resin from the upper layer to the top, moving the platform down. This process is liquid-based, so there isn't structural support during the building phase. Support needs to be added to help the part's creation. Some machines implement a blade system to move resin and create a smooth resin base to the following layer. In the end, the resin is drained. This method isn't applied to metal material [72].

1.2.7. Powder Bed Fusion

This technique is based on a machine that distributes a layer of metal powder onto a build platform using a roller or a blade. The powder is melted or sintered by an energy source (laser or electron beam). An electron beam method requires a vacuum environment to perform correctly. The build platform is then lowered, and the next layer of metal powder will be coated on top. An external tank provides fresh material. The process continues until the parts are built up layer by layer in the powder bed [72].

1.3. Lattice structures

The industry is greatly interested in lightweight structural concepts with high performances and lower costs. In the last decades, the efforts involved manufacturing techniques able to create cellular materials with high structural efficiency, high impact resistance, energy, and acoustic absorption and heat treatment [8].

The features of Additive Manufacturing permit building components capable of satisfying these requests.

In this scenario, it is possible to collocate lattice structures, also known as cellular structures.

Cellular structures are formed by the repetition of unit cells in all three directions. They can be defined as objects with internal symmetrical geometric micro-structures much smaller than the overall size [9].

There isn't a unique definition to describe a lattice structure, but many researchers express their opinion [7,17-18]:

- Ashby defined a lattice as a connected network of struts with the purpose of creating stiff, strong load-bearing structures using as little material as possible
- Tao et al. defined lattice structure as an architecture formed by an array of spatial periodic unit cells with edges and faces.
- Pan et al. defined lattice structures as three-dimensional structures composed of consecutively and repeatedly arranged interconnected cells, which can also be

understood as a porous material structure consisting of interlinked struts and nodes in a three-dimensional space

By ISO/ASTM, the lattice structure is a three-dimensional geometric arrangement composed of connective links between vertices (points), creating a functional structure.

They are part of the category called "architectured" materials. They are formed by a combination of bulk material and empty space, which creates a new lighter structure with mechanical properties close to the original bulk material. They are characterized by a relative density (ratio between cell density and bulk material density) lower than 0.3 [9,10].

This type of structure exists in nature (bones, coral, cork, sponge, wood, etc.) and is used to build constructions (Tour Eiffel, power line pylons, etc.).

Cellular metal structures can be separated into three different groups: stochastic (disordered lattice structures), non-stochastic (periodic lattice structures), and pseudo periodic lattice structures [10].

Stochastic foams are characterized by the random distribution of unit cells in different sizes and topologies and can be divided into open or closed-cell structures. Non-stochastic foams are characterized by the regular repetition of unit cells identical in topologies and dimensions. The last one has cells with identical topologies, but they differ in size and shape.
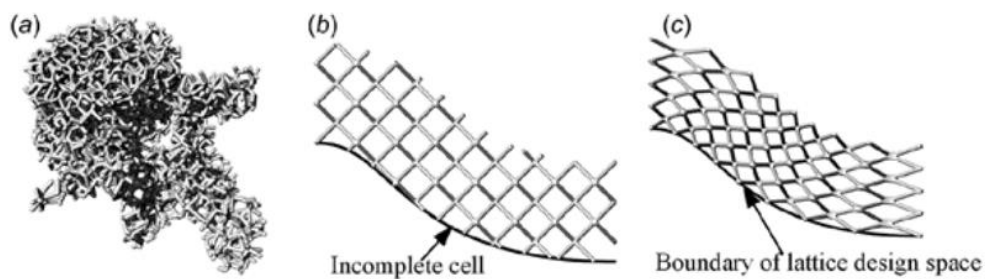
Figure 1 Different types of lattice structures: (a) Stochastic lattice structures, (b) Non-stochastic lattice structures, and (c) Pseudo periodic lattice structures

There are many methods used to make stochastic metal foams: closed-cell stochastic foams are typically produced by generating gas bubbles in a melt pool, and a good control permits to reach the desired porosity or using entrapped gas expansion, hollow sphere sintering, or other powder processing methods, while open-cell stochastic foams are formed using melt processing, powder processing or deposition processes [22].

This type of structure permits the topology optimization of parts. Two different methods exist to realize a topology optimization: the density-based approach (using sophisticated algorithms

to realize an optimal mass distribution) and the truss-based approach (replacing solid regions with lattice structures) [15].

Lattice structures are becoming interesting in designing and fabricating because they permit metamaterials with unique properties such as ultra-strong and ultra-stiff. The unit cell is a micrometrical scale so it can be seen simultaneously as material and structure.

In this working thesis, a non-stochastic open-cell lattice structure is selected because recent studies showed that using this cell is better in terms of mechanical properties than stochastic foams.

1.3.1. TPMS

TPMS (Triple Periodical Minimal Surfaces) is a category of lattice structures. They are generated from trigonometric functions. TPMS are minimal surfaces, which are a subset of hyperbolic surfaces. A hyperbolic surface is constituted of hyperbolic geometry, a non-Euclidean geometry. The main difference between a surface in hyperbolic geometry and standard Euclidean geometry is that in the first one, there are at least two distinct lines that pass through a given point and are parallel to a given line. Instead, Euclidean geometry has exactly one line through a given point in the same plane as a given line which is never intersected. In mathematics, a minimal surface is a surface that locally minimizes its area [14].
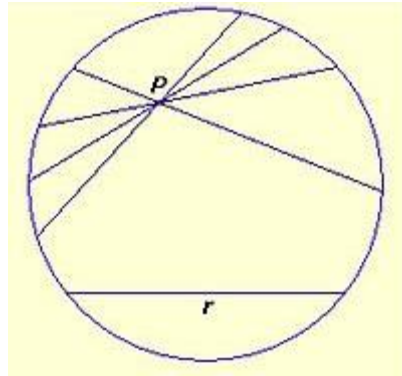
Figure 2 Hyperbolic geometry

Hence, TPMS is defined as minimal surfaces that are infinitely periodic in all three independent directions, without self-intersections and partitioning the space into two labyrinths [14-28].

Regarding manufacturability, TPMS structures are self-supporting, and this is a noteworthy feature that implies that support structures aren't required during the manufacturing process. Furthermore, due to this feature, TPMS is suitable for realization by L-PBF technology [11, 13].

The application of this kind of cell permits an improvement in the loading ability, stiffness, plateau stress, and energy absorption ability of the lattice structures because it deletes the presence of nodes, which are the weak points of the structure [63-66].
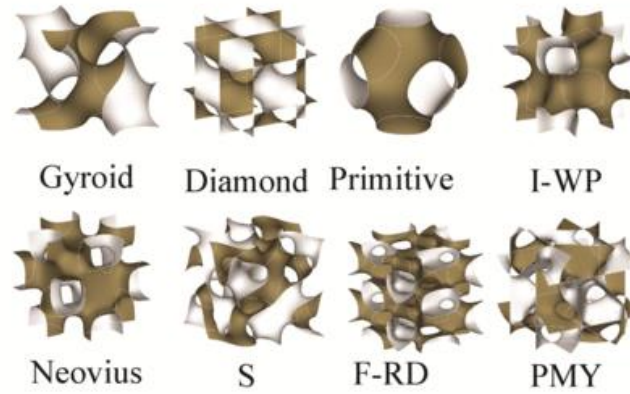
Figure 3 Different types of the unit cells for TMPS lattice structure

1.3.2. Shell-based

This structure shows a unit cell with plates and not struts to constitute itself. It is possible to divide shell-based lattice structures into two groups: close and open cells. The first one presents better elastic properties than strut-based with the same density. Close cell shows complexities to product through PBF because it challenges the powder removal. At the same time, the second one shows better stiffness and strength than strut-based with low density [13].
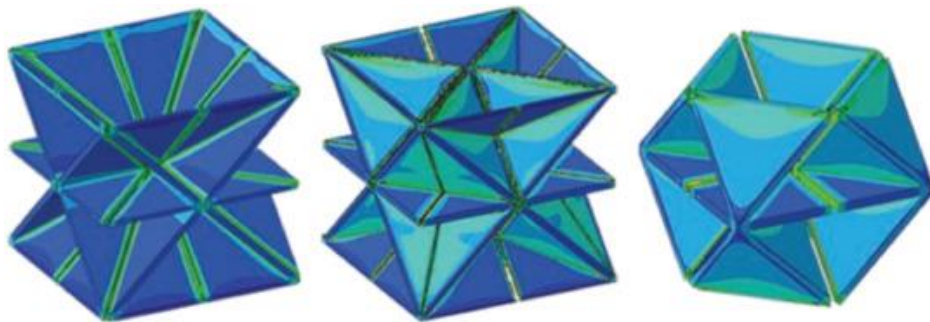
Figure 4 Different types of the unit cells for Shell-based lattice structure

1.3.3. Strut-based

This type of structure shows a unit cell that is formed by struts. These are similar to beams, and they are linked to each other to create a truss structure.

Strut-based lattice structures are chosen for their straightforward design. A topology optimization permits maximizing the efficiency of material distribution in the structure and using all potentialities of AM techniques [13].

A manufacturing technique commonly used to realize strut-based lattice structure is L-PBF because it guarantees good performance during the production phase and post-processing life.

1.3.3.1. L-PBF

Laser Powder Bed Fusion (L-PBF), also known as Selective Laser Melting (SLM), is an Additive Manufacturing technique. Metallic parts are fabricated from CAD data by the layer-wise fusion of metallic powders using a laser source to produce energy. Metallic powder is distributed above the previous layer for each layer, which is then selectively scanned by the laser to melt the powder locally. This is relevant because melting powder, compared to sintering, permits limiting risks of the birth of micro-porosity (voids) in the elements of the part and so preserves the mechanical performances [29,43].

L-PBF has certain limitations, like geometrical constraints, and sometimes it needs support to fabricate parts with complex geometry. Still, this solution isn't standard because supports are difficult to remove, representing material and energy waste. About geometry, this technique shows a tremendous geometrical accuracy compared to other Additive Manufacturing techniques [30].

The advantages of this technique are the capacity to create near fully-dense, complex components with high resolution and superior properties compared with those realized by traditional methods like casting [67].

On the contrary, the disadvantages related to manufacturing technique are: the minimum feature size (it depends on the laser beam spot size), metallurgical and microstructural defects (difficult to estimate), potential geometrical defects (caused by laser scanning, which doesn't perfectly melt the powder between layers and by suboptimal process parameters), thermal gradients (due to the rapid heating and cooling of powder) origin residual stresses which can produce deformation and geometrical defects [32-35,44].

Furthermore, L-PBF's powder must respect characteristics such as morphology and size. Much time is necessary to realize a part because the laser can melt small quantities of material per unit time, so manufacturing costs are expensive [38].

The features of Additive Manufacturing listed in the previous paragraphs, the advantages and disadvantages of L-PBF permit the realization of complex structures like lattice ones.

The effects of L-PBF on lattice structure performance are due to many factors like powder morphology, size and chemical composition, particle size distribution, laser exposure power and strategy, laser scan speed, and layer thickness [38-39].

It is noteworthy that PBF is the favorite technique for metallic lattice manufacture due to its great geometric accuracy, which reduces the number of defects and confers excellent performances [31].

The defects of lattice structures are related to the fabrication process and mainly involve the internal structures, which are thin and sensitive to the manufacturing parameters [40].

Typical lattice defects are: the staircase effect (phenomenon associated with 3D printing when the layer marks become distinctly visible on the surface of the parts and give the perception of a staircase, and it is omnipresent independently from the 3D technique), structural irregularities (strut waviness and non-idealized strut intersections/nodes), residual stress, shrinkage effect (phenomenon associated with 3D printing where there is a dimensional deviation between CAD and final product) and bonded particles on the surfaces of internal structures (they are caused by balling or partial melting of metal powder) [13,16,26,46,47,48,54,62].

These defects affect the property of fabricated parts, dimensional accuracy, and surface roughness. These defects cannot be completely deleted because they are characteristic of the fabrication process, but they can be minimized with process optimization [42,45].

This manufacturing process of a lattice geometry has two essential constraints:

-       The orientation angle → It represents the minimum inclination angle which indicates the inclination of the struct (lattice's internal structure like a beam) to be realized without supporting structure and without considerable geometric distortion. It depends on the material, processing parameters, and powder characteristics. The minimum angle is around 45° from the building plate, but some studies state that 30° is the low limit [50,51,53].

-       The minimum diameter → It represents the minimum diameter of the strut, which permits its successful building and not origins significant discrepancies with the CAD model. Some studies state that 300 μm is acceptable as a limit [20,52]

All these geometrical parameters must be related to the specific material.

After all considerations, L-PBF is selected as Additive Manufacturing technique in this working thesis to realize lattice structures.

L-PBF technique is characterized by features and constraints, as underlined in the previous lines. These generate many defects during the creation of struts, which implies a variation in the part's mechanical properties. The most common defects are a variation in cross-sectional geometry, waviness (deviation of the strut's axis across its length), and micro-porosity. Across an optimization of processing parameters is possible to reduce them and preserve the structure's performance [41].

This working thesis selects this type of lattice structure and the L-PBF technique to realize the lattice structure for the above characteristics.

1.4. Cell topology

In this paragraph, the attention is focused on the lattice structures with strut-based unit cells.

It is essential to underline that the cell's shape is more important than its dimensions to describe its properties.

Many research and works are made to discover better cell shapes and develop many cell geometries.

Production of complex cell geometries on whit small scale is challenging, but the use of Additive Manufacturing permits one to face this challenge efficiently, and new geometries are realized.
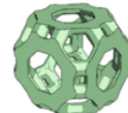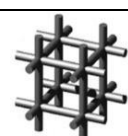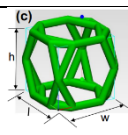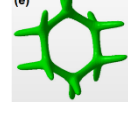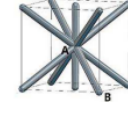
Commonly a unit cell is defined by three parameters that define the volume: length, width, and height.

The most common strut-based lattice structure unit cells are shown in the following table [13,36,49,63]:

Table 1 Strut-based lattice structure unit cells

Unit cell's name	Structure
BCC	
FCCZ	
FBCCZ	
FBCCXYZ	
BCCZ	
FCC	

Diamond	
Octet truss	
Truncated cuboctahedron	
Rhombic dodecahedron	
Cubic	
Hexagonal	
Vintiles	
Tetra	

The rhombic dodecahedron unit cell is selected to realize the lattice structure in this thesis work.

1.4.1. Selection of the cell topology

This cell topology wasn't the initial idea to fill the volume of the lattice structure. The first idea about unit cells differed from this one, which was more straightforward.

It consists of a tetrahedral base formed by three struts and a vertical strut at the top of the tetrahedron.

This unit cell is different from previous ones because it cannot be inscribed into a cubic cell, but it can be inscribed in a regular parallelepipedon. The base's angles are around 70°, and the struts on the base are located at an angle of 120° to each other, while the struts' length depends only on the manufacturing process and the final dimensional part.
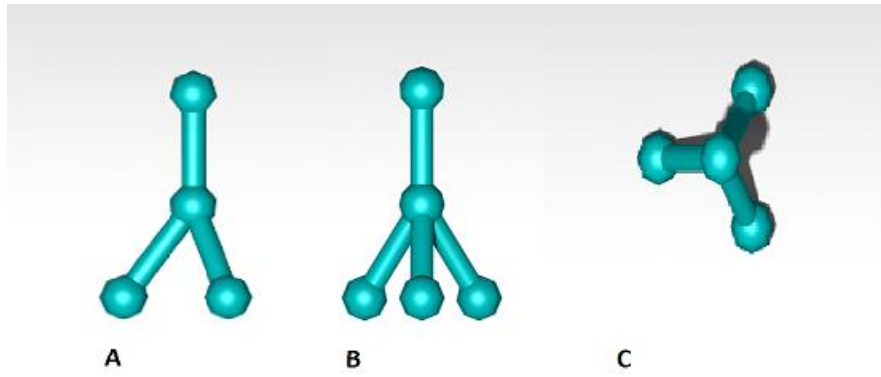
Figure 5 Initial idea of the unit cell: A lateral view, B front view, and C top view

This working thesis discovered another unit cell with a geometrical characteristic similar to the initial one and more attractive. So, it is adopted to substitute the first one.

This unit cell is more complex because it is the development in the three directions of the last cell. So it presents different and better mechanical performances than the simple unit cell. Compared to the old one, this new cell doesn't show favorite loading directions, which are evident in the preceding. Furthermore, some studies state that this cell can absorb energy due to its structural deformation [49].

This unit cell is close to the rhombic dodecahedron, a geometrical solid composed of 12 faces, 24 edges, and 14 vertices. The faces present a rhombic shape with angles around 70.53° and 109.47°.

The unit cell differs from the rhombic dodecahedron geometrical solid because there are eight struts in addition, one for each vertex of the cube, so they are inclined with an angle of 45°.

The selected unit cell presents a symmetrical structure in all planes (XY, XZ, and YZ).
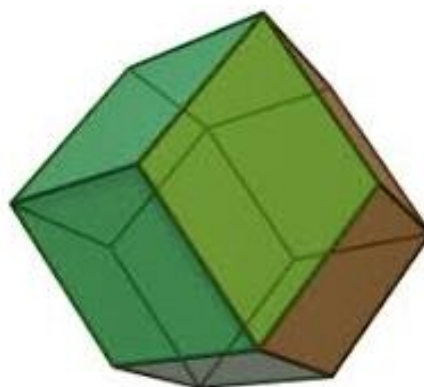
Figure 6 Rhombic dodecahedron geometrical solid

11
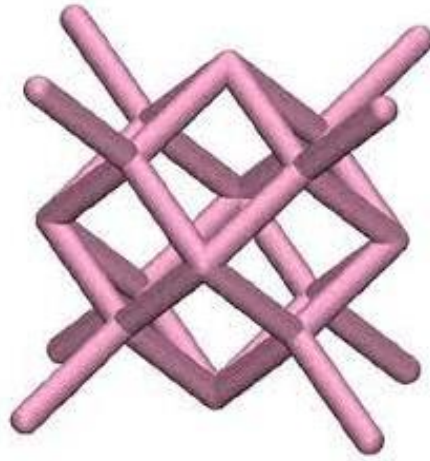
Figure 7 Rhombic dodecahedron unit cell

1.4.1.1. Design parameters

After choosing the unit cell, it is fundamental to analyze the main factors influencing the lattice structures' mechanical performances.

Generally, the properties of three-dimensional lattice structures are influenced by cell topology, cell's and strut's size.

The influence of cell topology will be discussed in the next paragraph. At the same time, the other influencing factor will be discussed in this one.

First, it is necessary to consider that lattice structures present three different failure mechanisms: yield, buckling, and brittle fracture [55,60,61]. During a preliminary phase design, it's essential to delete buckling and brittle fracture mechanisms because the structure must only fail through the yield mechanism.

Buckling must be deleted because if the structure is designed to support a specific load, the strut must resist almost the same load without showing buckling instability with a smaller load. If the buckling appears, the structure cannot support the load, the design is incorrect, and there is material waste.

The brittle fracture must be deleted because the entire component becomes useless if the structure collapses. At the same time, the yield mechanism must be considered because it represents the structural limit of the part, and so if the struct collapses under this type of load, the design is correct.

The unit cell's size is influenced by the Additive Manufacturing process, and considering an L-PBF technique, it must be adapted to permit easy removal of unmelted powder when the part is completed. Some studies report a low limit for this parameter of 2 mm (length, width, and height) [20].

Regarding the strut's size, there are many aspects to evaluate. Some of them are related to the manufacturing process, like the strut's orientation angle, length, and diameter.

The orientation angle was analyzed previously, and the value identified as a low limit was 30° for an L-PBF process.

The strut's diameter is a relevant parameter because it strongly influences its quality. When a part with small features of the exact sizes of the melted volume is built, many discrepancies could be created between the CAD design and the fabricated model. The strut's diameter must be more significant than the melted volume to avoid this geometrical mistake. This size is influenced by the energy of the heat source. For example, an EBM process suggests forming a strut with a diameter greater than 800 μm [20], while for a laser application, 200 μm is almost recommended [13].

The strut's length represents a constraint imposed by both the Additive Manufacturing technique and by the final application of the part. Considering L-PBF as a manufacturing process, the structs must be smaller than 5 mm to avoid the birth of deformation during the process itself. Still, it depends on the strut's diameter [30].

Two design parameters are represented by the ratio of strut and cell dimensions. The first one is the slenderness ratio, meaning the ratio between the strut's diameter and length. The second one is called the aspect ratio, and it can be defined as the ratio between the cell's size and the strut's diameter. These last parameters are important because they take into account the buckling problem related to the unit cell's strut.
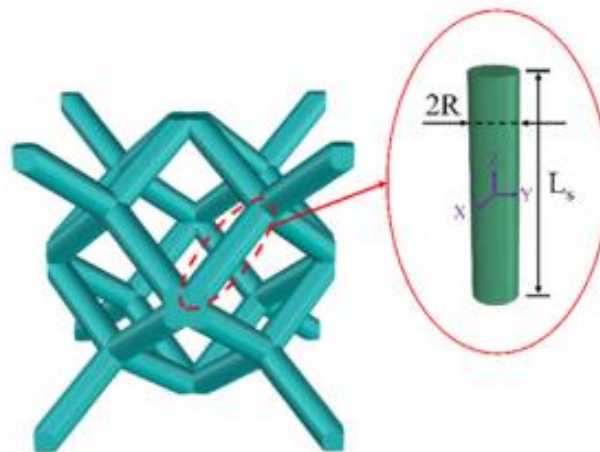
Figure 8 Slenderness ratio detail
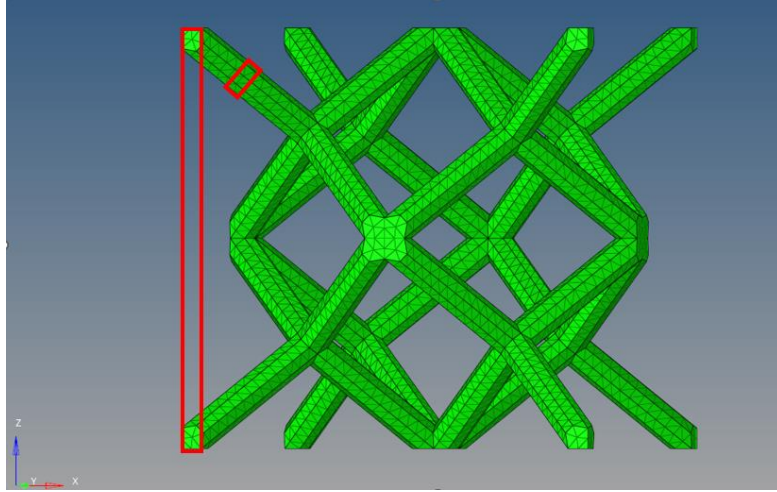
Figure 9 Aspect ratio detail

Considering the rhombic dodecahedron unit cell is evident, the most critical area is close to the nodes. A relevant aspect of the unit cell is the stress concentration in these points. To avoid a structure's failure, there is the need to reinforce them. There are different ways to do this: using a tapered beam instead of simple ones with a constant diameter or using a spherical element in place of the struts' joint [5].

The last design parameter is the relative density, and it is a combination of all geometrical cell and strut dimensions. It is calculated by the ratio between the cell's density and the parent material's [5,18,26]. In the following chapters, it will be shown as this parameter affects the structure's mechanical properties.

These design parameters will be associated with a value in the chapter dedicated to structural analysis.

1.5. Mechanical behavior of lattice structures

The influence of cell topology on mechanical performances is analyzed in this paragraph thanks to Maxwell's Criterion. It consists of an algebraic rule to define the compression behavior of a unit cell, starting with its cell topology. This criterion is applied to 2D and 3D cells, and so two different formulations exist [9,11-13]:

$$M = b - 2j + 3 \qquad 2D$$
$$M = b - 3j + 6 \qquad 3D$$

Regarding the relation: the "b" parameter is the strut's number, the "j" parameter is the joint's number, and "M" is Maxwell's parameter. The rhombic dodecahedron unit cell (3D structure) selected comprises 32 struts and 14 joints, so Maxwell's parameter counts -4.

The value of Maxwell's parameter predicts the unit cell behavior, and so there are three cases [9,11,37,47,62]:

- M<0 → There are too few struts to be statically determinant, and so the structure shows bending-dominated behavior
- M=0 → The structure has the minimum number of struts to be statically determinant, and so it shows a stretch-dominated behavior
- M>0 → The structure has more struts than necessary to be statically determined, and so the structure shows a stretch-dominated behavior

The stress-strain curve of a lattice structure can be divided into three different phases: linear elastic, plastic, and plateau region and then densification [49,55].

The material's response is linear elastic in the linear elastic region with Young's modulus proportional to the parental bulk material. The reaching of the elastic limit defines the next region, the cells begin to yield or buckle, and then a plateau zone appears, which shows a large deformation with a bit of stress variation. The last area offers a phenomenon which is called densification. It starts when the cells are deformed enough and are in contact with each other, and a substantial increase in stress characterizes it. In this last phase, the structure's failure can be reached in three different ways: successive cells collapse, crack propagation, and diagonal shear [36,47].
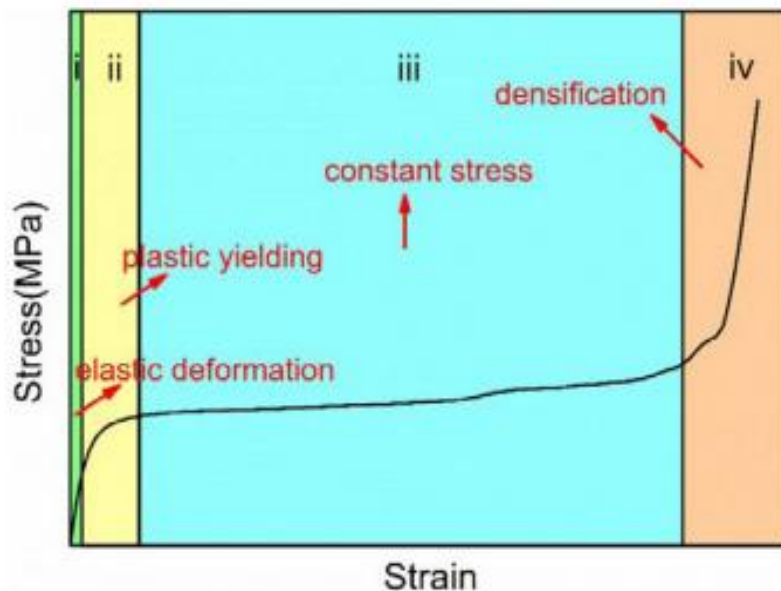
Figure 10 Typical stress-strain curve of a lattice structure

The predicted behavior of a unit cell characterizes the second region of the stress-strain curve after the plastic deformation and so the mechanical performances of the lattice structure.

A stretch-dominated behavior presents a drop and an oscillating stress trend. It is essential to underline that Young's modulus and initial yield strength structures are more remarkable than bending-dominated ones, and so these types of structures are high-strength and low-compliance. They are dominated by tensile or compressive forces generated in struts. These produce plastic deformation and failure characterized by yielding, buckling or the brittle collapse of struts [9-11,27,56,59,60-62,70].

While a bending-dominated behavior shows a constant stress trend without a stress reduction and considerable plateau stress, which represents the amount of energy stored by the cell until the failure. These types of structures are dual compared to the stretch-dominated, so they are low-strength and highly compliant. They deform via generation of bending moments at strut intersections and subsequent forming plastic hinges like a ductile material [9-11,27,56,59,60-62,70].

Due to these characteristics, lattice structures with stretching-dominated behavior are used for structural applications. In contrast, lattice structures with bending-dominated behavior are applied where energy absorption is requested [9].
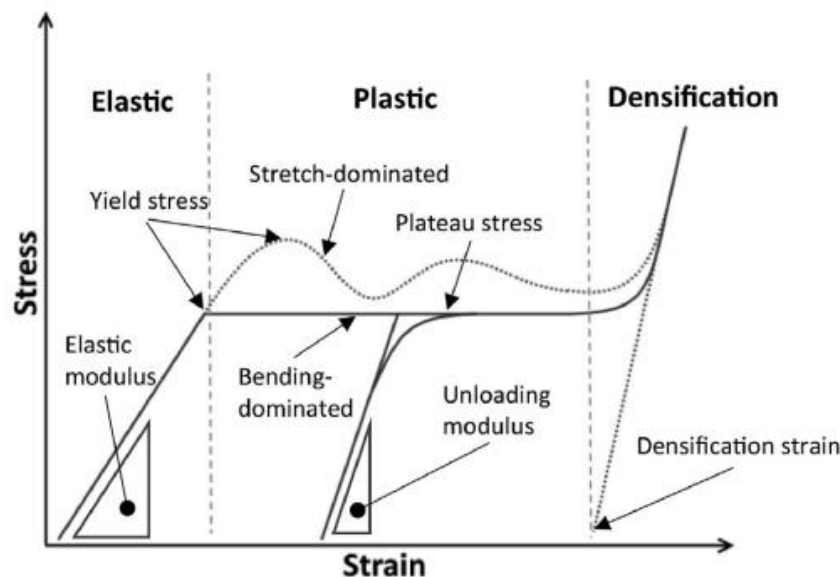
Figure 11 Bending and Stretch-dominated behavior

At the end of this first chapter, it is evident that mechanical performances are influenced by material, building process, structural constraints, and load conditions.

In this chapter, some decisions are taken: first of all, L-PBF is selected as the manufacturing technique, and then a rhombic dodecahedron unit cell is chosen to form the lattice structure, which will be studied in the following chapters.

2. RESEARCH

This chapter is divided into main paragraphs: the first is dedicated to finding the material to produce the sample, and the second is related to exploring the Finite Element Software world to know how they approach the lattice structure analysis.

2.1. Material

2.1.1. Metal Additive Manufacturing Materials

Printing metal with a 3D printer is the last frontier of additive manufacturing. It consists of the deposition and melting, layer by layer, of metal powder to realize a part.

Metallic materials are largely used in industrial fields. The goal is to transform the production process by introducing Additive Manufacturing systems to replace, in some cases, the actual ones.

The initial problems related to the velocity and costs are disappearing; this permitted the rapid diffusion of this manufacturing technique [23].

Research and investments improve the development of new technologies and methods with better performances and cheaper than before. Added to this, the introduction of design 3D software to improve the topological optimization of components can completely change manufacturing, passing from subtractive to additive manufacturing [19,21,57].

The interest forwards this technology is due to different factors [19-21]:

- Speed is a great benefit compared to subtractive manufacturing processes. Sometimes, the time to build a part can be reduced from months to a few hours. This permits engineers and designers to develop new concepts and companies to produce faster than traditional methods

- There are no added costs in the production because dedicated infrastructure isn't necessary, while tools and machines' costs are confrontable with CNC's systems (Computerized Numerical Control). It is possible to use the same device to realize parts with different sizes and geometries

- The waste of materials is primarily minimized thanks to the additive method; indeed, the material is put where it is necessary compared to traditional methods, and there is enormous design freedom

- Entire manufacturing process (from CAD model to physic model) is faster because it is possible to conduct all phases in the same workspace (the process is completely made with PC software)

- A difference with traditional methods is the excellent design freedom due to the absence of geometrical constraints

- On-demand process and customization are permitted thanks to the possibility of realizing small, medium, or large volumes of parts, and they are used in different fields
- The most important aspect is the introduction of new materials and the possibility of mixing them to obtain better performances which are impossible to reach with traditional methods

Related to the last advantage, some of the more common metal materials available for Additive Manufacturing are listed below [19,21]:

- Titanium and its alloys → It is strongly reactive, so this powder must be used in a controlled atmosphere (Argon or vacuum). Moreover, it presents an excellent surface finishing and an elevated mechanical resistance. It is used mainly in the medical industry to realize prostheses. It has optimal performances related to lightweight and hardness, which permits its application in the aerospace and automotive industries. Other essential features are corrosion resistance, biocompatibility, low thermal distortion, and low thermal conduction
- Nickel superalloys → They are materials that are corrosion, high temperature, and oxidation resistant. These properties are essential for the airplane flight data recorder and the critical engine components such as turbine blades
- Precious materials (gold, silver, and platinum) → The jewels industry is particular interests in Additive Manufacturing technologies. The additive features allow one to realize complex and unthinkable geometry quickly. Moreover, the part's dimension permits serial production, and so this aspect makes it possible to reduce time and create more pieces than before
- Aluminium and its alloys → It is vital because it is very lightweight and has relevant mechanical properties. Moreover, low density, high thermal and electrical conduction with dynamic resilience make it fundamental in the aerospace and automotive industry
- Chrome-cobalt alloys → It is primarily used in Metal Additive Manufacturing and, thanks to its characteristics, is applied to realize medical components and in the engine part as turbine, where corrosion and thermal resistance are essential
- Stainless steels → Nowadays, it is the cheaper metal material used to print. The relevant applications involve automotive, aerospace, and medical industries, where its characteristics such as excellent corrosion resistance, high strength under elevated temperatures, and high ductility era exploited.

Nowadays, many companies produce and sell metal powder for Metal Additive Manufacturing printers with different properties and dimensions.

The research focuses on the L-PBF powders because this technique is selected to realize the previously chosen cell.

Many companies worldwide produce powder metal able to perform in an L-PBF printer and build an additive manufacturing part. In the following tables are listed two of the most relevant companies, the sector's leader, and their products [3,6]:

Table 2 Companies powders available

Company's name	Alloys	Powder's name	Datasheet (*)
SLM Solutions	Al-Based Alloys	AlSi10Mg	
		AlSi7Mg0.6	
		AlSi9Cu3	
	Ti-Based Alloys	Ti6Al4V ELI (Grade 23)	
		TA15	
		Ti (Grade 2)	
	Ni-Based Alloys	HX	
		IN625	
		IN718	
	Co-Based Alloys	CoCr28Mo6	
		SLM MediDent	
	Fe-Based Alloys	316L (1.4404)	
		15-5PH (1.4545)	
		17-4PH (1.4542)	
		1.2709	
		H13 (1.2344)	
		Invar 36	
	Cu-Based Alloys	CuNi2SiCr	
		CuSn10	
		CuCr1Zr	
EOS	Al-Based Alloys	AlSi10Mg	
		AlF357	
		Al2139 AM	
	Steels	20MnCr5	

	Co-Cr-Based Alloys	MP1	
	Cu-Based Alloys	Cu	
		CuCP	
		CuCrZr	
	Ni-Based Alloys	IN625	
		IN718	
		IN939	
		HX	
	Precious metal	Gold	
		Silver	
		Platinum	
		Palladium	
	Refractory Metals	Tungsten W1	
	Fe-Based Alloys	316L	
		316L VPro	
		17-4PH	
		254	
		SuperDuplex	
		CX	
		PH1	
		GP1	
	Ti-Based Alloys	Ti64	
		Ti64ELI	
		Ti64 Grade 5	
		Ti64 Grade 23	
		TiCP Grade 2	

(*) Green is associated with the presence of the material datasheet, while red represents the absence of one.

2.1.2.Material selection

At the end of this section, SS316L is chosen to build the part. There are two main reasons for this choice: the first is the discovery of a paper titled "Mechanical properties of an improved 3D-printed rhombic dodecahedron stainless steel lattice structure of variable cross section" published by Xiaofei Cao, Shengyu Duan, Jun Liang, Weibin Wen, and Daining fang [5].

This paper uses an accurate study to optimize a rhombic dodecahedron lattice structure built by Selective Laser Melting (SLS) with SS316L. A quasi-static compression test is conducted on the samples.

The paper is fundamental for this working thesis because it gives the experimental test results to calibrate and define the material's behavior in FEM software. Indeed this type of test constitutes the first step of the methodology to determine the equivalent solid's characteristics. The metal material defines the second reason: it is austenitic high chromium steel with excellent processability on the L-PBF Additive Manufacturing machines. It is often used in applications requiring good mechanical properties (high ductility and strength), excellent corrosion, and high-temperature resistance. It is employed in aerospace and automotive and medical applications as surgical instruments [3,6].

2.1.3. AM Printer

The printer covers an important role in defining the properties of parts. Regarding a laser printer (L-PBF), it is possible to identify six main elements:

- Laser entry lens → The power to melt powder is provided by a laser. It enters from a lens put on the top of the chamber. The powder is located on a platform that descends after the fusion of the upper layer
- Argon inflow door → This door is fundamental because the use of laser imposes an inert atmosphere which is created using argon or other gases
- Argon aspiration door → This door permits the removal of gas at the end of the process
- Powder tank → The powder is stocked in a tank to provide raw material during part forming
- Dosing system → This system guarantees the correct quantity of metal powder
- Dust recovery door → At the end of the process, this opening is helpful because the unmelted powder is recovered and filtered to be reused later
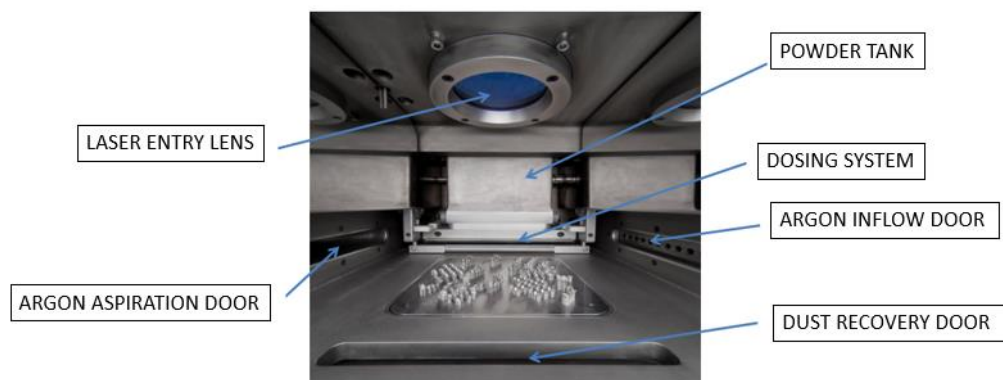
Figure 12 AM400 3D printer (RENISHAW): L-PBF printer main elements

The principal feature of the L-PBF printer regards laser power, which is lower than Electron Beam Melting, and its value is higher than 100 W, but it depends on the printer itself. Another aspect to consider is related to preheating. Indeed, the laser power isn't sufficient, so installing electric heaters under the platform is necessary to improve the process efficiency limited to the lower layers. For this reason, this process is called a "cold process". The work chambers have a limited size of around 1000x400x400mm, and often they are divided into two parts where two lasers work together [74].

Moreover, the layer thickness highly influences the mechanical characteristics of the part, and it is around 30-50 µm. This thickness affects the production velocity, reaching 1.8-11 cm3/h. The layer is thinner than an EBM method because the power is lower and the laser focus is smaller, so better precision, roughness, and finishing are obtained [74].

Other parameters to evaluate during preliminary design phases include laser velocity, around 3500 m/s, hatching distance, and scanning strategy. Hatching distance is the distance between two adjacent working lines, and it is relevant because if it is significant, the process is faster, but the risk of having unmelted powder is elevated, and it must be optimized to improve the process efficiency. Scanning strategy highly influences microstructure and so mechanical performances. Therefore its optimization must occur too.

The reference paper defines the printer machine and the manufacturing technique to produce experimental samples. They are made by SLM using the AM400 3D printer from RENISHAW with SS316L powder. On the paper are reported some characteristics: laser power of 110 W, laser exposure time of 200 µs, and scanning speed of 8 m/s [5]. More printer features are described in an attached datasheet [A].

Figure 13 Additive Manufacturing Printer

2.2. Software

During this phase of the thesis, an overview of FE Software is defined, and in particular, the purpose is to find out if there are and how software work to solve a lattice structure analysis. The main principle and knowing software available are reported in the following table:

Table 3 Software available

Software	Tool (*)	Software operation (**)
Ansys	Multiscale.Sim	Homogenization
Abaqus		
Nastran		
LS-Dyna		
MS Marc		
Pam Crash		
Optistruct		
Samcef		
MSC hexagon		
Hexagon digimat e-Xstream	Digimat FE	Homogenization
	Digimat AM	This tool works on plastic Additive Manufacturing, but it focuses on the process optimization and not on the FE analysis
Altair Inspire		

(*) The red color underlines the absence of a tool to approach the analysis, and the green color defines the presence of one.

(**) It contains the technique used to face the study.

In this research, it has emerged that at the state of the art, there isn't or isn't find out software that has a tool or method to deal with a complete analysis of a lattice structure rapidly and efficiently [75,88].

Software scenario shows the presence of many tools or methodologies to analyze lattice structure formed by Additive Manufacturing from the point of view of optimizing the manufacturing and design process. In particular, many of them study how to reduce the waste of material finding what component's parts are more stressed and underline the need to put

many materials in that area. Other software tools study the better way to form the piece to avoid stress and thermal distortion during and after the process [75,88].

Currently, the research shows that there are a few software that implements this type of analysis. In particular, Ansys sells a tool to study the mechanical properties of the lattice structure in a simple way. This tool is called Multiscale.Sim and its mode of operation is based on a method defined as Homogenization [2].

2.2.1. Multiscale.Sim

Multiscale.Sim is part of the Ansys Workbench GUI using the Ansys Customization Toolkit (ACT) techniques. It is straightforward to use and guarantee high-performance productivity for Ansys Workbench users [2].

The Multiscale.Sim tool helps customers solve complex materials problems and challenges around materials modeling and characterization. Its operational mode consists of two functions: homogenization and localization. These make it possible to perform analysis of the inhomogeneous material microstructure: composite material, honeycomb, filler dispersion, lattice structures, and others [2].

The entity of the material's properties is estimated by a numerical material test of microstructure without material tests required in a traditional approach. The results enable the prediction of the macroscopic behavior by the macro structural analysis. Later, it is possible to obtain the microscopic behavior by returning to the microstructure analysis [2,62].

The following reported picture shows the Multiscale Analysis flow:
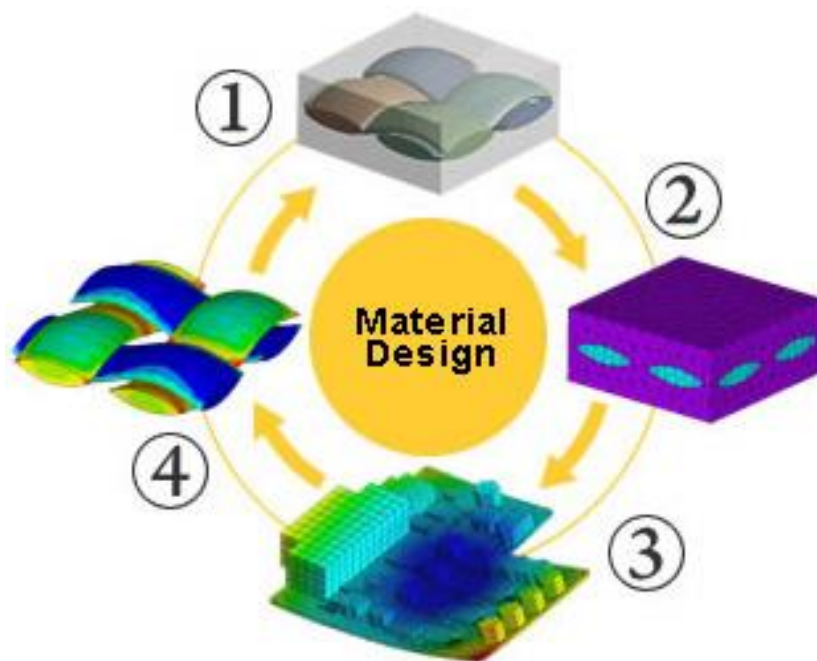
Figure 14 Multiscale Analysis flow

It is composed of four main steps [2,70]:

1. Create a Micro Model → The creation of a micro model exploiting a 3D CAD or Ansys Design Modeler to realize material test

2. Homogenization Analysis → The equivalent properties are calculated after meshing, defining the boundary conditions in Ansys, and performing a numerical material test

3. Macro Structure Analysis → The previous defined materials properties are attributed to the macro model, and then perform verification and analysis of the macro model are repeated

4. Localization Analysis → It is possible to know the local behavior by selecting the area from the macro model

The benefits given by this tool are considerable: it is possible to improve product performance and reduces product development time, make parametric studies, improve product design, productivity, and quality, and reduce time to market and real material testing cost and resources [2,70].

2.2.1.1.   Homogenization method

This approach is based on studying the microscopic behavior of the unit cell to define the macroscopic one. This way, the lattice properties are described with an equivalent material treated in the analysis as a bulk material. The geometrical and boundary conditions periodicity helps to implement this method. Homogenization aims to reduce the degree of freedom of a lattice structure. In this process is generated a linear orthotropic medium material whose properties are estimated by compression and shear simulations along with the principal directions. The core method is that a periodic unit cell represents the entire component. So it is evident how the reduction in time and cost calculation is significant, permitting to get information faster and easier than a more detailed analysis [24,62,70].

The results are not accurate, but it becomes helpful in the preliminary design phases where a global behavior is requested.

At the end of this second chapter, SS316L metal material is chosen to realize the lattice structure. Moreover, homogenization is the only way to analyze this type of manufacturing quickly and straightforwardly. This method is the same thinking at the beginning of the work, and so it is followed in the next chapters to define equivalent solid's properties.

3. ANALYSIS

The previous paragraphs underlined the advantages of realizing a component using an additive manufacturing technique and the enormous potentialities of building a lattice structure. These parts' diffusion is spreading rapidly in the last period, and a reliable method to analyze and predict the behavior has become essential. The complexity of a simulation conducted by FEM software is evident considering the number of nodes and elements necessary to mesh the entire lattice structure. In this scenario, the thesis goal is inserted. It is to define a methodology to simplify a lattice structure analysis using an equivalent solid. The strategy is to extrapolate the true mechanical properties of a lattice structure and then transfer them to an equivalent solid to reproduce the same behavior as the reticular one.

This chapter is the core work thesis. The analysis is divided into different phases, which are explained in detail in the following.

The methodology analysis consists of conducting an experimental test to determine material characteristics to define the lattice structure properties. Then, many virtual tests are made on an Additive Manufacturing part to extrapolate the equivalent characteristics.

In the last part of the chapter, the same tests are conducted on the equivalent volume to validate the obtained results.

3.1. Material definition

3.1.1. Material definition: Experimental test

A relevant aspect of the methodology is represented by using FEM software that permits the simulation of the lattice structure behavior. The adopted software needs information to define the material characteristics and reproduce the reticular one. This information must be provided by an experimental test, which produces a stress-strain curve. The experimental campaign isn't comprised of the project program for this working thesis, so they aren't available. In the previous chapter, a paper is mentioned. Its importance is relevant because it gives the experimental results, which are crucial to define the simulation material. They are the first step of the helpful methodology to determine the equivalent solid properties. More details are given in this paragraph about the test.

After choice, the manufacturing technique, unit cell type, and metal material are necessary to know the properties of the material produced by Additive Manufacturing because they differ from a bulk material built with the same material.

The process greatly influences the properties, so knowing them is a focused aspect to be considered.

The paper describes the test process to extrapolate the material behavior: a single beam is produced and tested, and the results are reported in a stress-strain curve that underlines its behavior.

The beam has this size:

- Core length → 9 mm
- Core diameter → 1 mm
- Radius curvature base → 0.5 mm
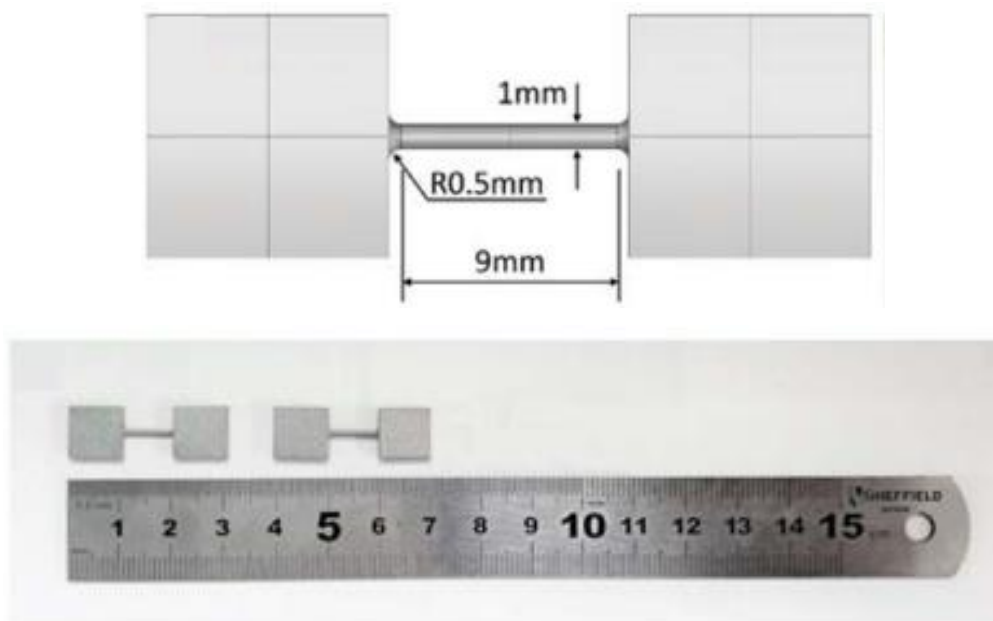
Figure 15 Single strut tester dimensions

A uniaxial tensile test is performed on a 30 kN Instrom universal testing machine at the tensile rate of 1 mm/min. A quasi-static compression test is made in the same testing machine with a compression rate of 0.9 mm/min. Stress is determined by the ratio between force and starting sample area, while the strain is determined using the displacement that occurred and the initial length.
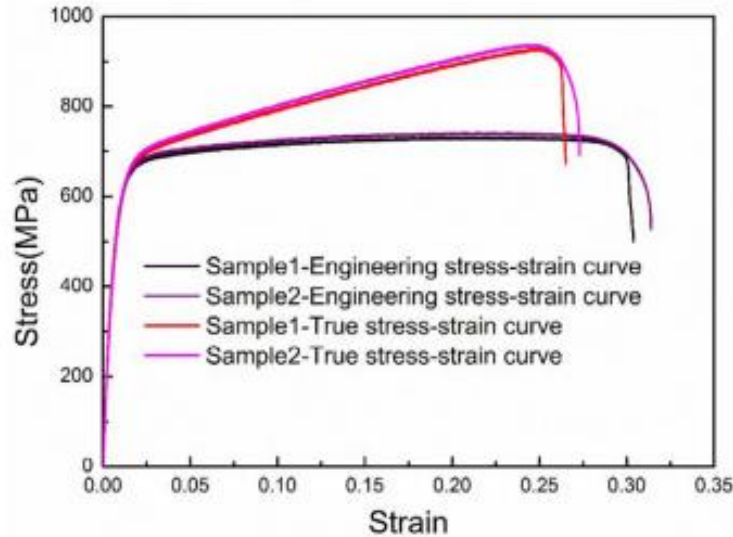
Figure 16 Single strut test: Engineering and True stress-strain curve

This test is performed on two identical samples, and the results are reported in the above figure. It is possible to recognize two different curves: the true curve presents higher stress than the engineering curve because the stress values are calculated by the ratio of applied force and the true area, and so the striction is considered. In contrast, the engineering one considers the area constant during the force application, so stress values are lower.

For the thesis, the curve to be considered is the true curve.

Using these results is possible to define the material characteristics:

Table 4 Material characteristics

Sample	Density [g/cm³]	Elastic modulus [GPa]	Initial yield stress [MPa]	Ultimate stress [MPa]	Ultimate strain
1	-	95	516.0	927.0	0.2365
2	-	91	509.0	937.0	0.2374
Average	7.96	93	512.5	932.0	0.2370

Referring to the stress-strain curve permits obtaining many points belonging to the plastic zone and defining the "virtual" material used in the software.

The plastic deformation values are extrapolated considering the plastic strain, so starting from the deformation is necessary to remove the elastic one.

In the picture below is reported this procedure:
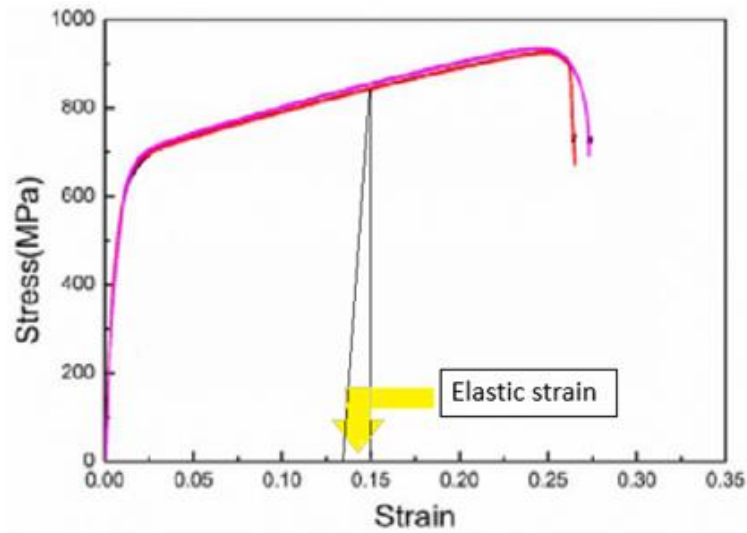
Figure 17 Method to extrapolate the plastic strain

In the following table are reported the points considered to draw the characteristic curve:

Table 5 Plastic stress-strain curve

Global strain	Plastic strain	Stress [MPa]	Elastic strain
0.0055	0.0000	512.5	0.0055
0.0075	0.0020	540.0	
0.0090	0.0035	580.0	
0.0100	0.0045	600.0	
0.0125	0.0070	620.0	
0.0150	0.0095	640.0	
0.0175	0.0120	680.0	
0.0200	0.0145	700.0	
0.0325	0.0270	720.0	
0.0450	0.0395	740.0	
0.0650	0.0595	760.0	
0.0850	0.0795	780.0	
0.1000	0.0945	800.0	
0.1150	0.1095	820.0	
0.1350	0.1295	840.0	
0.1500	0.1445	860.0	
0.1700	0.1645	880.0	
0.1950	0.1895	900.0	
0.2150	0.2095	920.0	
0.2370	0.2315	932.0	

Starting from the stress-strain curve and table reported parameters is possible to verify if and how FEM Software describes the natural behavior.

3.1.2.Material definition: FEM test

At this point, choosing Software is necessary to simulate the material behavior and compare the experimental results with simulation one.

Hypermesh is selected as the pro-processor to realize the CAD model and to test the sample. The solver is Optistruct, and the results are displayed on Hyperview, which is the post-processor. First of all, the solid is built. It is approximated with a cylinder whose dimensions are the same as the experimental strut test. This model has meshed with first-order CHEXA elements (8 nodes). The element number is 1600, and the node number is 2091.
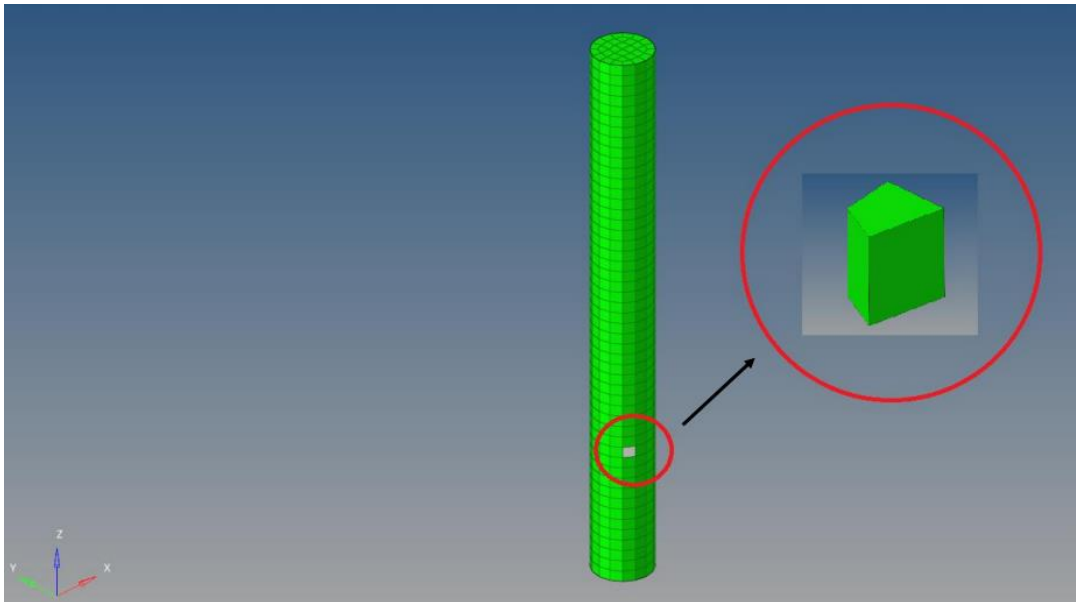
Figure 18 Element's detail

Successively constraints are given, and to avoid the "barrel" effect, isostatic constraints are imposed. This solution permits to display the displacements of the struts. They set a no translation in the Z direction to simulate the inferior plate of the testing machine.

The realization of the virtual test requests the applied load as input. In the paper, it isn't specified, and so it is calculated considering the final global displacement. It is extrapolated by the stress-strain curve starting from the ultimate strain value:

$$displacement = ultimate\ strain \cdot strut\ length$$

The applied displacement is 2.133 mm in the negative Z direction. The test runs, and the "virtual" stress-strain curve is drawn.

In the following graphs, the trends are shown:
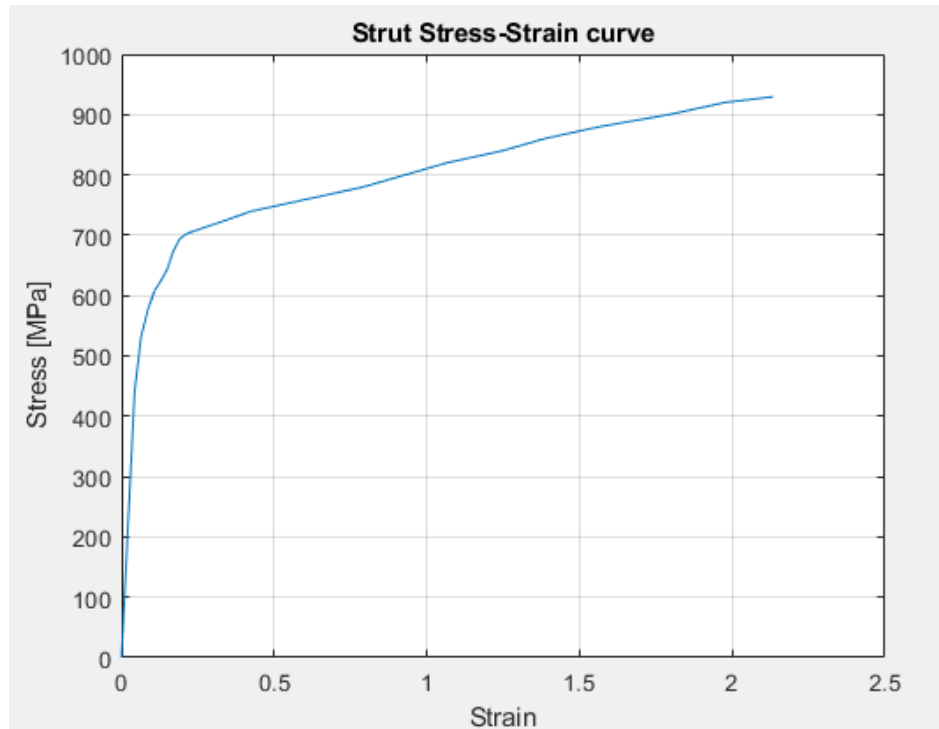
Figure 19 Stress-strain curve FEM
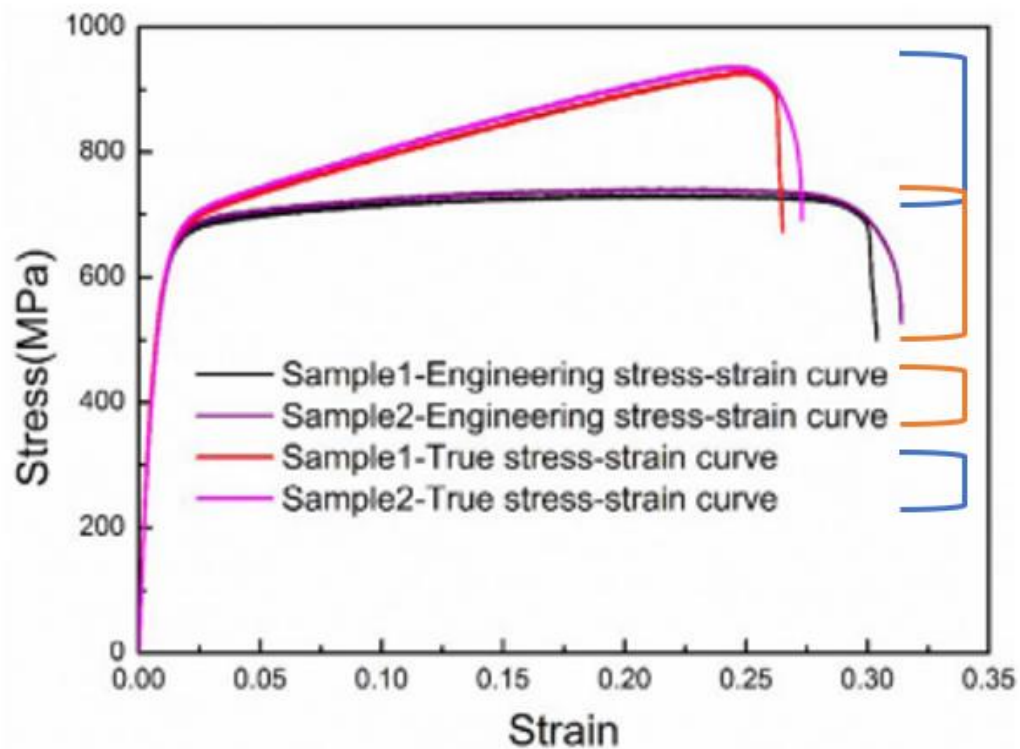
Figure 20 Stress-strain curve real test

As is expected, looking at the comparison between curves, it is evident how the software can describe the real material behavior excellently, so it can be attributed to a lattice structure to analyze more complex structural solutions.

If the curves are compared, it is possible to note that the trends differ only in the ultimate stress value. Indeed for the FEM simulation, it is 929.55 MPa, while for the real test, the result is 932 MPa. The solver approximations cause this short discrepancy. While strains are imposed, and so they are the same.

3.1.3.Material definition: Plastic zone

During the material research, it is evident that some powders have different behavior in horizontal (in plane) and vertical (out of plane) directions, and others where properties are similar in both ones.

This working thesis selects a powder type with different properties (anisotropic) to define a more general methodology. This method can also be adapted to material with similar mechanical properties (isotropic) in other directions.

The previously mentioned datasheet provided by SLM Solutions reported the most relevant parameters to describe a stress-strain curve for the horizontal and vertical directions [B]. There are:

- Tensile strength
- Offset yield strength
- Elongation at break
- Young's Moduli

The sample is produced with FE-Alloys 316L (1.4404), where the layer's thickness is 30 μm and the laser power is 400 W. In the following table are reported the reference values obtained by the experimental test, and so they are engineering one:

Table 6 Mechanical characteristics of metal powder

Parameter	Horizontal	Vertical
Tensile strength [MPa]	692	618
Offset yield strength [MPa]	591	541
Elongation at break [%]	39	45
Young's modulus [GPa]	239	178
Mass density [g/cm^3]	7.9	

Starting from the parameters reported in the table is possible to define the elastic and plastic zone of the stress-strain curve. In particular, considering the plastic zone, it is dominated by a

Non-Linear law. So a law must be chosen to interpolate the values and create a material trend to put in the FEM software and simulate the proper behavior.

The selected law to reach this goal is Johnson Cook. It consists of the definition of stress by the translation of an exponential curve:

$$\sigma = a + b \cdot \epsilon^n$$

Capgemini Engineering provided a tool to calculate the stress-strain plastic segment starting from mechanical characteristics. In particular, using Young's modulus, Poisson's coefficient, yielding stress, ultimate stress, and elongation at the break, the tool estimates the equation above reported to better approximate the real material behavior. The best solution is obtained by minimizing the error sum between real stress and the calculated one considering yielding stress, ultimate stress, and plastic strain.

This tool considers an intermediate value in the linear section as the first stress of plastic behavior and not the true yielding stress material. This solution permits a better approximation of the Non-Linear trend.

The true curves are reported below:
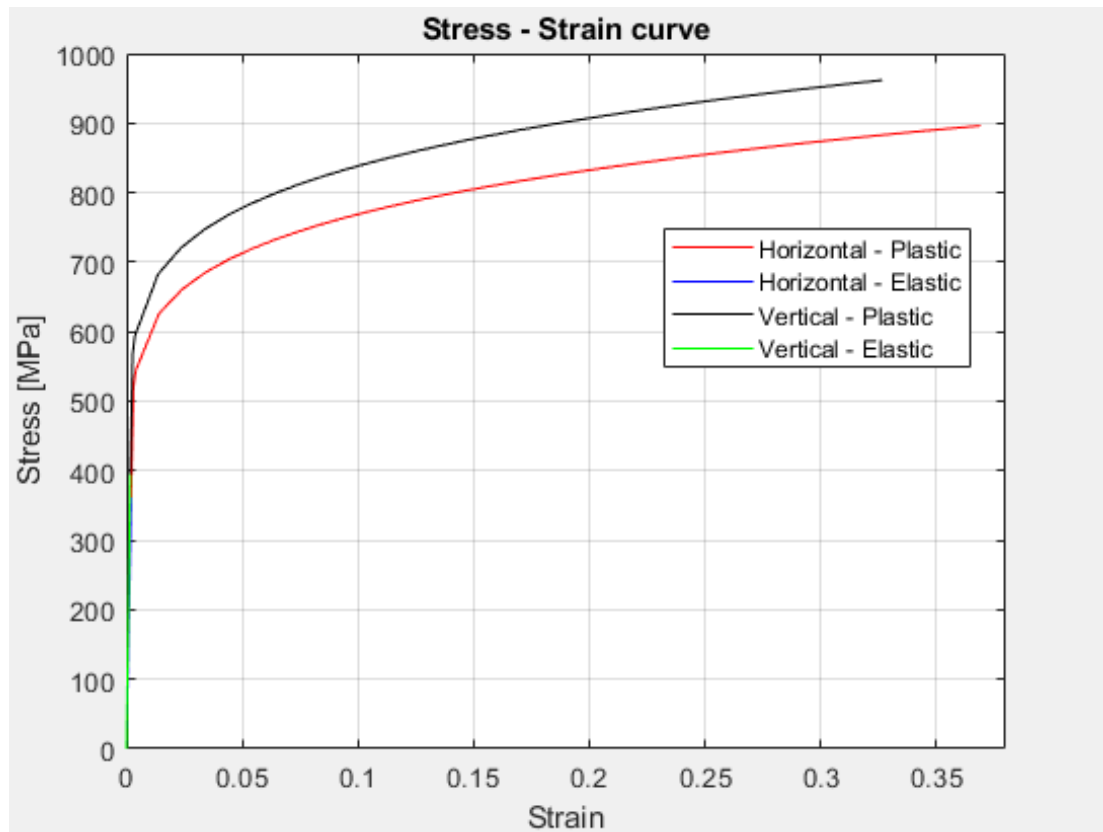
Figure 21 Plastic strain curve for Vertical and Horizontal directions

3.2. Single lattice unit cell

In the previous paragraph, it is demonstrated that FEM software can describe with excellent results a part's behavior produced by Additive Manufacturing starting from an experimental test.

Following this idea and using the results produced in material research made in the first step of the thesis, it is possible to obtain the stress-strain curve of the metal to realize the component and the lattice structure.

Referring to the datasheet provided by SLM Solutions, the mechanical properties and physical characteristics of Fe-Alloy 316L powder (1.4404) (SS316L) are defined.

In this paper, it is possible to underline that the thickness layer highly influences the final mechanical performance of the part; indeed, the sample shows significant differences in the horizontal and vertical direction if it is small. While if the thickness is more significant, horizontal and vertical values aren't much different, so the material can be considered isotropic.

This condition is analyzed deeper in the following paragraph to treat the most generic condition possible and to define a universal methodological approach.

3.2.1. Unit cell design

A rhombic dodecahedron unit cell is selected to form the lattice structure. The cell creation consists of multiple rotations and reflections of a tetrahedral structure that is the base cell's element. According to ISO 13314:2011, the dimension of a unit cell must be at least 10x10x10 mm, and the cell is created by coordinate method knowing ISO and geometrical characteristics of the tetrahedron. Successively it has meshed, and a global rhombic dodecahedron unit cell is built, rotating the single one.

The base element of the rhombic dodecahedron unit cell is a tetrahedral structure. It is reported below:
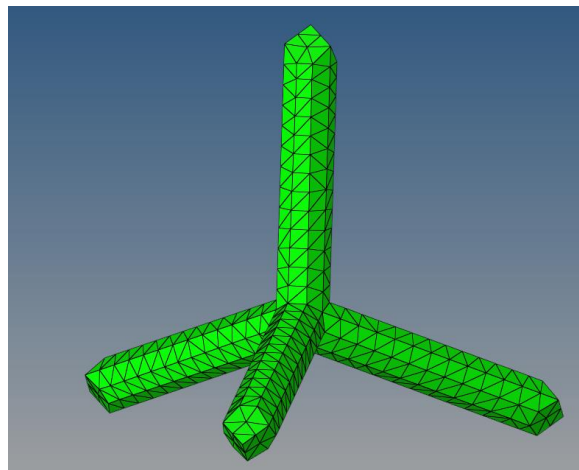
Figure 22 Tetrahedron element

35

Referring to the rhombic dodecahedron unit cell, its geometrical characteristics are:

- Strut length → 4.33 mm
- Strut diameter → 0.4 mm
- Slenderness ratio →0.1847
- Aspect ratio → 0.433
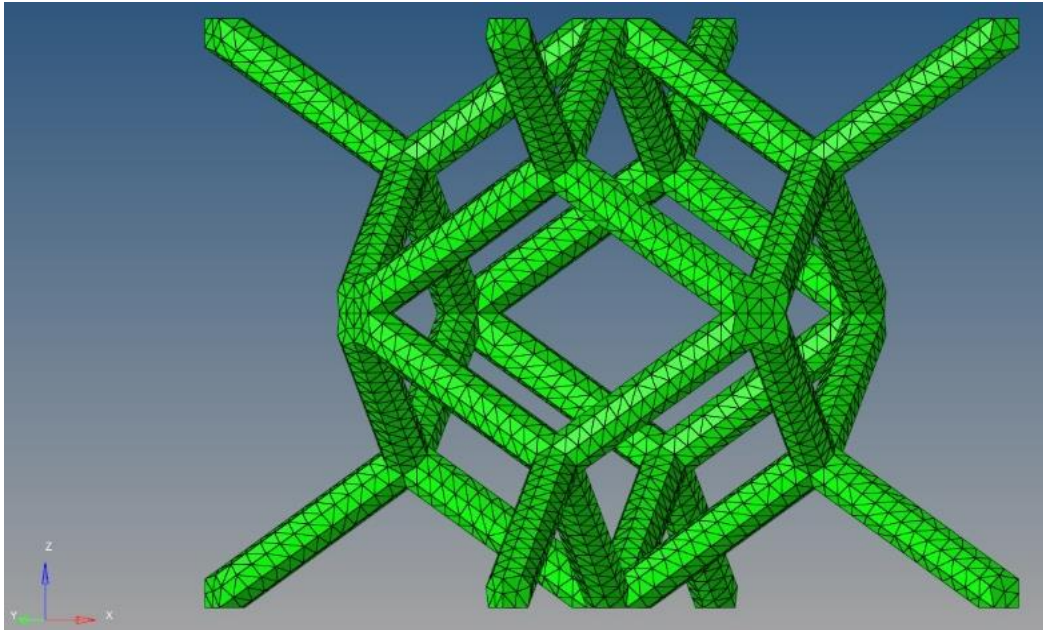
Figure 23 Rhombic dodecahedron unit cell created in Hypermesh

The mesh comprises 17425 elements, first order CTETRA (4 nodes), and 5059 nodes. In the figure below, there is an enlargement of the CTETRA element:
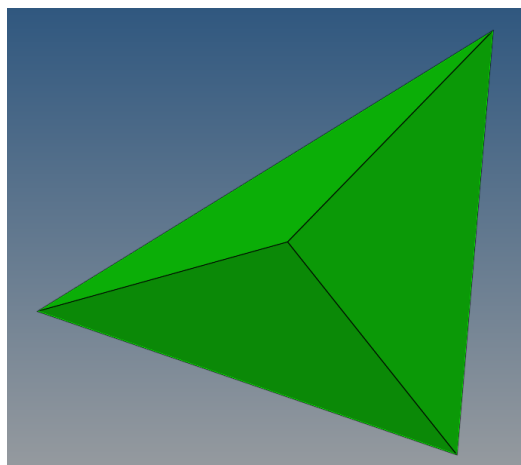
Figure 24 CTETRA detail

This cell is built considering the information acquired in the first phases of the work. In particular, the strut diameter in an L-PBF must be more significant than 200 µm, and in this sample, it is 800 µm. The orientation angle is identified as the lower limit for this manufacturing technique at 30°, and the sample presents 45° one. Regarding the strut length, 5 mm is indicated as the upper limit to avoid deformation during the process, so 4.33 mm is selected.

3.2.2. Unit cell behavior

The following paragraphs evaluate the importance of anisotropy and Non-Linearity in the analysis.

In Hypermesh, many functions help study these two different aspects. It is essential to underline that a Non-Linear anisotropy analysis isn't permitted using this software, so these concepts are analyzed separately.

In this type of software, it is common to create the component, primarily defining geometry and, successively, material and property. Material definition recovers one of the most critical aspects of the analysis because it characterizes the global behavior and the component answers to stress.

In Hypermesh, the material is defined by using a card image. To treat anisotropy, it is necessary correctly to choose the material card. There are two different anisotropy cards: MAT9ORT e MAT9. The first one requests Young's modulus (X, Y, Z), Poisson's coefficient (XY, YZ, XZ), and Shear's modulus (XY, YZ, XZ). Still, in the software, the only parameters to enter are Young's modulus and Poisson's coefficients because Hypermesh calculates the third one. This approach permits a faster analysis, but the complicated geometry of the problems made it necessary to change strategy. The other possibility faces the problem with a matrix approach, which needs all 36 matrix coefficients.

In the following paragraphs, the difference between cards is mainly underlined by using them in the definition of equivalent moduli.

It is notable that this software requests some load collectors to run different kinds of analysis. In particular, a Non-Linear one asks two load collectors: NLPARM permits the execution of Non-Linear analysis, and NLOUT provides the results at the end of the study. NLOUT demands a set time to specify the load/displacement percentage where the results are captured. In this case, the set time is defined as 101 steps to describe a 1% increment starting from zero condition.

The unit cell in the following paragraph is studied by imposing elastic constraints on the base node and introducing a rigid element (RBE2) to the top surface nodes to simulate the plate of a compression test machine.

RBE2 is a rigid element realized by the definition of a master node and many slave ones. In particular, it introduces a constraint on the displacement ($U_{slave} = U_{master}$) of all element nodes. This equation is imposed on all constrained degrees of freedom (in this case, all six are defined). This equation simulates an infinitely stiff body behavior, so it doesn't permit a differential displacement between nodes. Regarding its features, it is commonly used to consider: model parts with a stiffness bigger than modeled components (stress cannot be calculated on them), to distribute a constraint on a surface, or to model bolted joints where the stress definition on the bolt isn't necessary.

In the following picture is reported an RBE2 application on a single unit cell from different views:
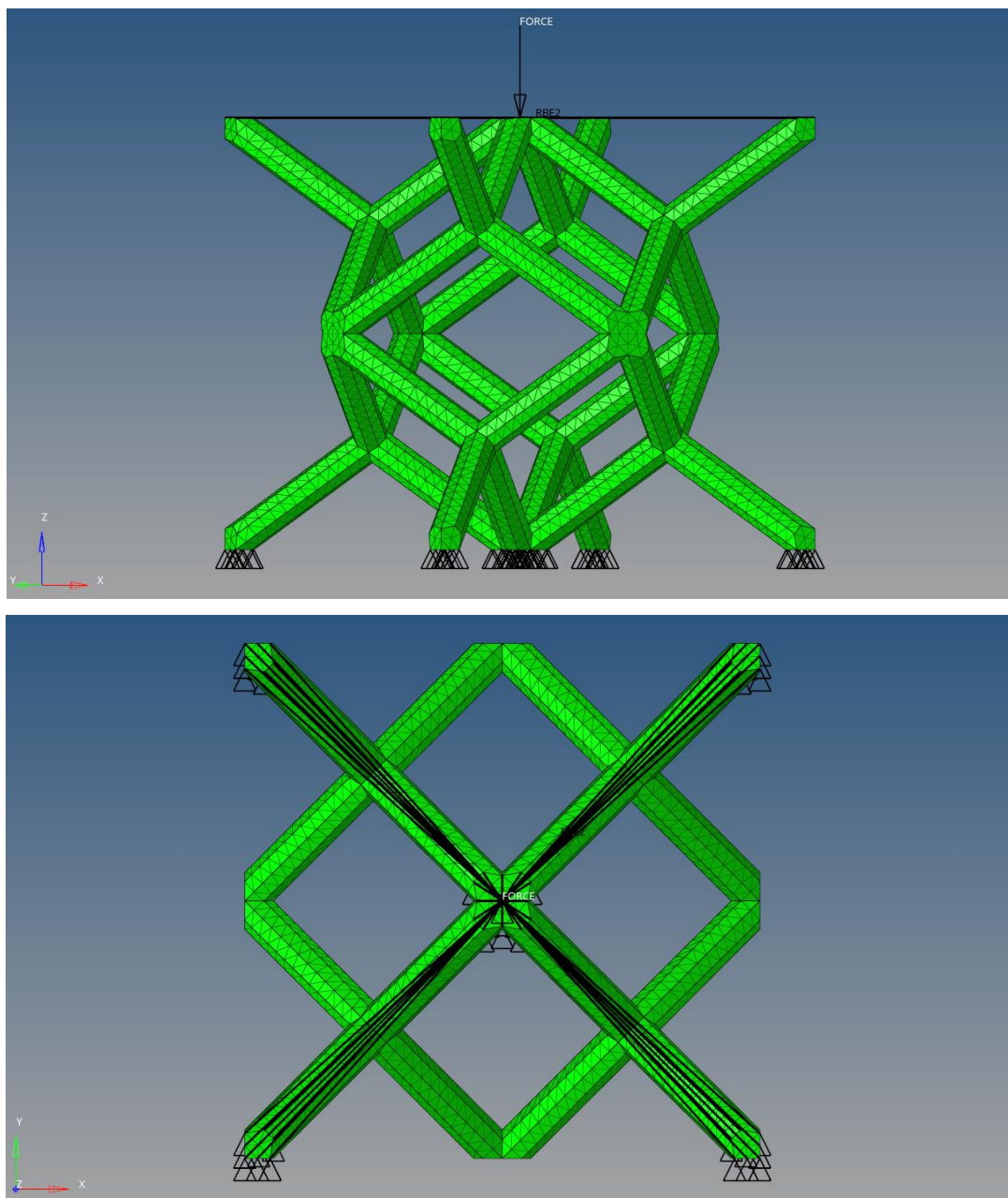
Figure 25 RBE2 application from different points of view: lateral (T) and superior (B)

3.2.2.1.   Isotropy or anisotropy: the importance of anisotropy

This paragraph analyzes the impact of anisotropy on the test results and how it is relevant to be considered in the analysis or if it is negligible because there aren't considerable variations in horizontal and vertical directions.

Two different analyses are conducted to persecute this purpose considering a rhombic dodecahedron unit cell compressed in a negative Z direction with a force of 150 N:

1. Comparison between isotropy Linear unit cell considering vertical and horizontal properties alone

2. Comparison between anisotropy and isotropy Linear unit cell

All analyses are requested and considered the same output:

- Displacement

- Element stresses

- SPCF forces

Regarding the first analysis, the following results are obtained:

a) Displacement:

Both cells present the same distribution scheme. The cell with a smaller Young's modulus shows a more significant displacement due to the paramount compliance of the structure. In particular, the ratio between two maximum displacements is 74.48%. This value is the same as the moduli ratio in the two directions. This result makes it possible to evaluate the deformation of different isotropy materials.

The displacement isn't caused only by the translation in the Z direction, but if enlargement is done, the importance of morphology deformation in the displacement scheme is underlined. Indeed, struts assume an "S" shape in joint proximities due to the plastic hinge's joint transformation.

In the following images are reported the comparison between displacements and the joint details:
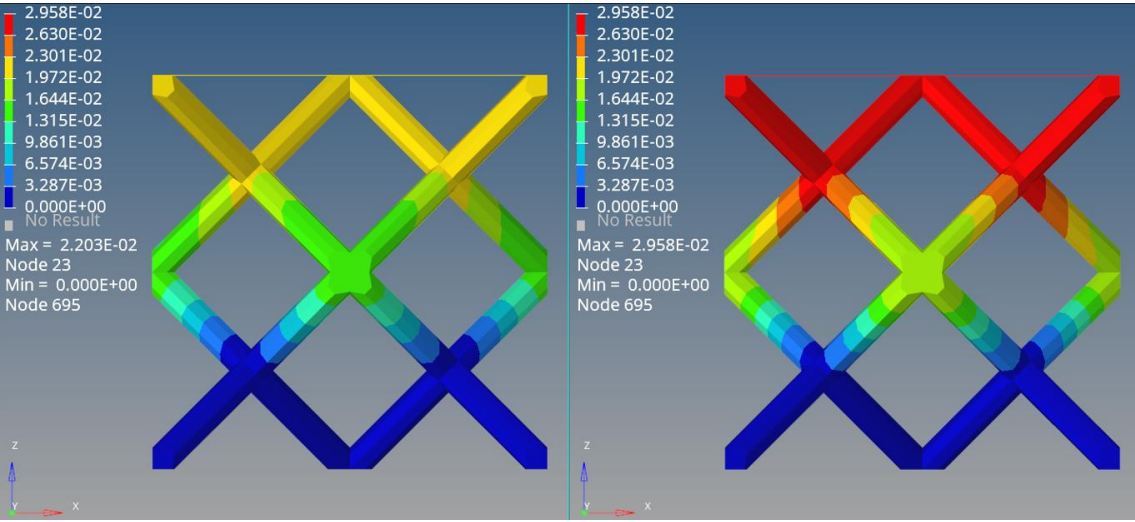
Figure 26 Displacement: Emax (L) and Emin (R)
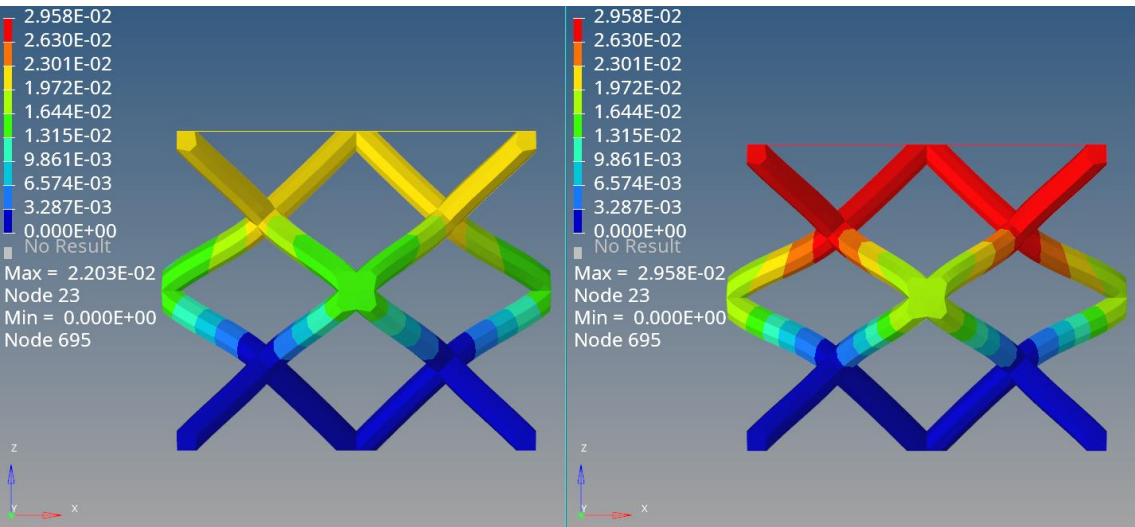
Figure 27 Amplification displacement (x50): Strut deformation detail

b) Stress element:

The distribution and entity are the same because it depends only on the geometry and forces applied. These remain identical in both cells.

The image below shows the stress element distribution:
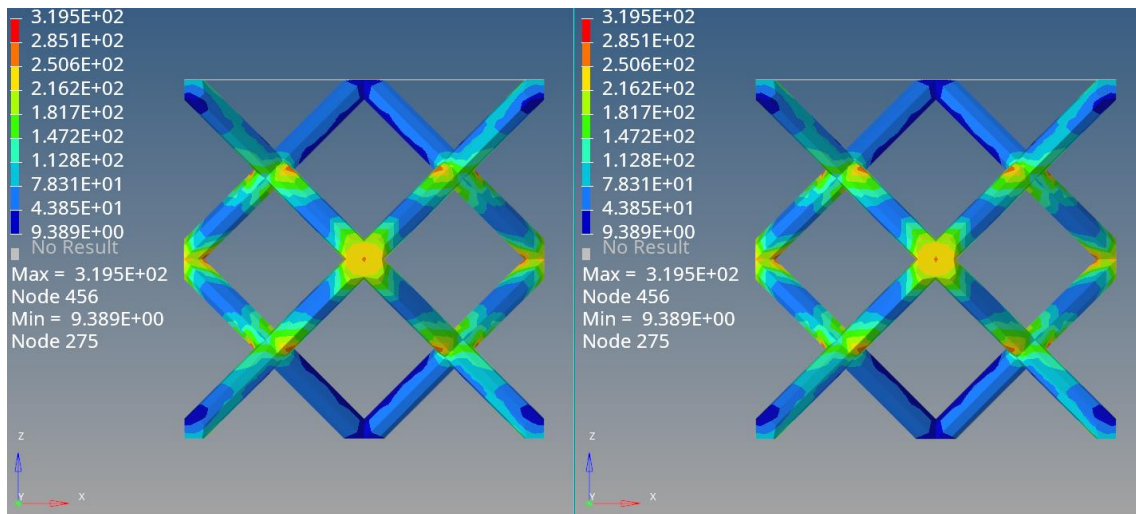
Figure 28 Stress element distribution (Emax (L) and Emin (R))

c) SPCF:

They are identical in all two cells because the applied load in the Z direction is identical.

The distribution is reported:
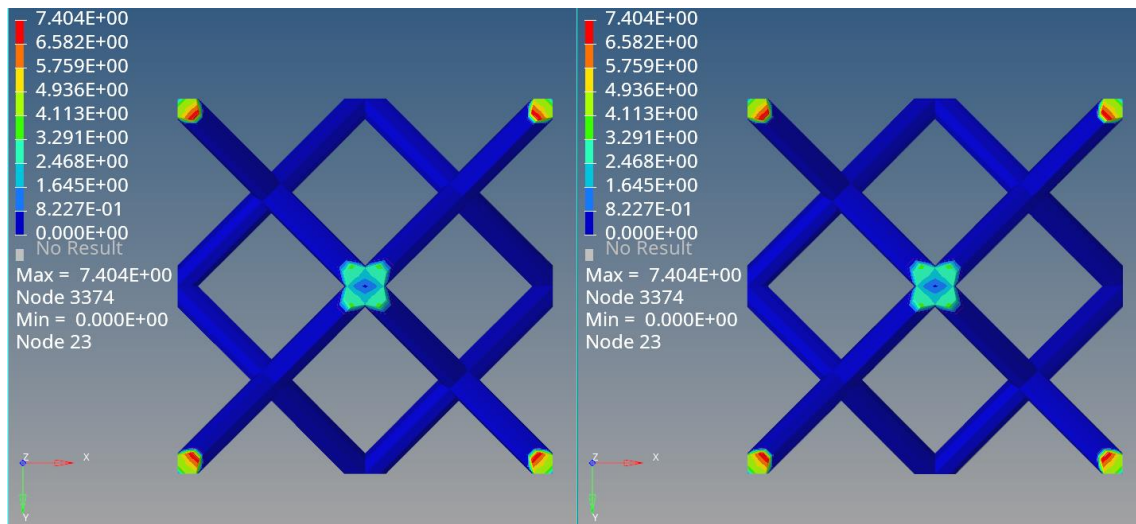
Figure 29 SPCF distribution (Emax (L) and Emin (R))

Regarding the second analysis, the following results are obtained:

a) Displacement:

Anisotropy material presents an intermediate behavior between maximum Young's and minimum Young's modulus. Starting from this information, the anisotropy rhombic

dodecahedron cell behavior, realized in L-PBF with the previously described powder, presents a Young's Modulus in a range between the horizontal and vertical modulus. In particular, it is very close to the maximum one (horizontal).

Indeed, the difference between displacement values is 18.69% respect the minimum Young's modulus and 8.39% respect the maximum one.

The combination of moduli produces improvement concerning the vertical modulus and deterioration of the horizontal one.

In the following there are the results:
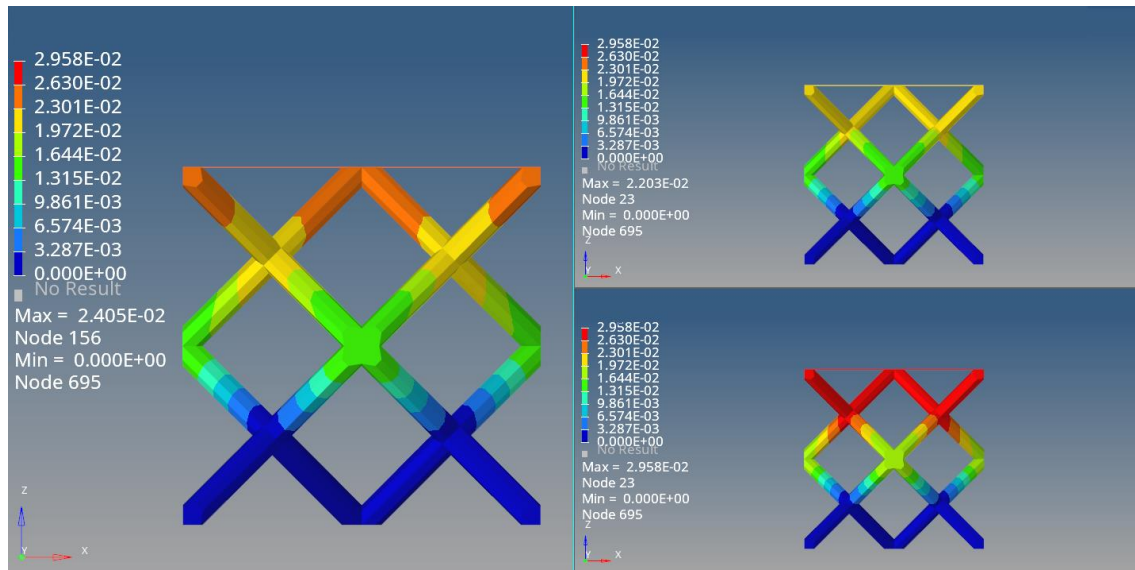
Figure 30 Displacement distribution: Anisotropy (L), Isotropy Emax (T), and Isotropy Emin (B)

b)   Stress element:

All three cells show the same distribution scheme because the applied force is the same and directed in the vertical direction. There is a reduction in maximum and minimum values of the anisotropy cell compared to isotropy ones, which is beneficial. The maximum values are different, around 9.67%.

Each material presents a peak of stress in the joint strut close area. Indeed, struts can be visualized as trapped cantilevers loaded with a bending moment, so the maximum stress is limited to the joint.

In the images below are shown these two analyzed aspects:
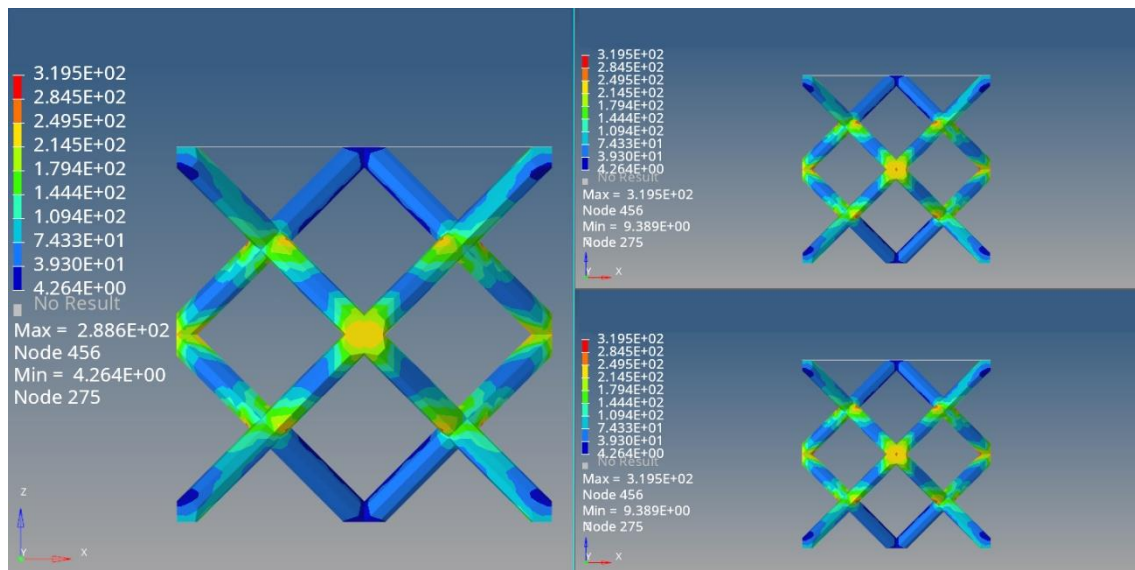
Figure 31 Element stress distribution: Anisotropy (L), Isotropy Emax (T), and Isotropy Emin (B)
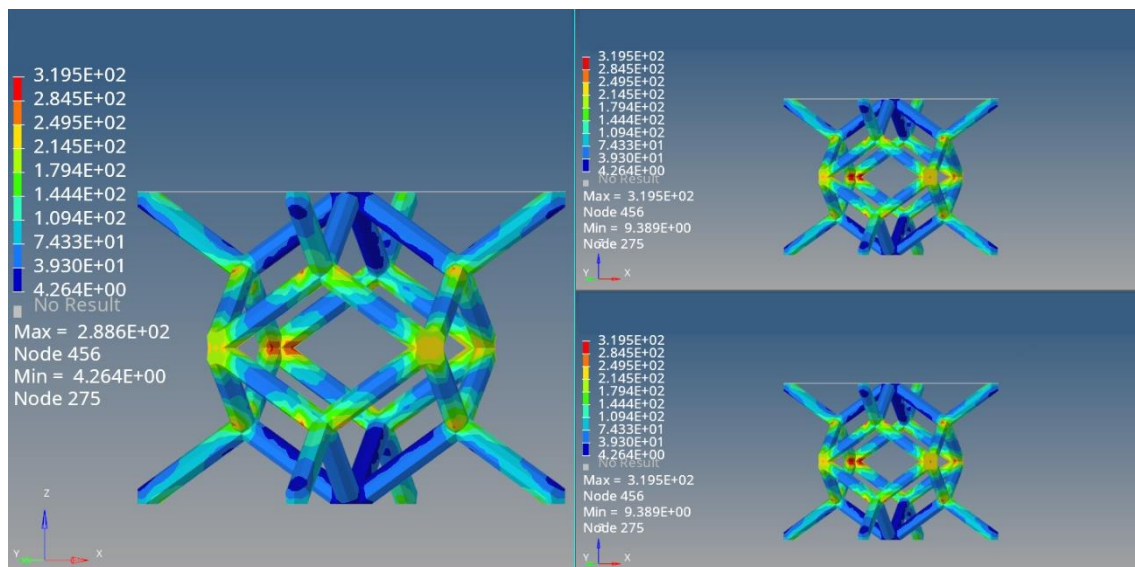
Figure 32 Element stress joint detail

This load entity doesn't produce plastic deformation. Indeed, the maximum element stress isn't more significant than yielding vertical stress (543.73 MPa) and yielding horizontal one (593.64 MPa).

    c) SPCF:

The applied force is the same in both three cells, and so the distribution scheme is the same and symmetrical. There is a short difference between the maximum and minimum magnitude

values. The anisotropy cell shows a smaller leading force of around 2.33% compared to the isotropy one. This difference can be attributed to the geometrical complexity and anisotropy characteristics. During compression, the anisotropy cell deforms itself differently from the others, so SPCF changes.

The image below shows this distribution:
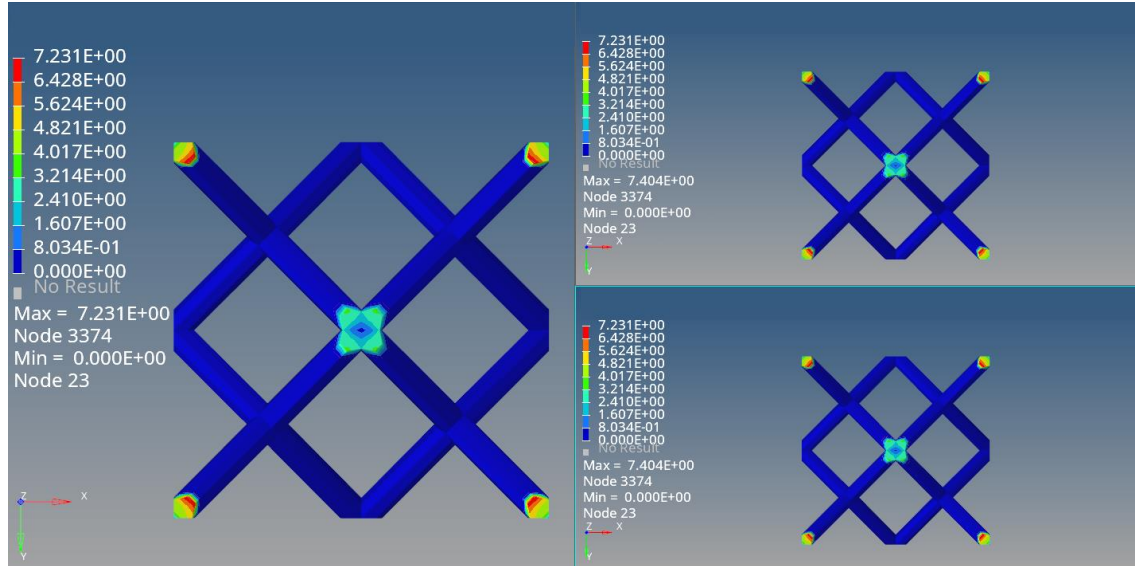
Figure 33 SPCF distribution: Anisotropy (L), Isotropy Emax (T), and Isotropy Emin (B)

This first analysis is concluded. It has emerged that the anisotropy behavior is essential because it changes the material properties, and so it must be considered to define the characteristics of an equivalent solid better.

3.2.2.2. Linearity or Non-Linearity: the importance of Non-Linearity

In this paragraph, a comparison of Linear and Non-Linear materials is made. Two studies are conducted by loading unit cells with forces of 150 N and 1000 N. These forces are chosen to show the different behavior of cells. The first load doesn't produce an element's stresses bigger than the yielding stress material, while the second one exceeds the yielding one. So some elements sample reach plasticization showing a Non-Linear behavior permitting to compare different deformations.

In the following significant details are reported in both load cases:

a) Type of load: Compression Z direction

Load entity: 150 N

- Minor Young's modulus (Vertical):

o Displacement:

The distribution scheme is symmetric and the same in both types of analysis, thanks to the elastic constraints. No one exceeds the yielding stress material regarding maximum element stresses, so the deformation is elastic. The difference between maximum displacement should be zero, but solver approximation produces a slight difference of around 0.37% due to different conditions analysis.

In the image are reported the displacement trends:
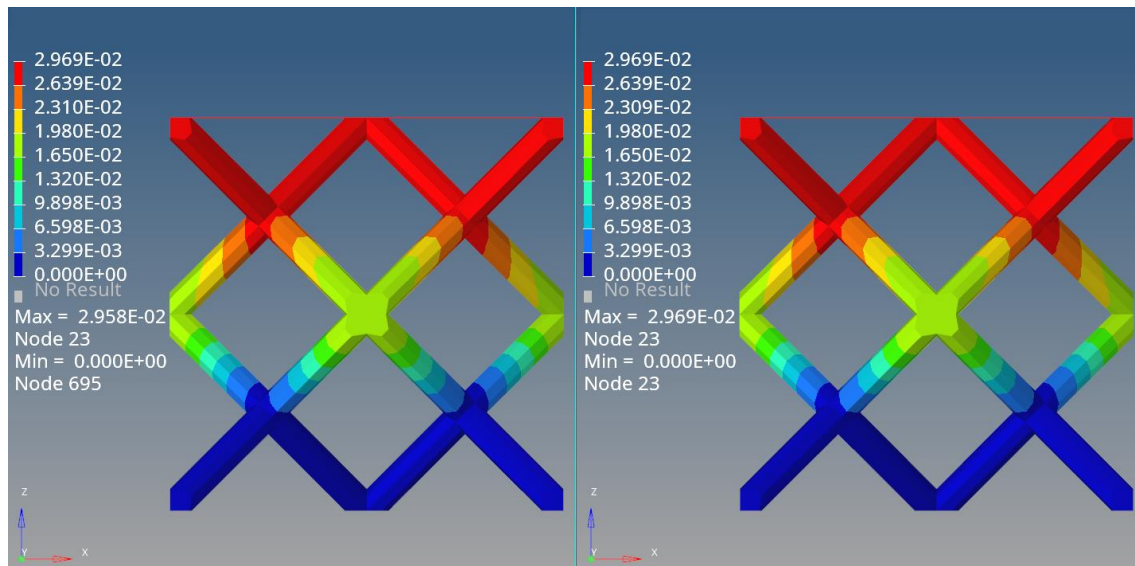
Figure 34 Displacement distribution: Linear behavior (L) and Non-Linear behavior (R)

o Element stress:

Element stress distribution, like displacement, is symmetrical and the same in both unit cells. Under material yielding stress, the values should be the same, but it is possible to evaluate the difference between maximum values of around 5.1%. This discrepancy is due to solver approximations in the analysis.

If the plastic strain is shown in the cell, there aren't any areas with values bigger than 10^{-3}. This result confirms that Non-Linear material works in the stress-strain curve's linear section. Indeed, 0.2% of plastic strain is considered as starting point for plasticization effects.

This aspect is reported below:

45
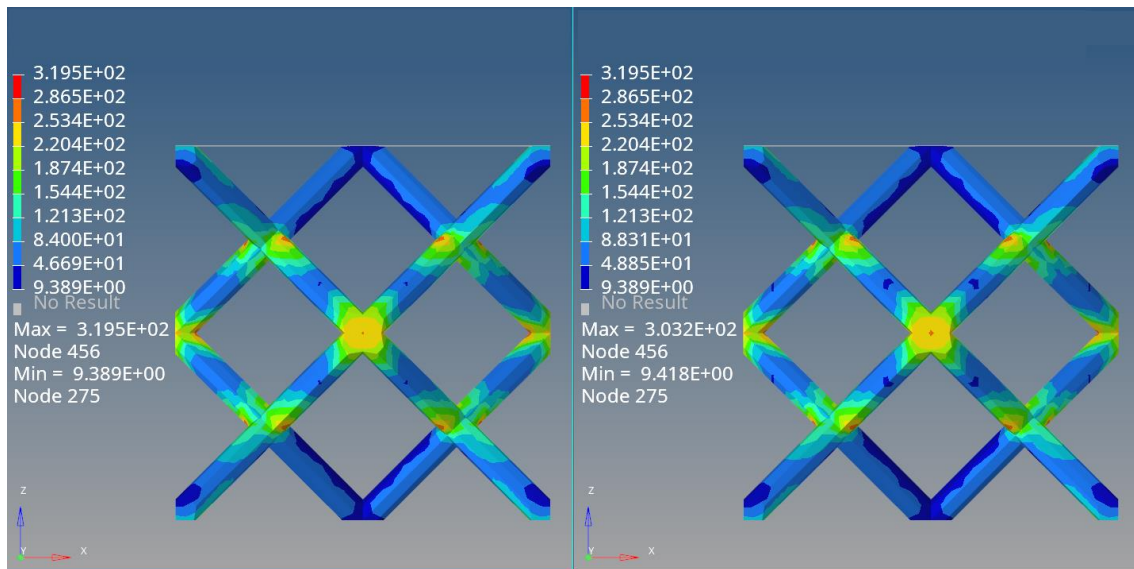
Figure 35 Element stress distribution: Linear behavior (L) and Non-Linear behavior (R)
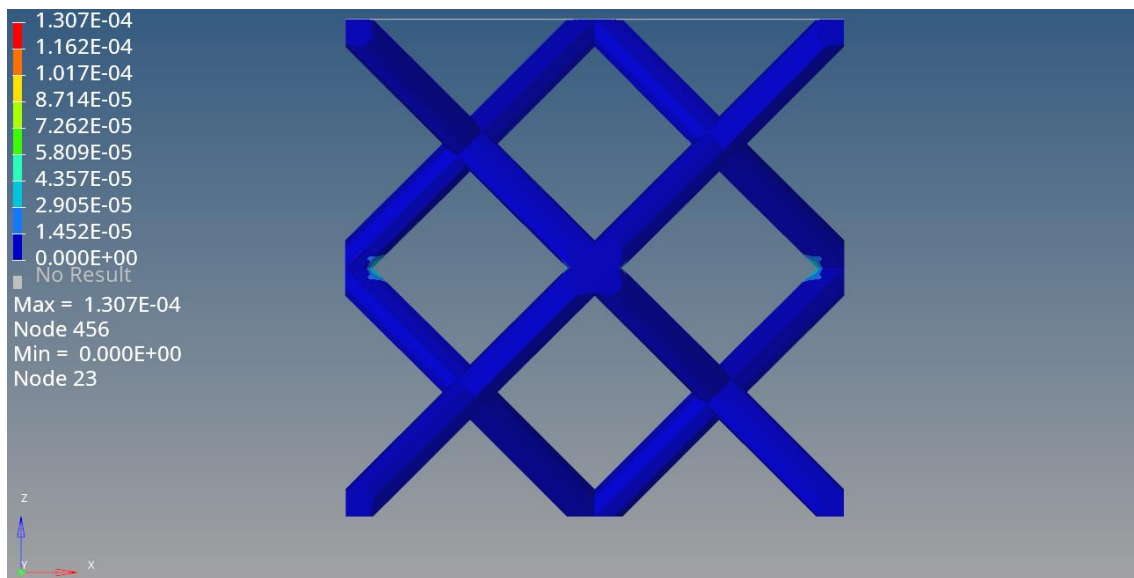
Figure 36 Plastic strain detail

o SPCF:

The distribution is symmetric and identical in both unit cells. SPCF entities are dependent only on the geometry and applied load, so they should be the same. Indeed, the difference assumes a negligible value of around 0.027%, caused by solver approximation as previous parameters. This distribution is shown in the picture:
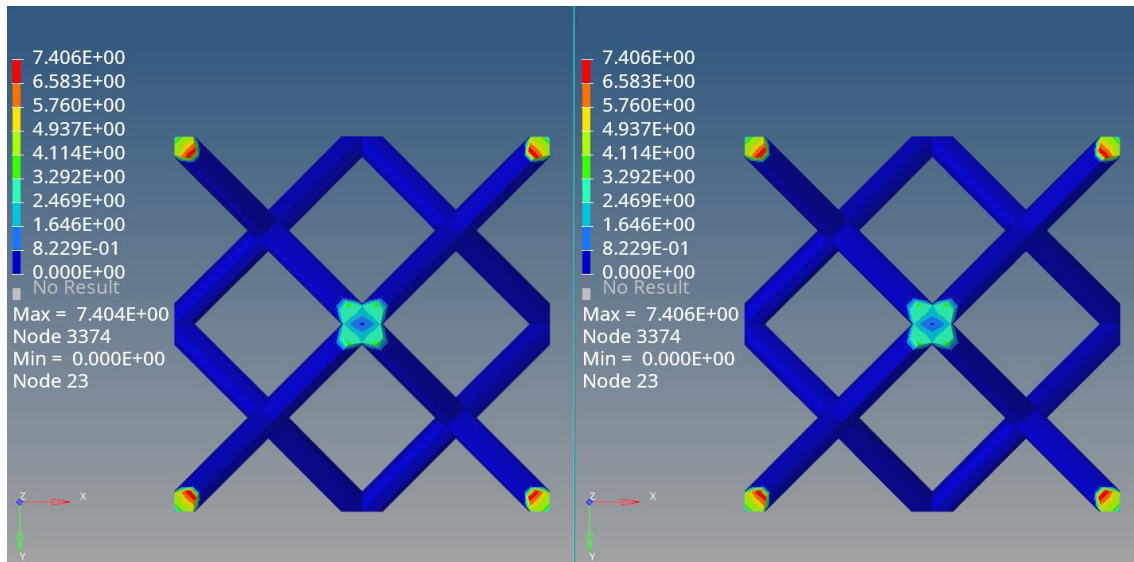
Figure 37 SPCF distribution: Linear behavior (L) and Non-Linear behavior (R)

- Major Young's modulus (Horizontal):
  o Displacement:

The scheme distribution is identical and symmetrical in both types of analysis. The difference between maximum values is negligible and around 0.22%. The discrepancy can be related to solver approximation caused by different material definitions. No one element stress exceeds the yielding stress. Indeed, Non-Linear material is working in the elastic section of the stress-strain curve, so values should be the same.

The picture below reports this aspect:
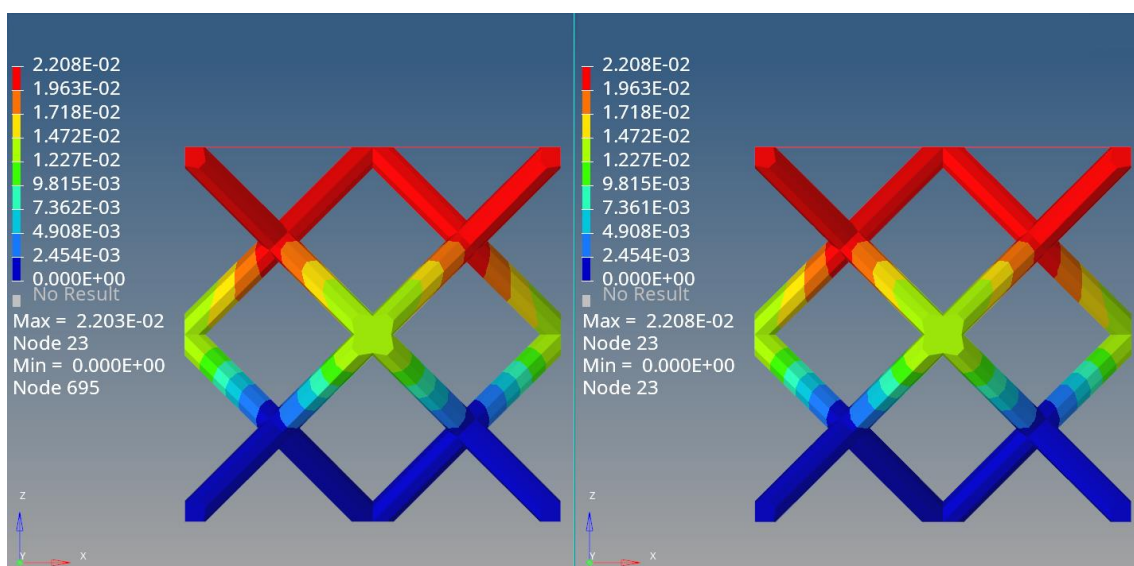
Figure 38 Displacement distribution: Linear behavior (L) ad Non-Linear behavior (R)

o   Element stress:

In this case, the distribution scheme is the same and symmetrical for both cells. Their maximum values differ only by 4.35%, but this difference is due to solver approximations in the analysis. Like minimum Young's modulus, the Non-Linear material works in a linear zone of the stress-strain curve. Indeed, no elements present stress bigger than material yielding stress.

Regarding plastic strain, they assume values smaller than 10^{-5}, which confirms the elastic behavior of Non-Linear material.

The images reported show these trends:
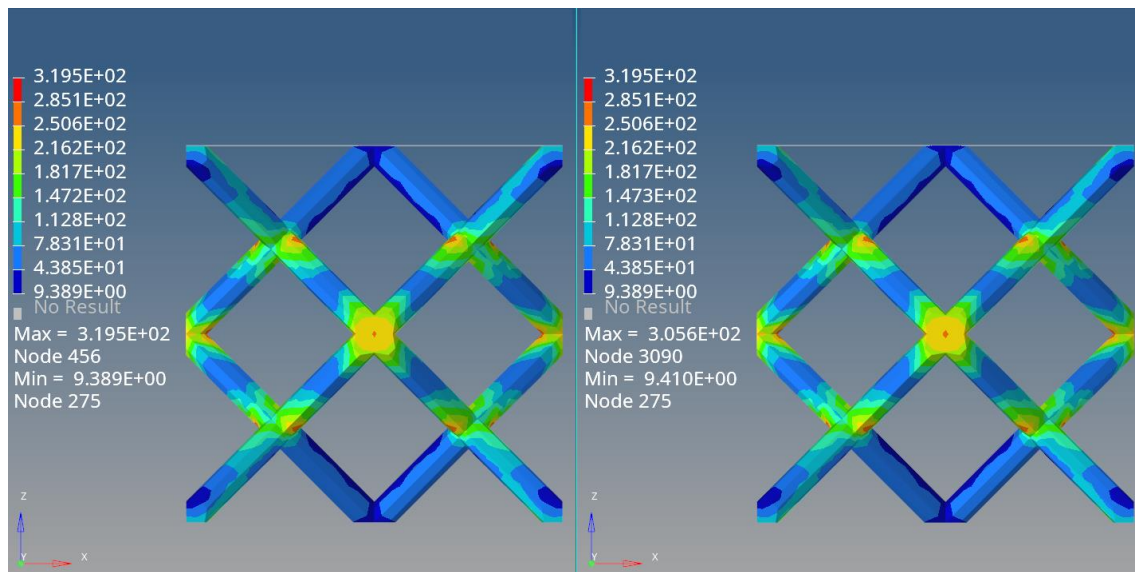
Figure 39 Element stress distribution: Linear behavior (L) and Non-Linear behavior (R)
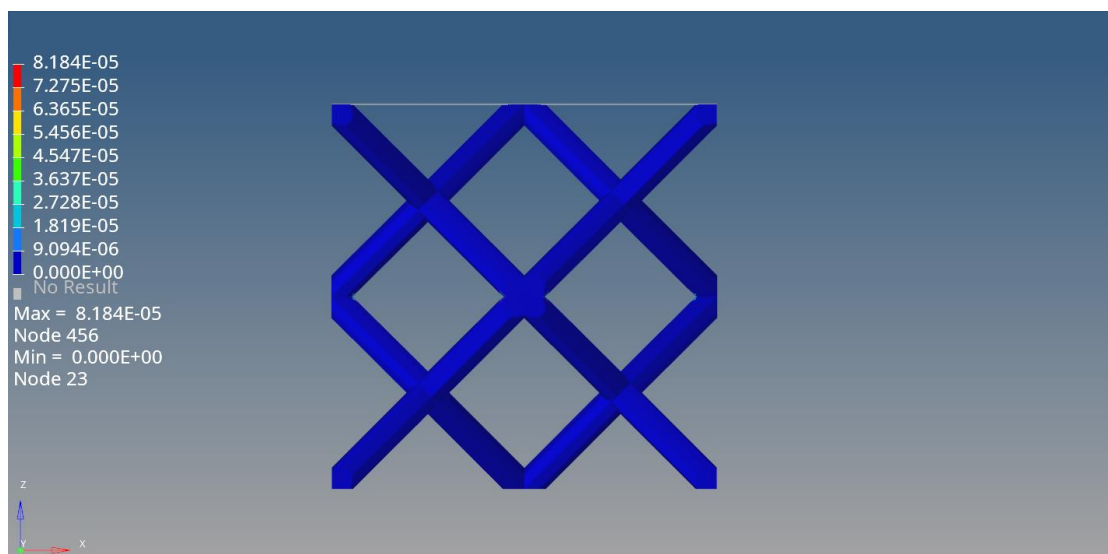
Figure 40 Plastic strain detail

    ○ SPCF:

As in the previous cases, the distribution scheme is the same and symmetrical. This parameter is influenced only by geometry and applied load, so they should be identical. The difference is limited to 0.013%, and this error is reconducted to solver approximations.

In the following image is reported this trend:
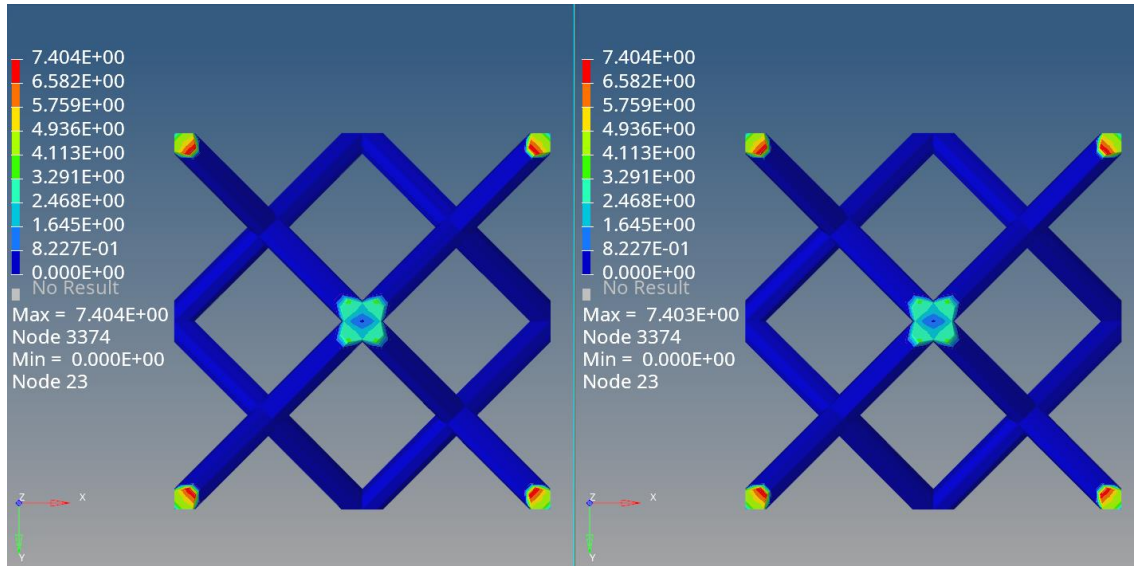
Figure 41 SPCF distribution: Linear behavior (L) and Non-Linear behavior (R)

  b) Type of load: Compression Z direction

    Load entity: 1000 N

 - Minor Young's modulus (Vertical):

    ○ Displacement:

This load entity is more prominent than the yielding one, so the Non-Linear behavior is shown. Being in the Non-Linear section of the stress-strain curve (plateaux), the difference between maximum displacement values is relevant, and around 82.13%. So the displacement is mainly superior compared to the Linear case.

The picture below shows this behavior:
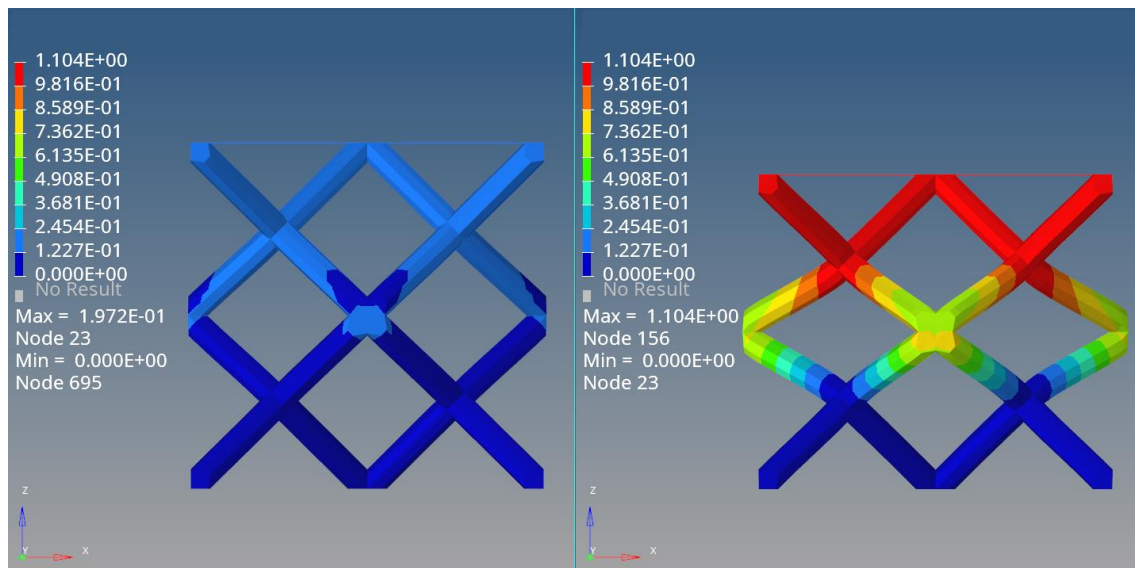
Figure 42 Displacement distribution: Linear behavior (L) and Non-Linear behavior (R)

    o   SPCF:

In this case, the distribution scheme and maximum values are different. The first one presents differences located in the footprint of external struts. The Non-Linear maximum value is smaller than the Linear one, around 3.01%. This discrepancy is related to different deformation modes; indeed, SPCF depends only on geometry and applied load. Geometry changes and the applied load remains the same.

This trend is reported in the picture:
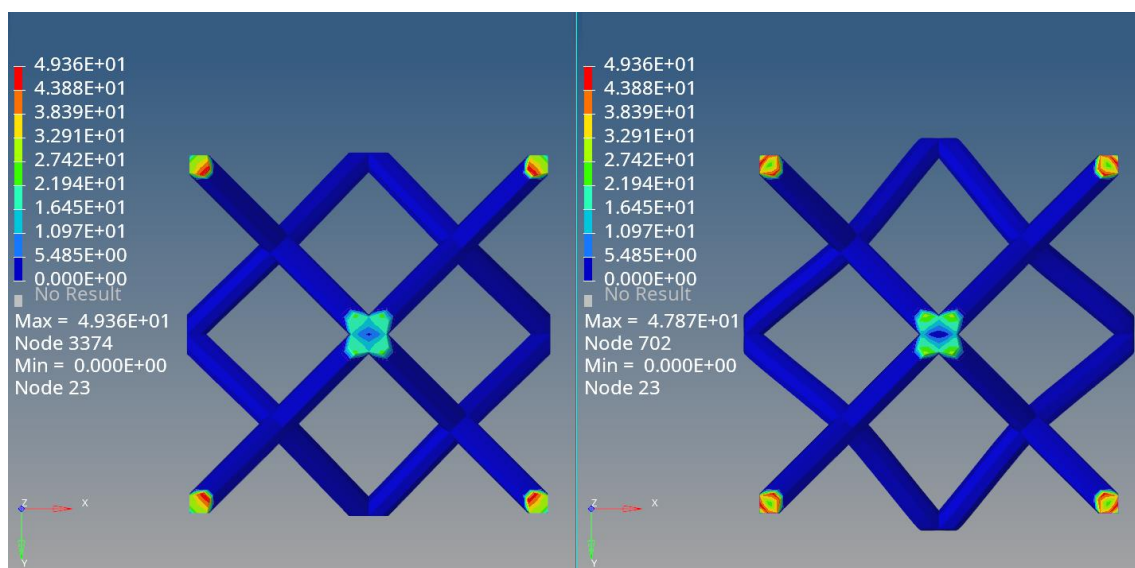
Figure 43 SPCF distribution: Linear behavior (L) and Non-Linear behavior (R)

o   Element stress:

Unit cells show different behaviors:

- Non-Linear presents minor stress due to the plastic zone where the deformation grows fast, and the stress slowly increases because energy is absorbed by deformation in the plateaux zone. Referring to the maximum value reached, it is included in a range between yielding stress (543.73 MPa) and the ultimate one (896.1 MPa)

- Linear shows critical stress because deformation is directly proportional to stress. So, in this case, ultimate stress (896.1 MPa) is vastly exceeded (2130 MPa), and cell breaks

The picture presents the distribution:
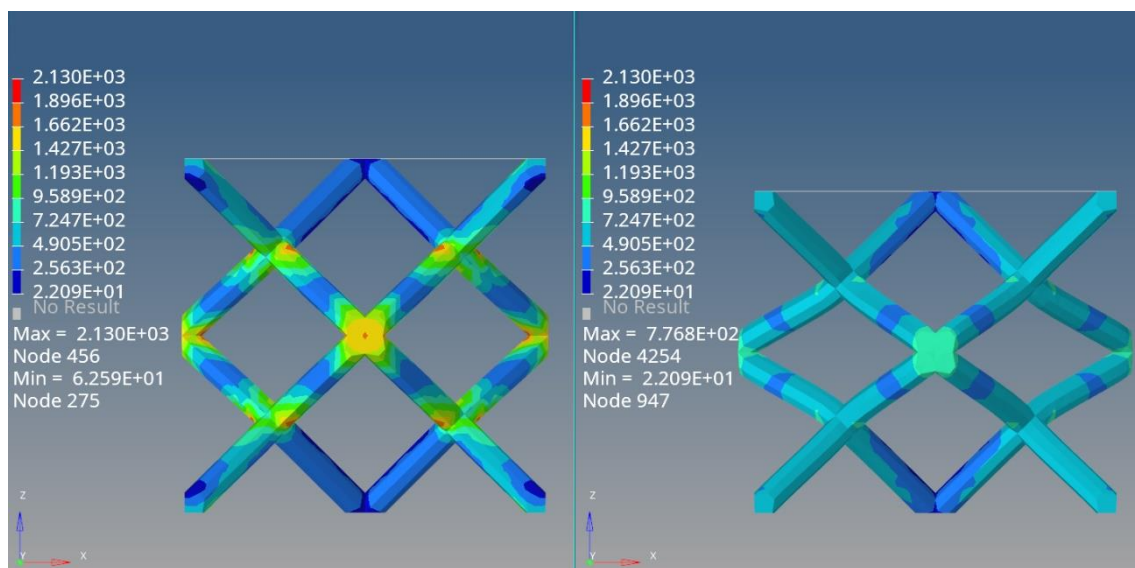
Figure 44 Stress distribution: Linear behavior (L) and Non-Linear behavior (R)

To better understand this situation is reported the stress trend related to the applied load. The node located in the external joint zone between four struts is considered to draw this trend. Linear and Non-Linear curves present an overlapping of the elastic section. Still, around 20% of the applied load, the Non-Linear curve divides itself from the Linear and enters the plastic zone (plateaux).

Previously describing Capgemini's tool used to approximate the plastic trend into the stress-strain curve, it said that an intermediate value in the linear section is considered the first stress of plastic behavior and not the true yielding stress material. This solution is adopted to better approximate the Non-Linear trend, so the curve's elbow doesn't correspond to material yielding stress (543.73 MPa).

In the following picture, it is reported:
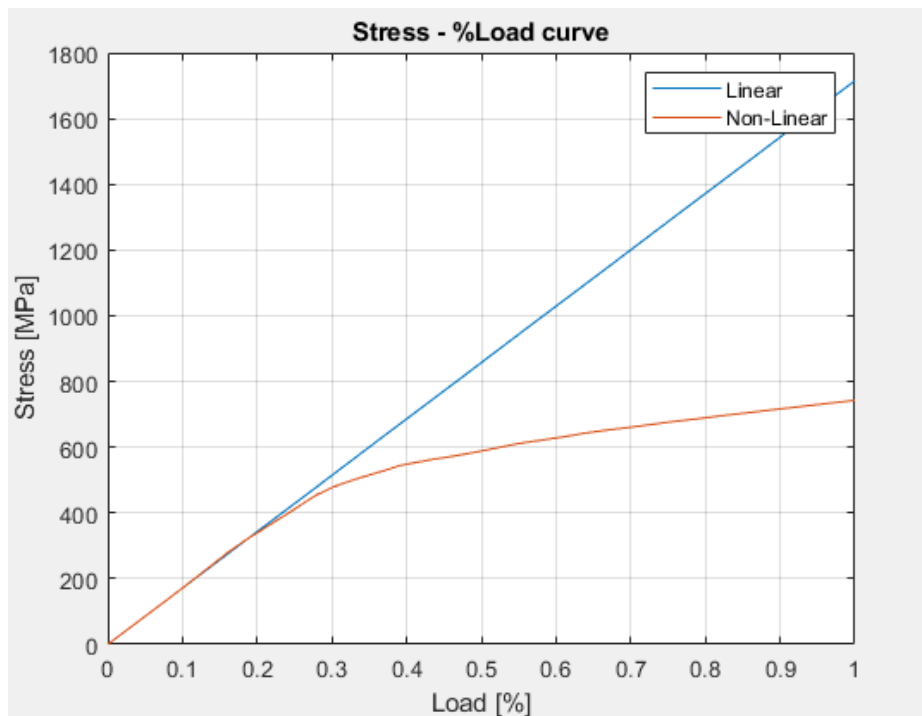
Figure 45 Comparison or trend of Non-Linear and Linear behavior

Graphically showing plastic strain, it is possible to observe that until 31% of applied force, there aren't plasticization zones if 0.02% is considered as starting point. At the end of loading, the joint zones and extremal struts areas are completely plasticized.

The following images report these plastic strains' distribution:
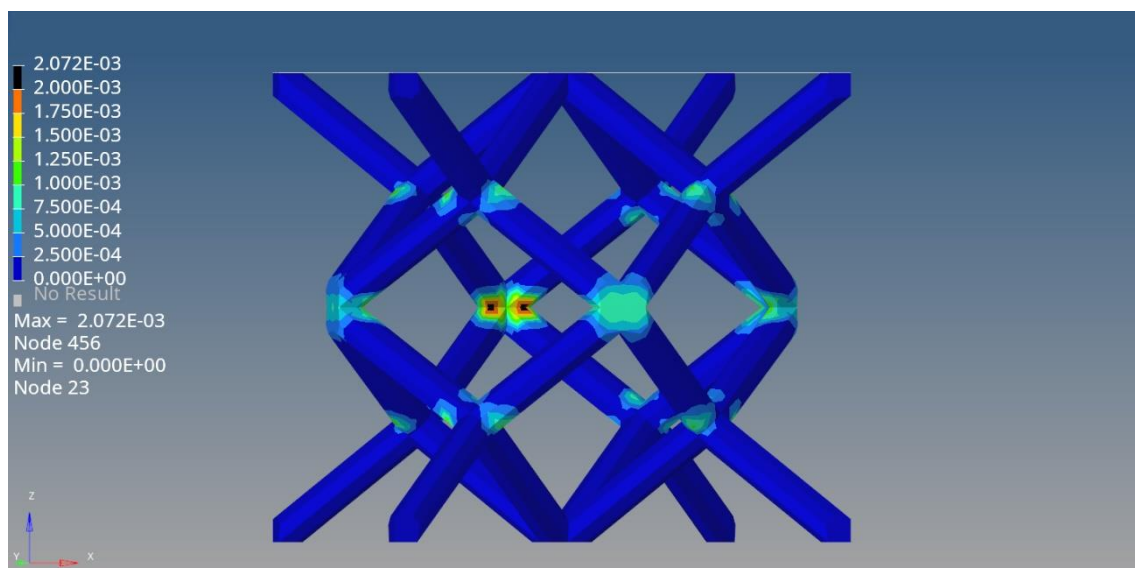
Figure 46 Plastic strain detail at 31% of load application

52
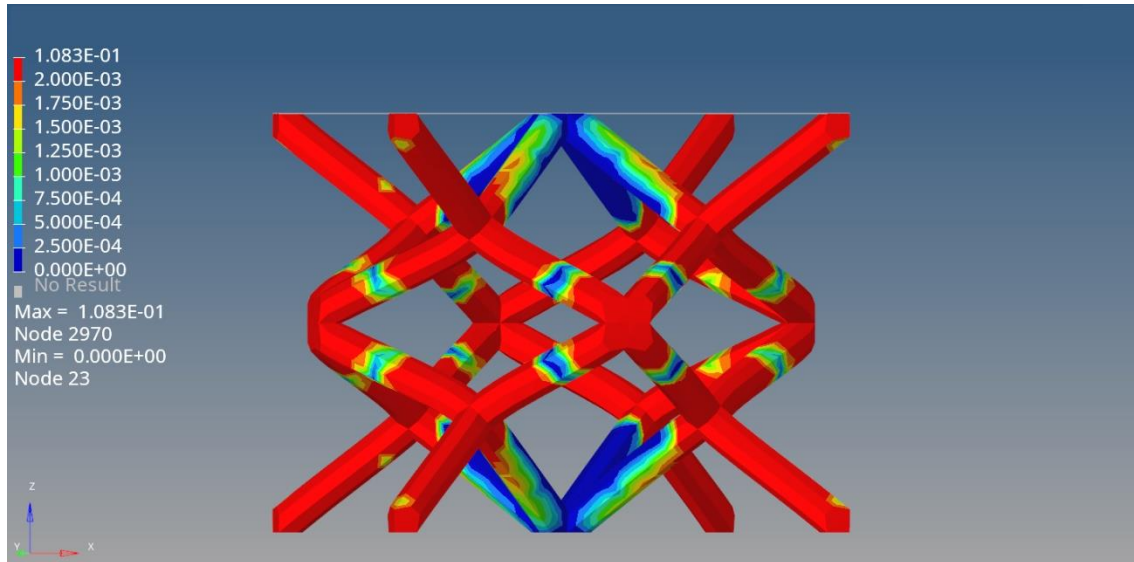
Figure 47 Plastic strain detail at the end of load application

- Major Young's modulus (Horizontal):
  - o Displacement:

The applied load is more significant than material yielding stress, so Non-Linear behavior emerges. Being in a Non-Linear stress-strain curve section, the displacement is more remarkable than in a Linear one. The discrepancy entity is elevated around 79.75%, vastly superior to Linear displacement. This result is due to the morphology of structure cell itself.

The picture reported shows this trend:
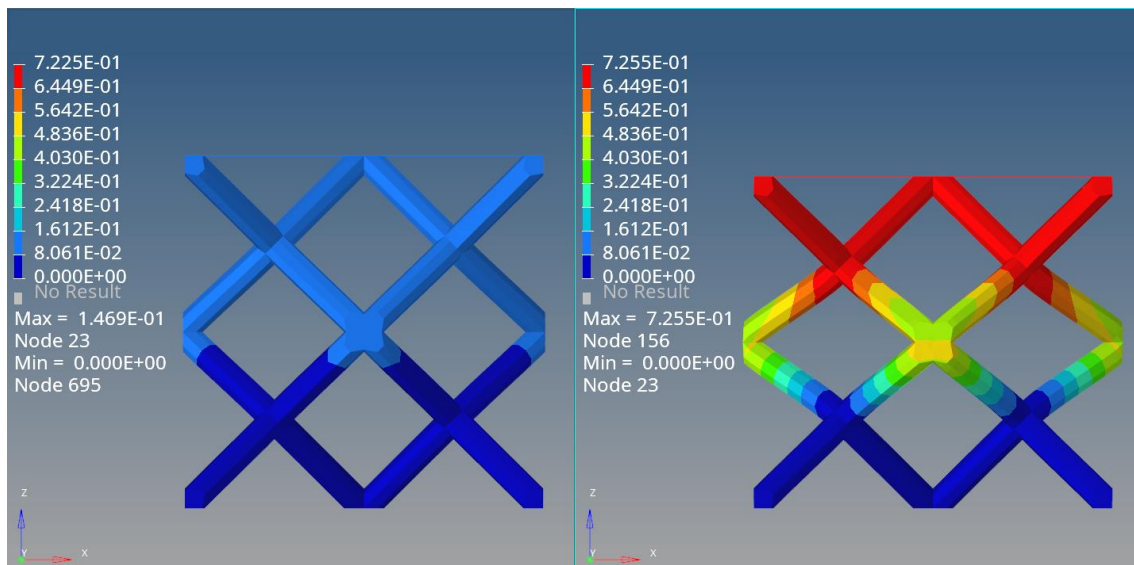
Figure 48 Displacement distribution: Linear behavior (L) and Non-Linear behavior (R)

o SPCF:

The cells show different distribution schemes and maximum values reached. The first one presents differences located in footprint external struts areas. Regarding maximum values, the Non-Linear material is smaller than Linear, around 2.91%. This discrepancy is attributed to different deformation due to Non-Linear behavior. Indeed, SPCF depends only on geometry and applied load.

The image shows this trend:
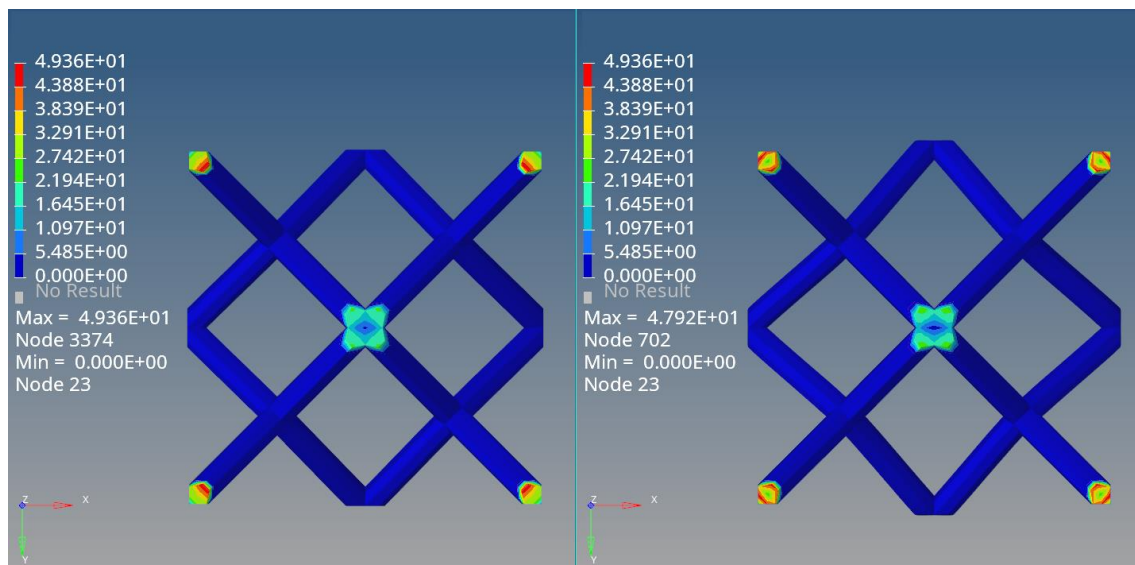
Figure 49 SPCF distribution: Linear behavior (L) and Non-Linear behavior (R)

o Element stress:

Cells have different behavior:

- Non-Linear presents values more minor than the other due to plastic deformation, which increases while stress slowly grows because energy is absorbed by deformation in the plateaux section. The broken is reached. Indeed, the maximum stress values are comprised in a range from yielding stress (593.64 MPa) and ultimate stress (961.78 MPa), so some elements overcome the yielding limit

- Linear one shows great stress values due to deformation, directly proportional to the stress. In this case, the cell collapses because some elements largely overcome ultimate stress (961.78 MPa), reaching a peak around 2130 MPa

The picture below shows these results:
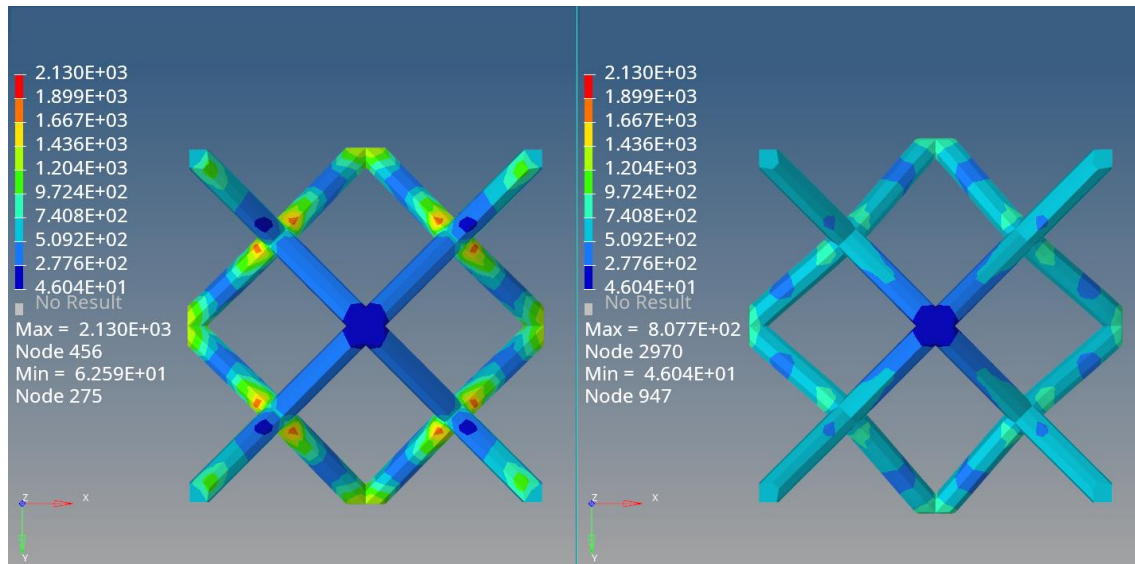
Figure 50 Element stress distribution: Linear behavior (L) and Non-Linear behavior (R)

To better understand this situation is reported the stress trend related to the applied load. The node located in the external joint zone between four struts is considered to draw this trend. Linear and Non-Linear curves present an overlapping of the elastic section. Still, around 20% of the applied load Non-Linear curve divides itself from the Linear and enters the plastic zone (plateaux).

Previously describing Capgemini's tool used to approximate the plastic trend into the stress-strain curve, it said that an intermediate value in the linear section is considered the first stress of plastic behavior and not the true yielding stress material. This solution is adopted to better approximate the Non-Linear trend, so the curve's elbow doesn't correspond to material yielding stress (593.64 MPa).

Trends are reported in the following:
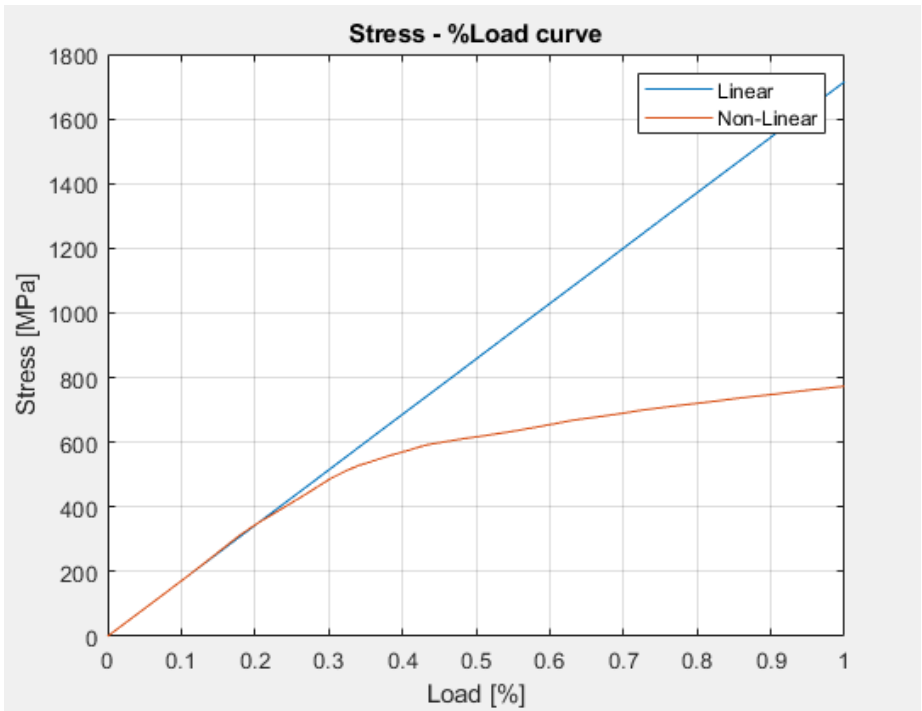
Figure 51 Comparison trend of Non-Linear and Linear behavior

If 0.02% of plastic strain is considered the starting point for yielding, it is possible to underline that until 35% of applied force, there aren't any elements showing plasticization. At the end of loading, the cell into joints and close to extremal strut zones is completely plasticized.

The following images report these plastic strain's distribution:
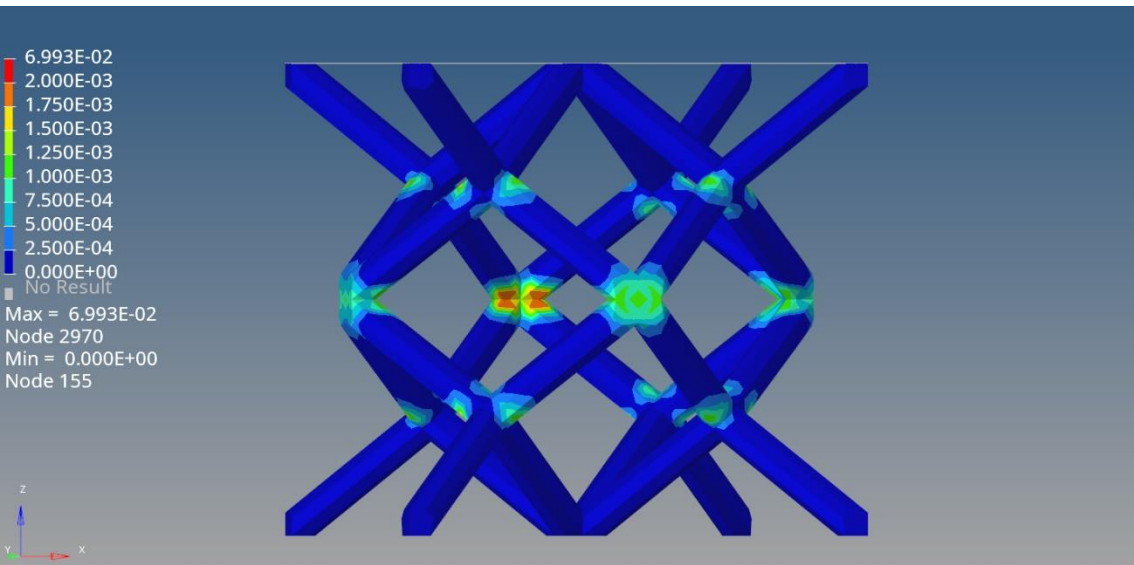
Figure 52 Plastic strain detail at 36% of applied load
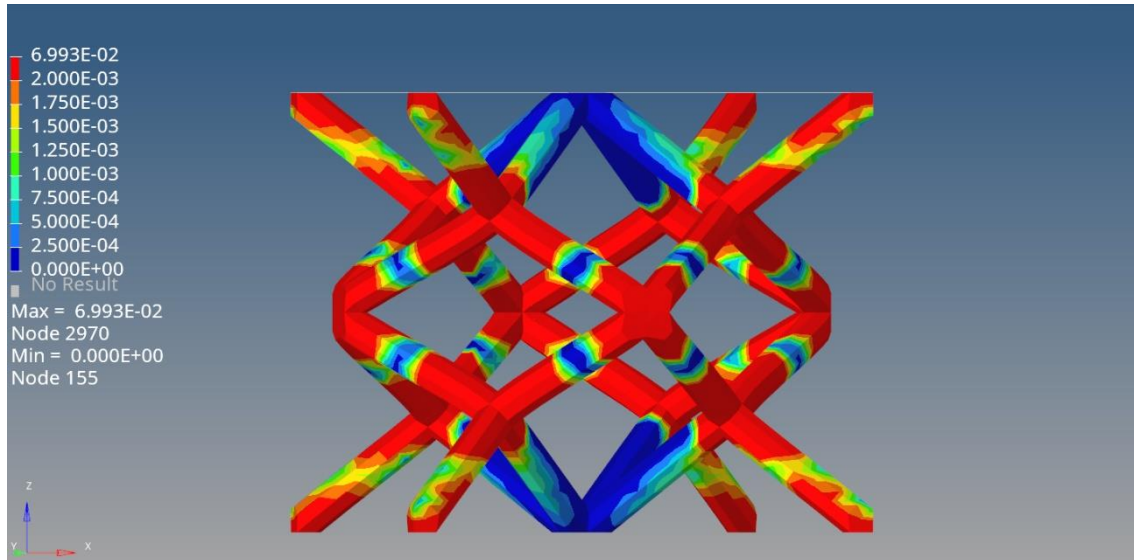
Figure 53 Plastic strain detail at the end of load application

These tests report very relevant results. Indeed if a load of 1000 N is applied to the single unit cell and the previous node considered is visualized, it is possible to notice that a Linear material shows a stress element around 1714.81 MPa, while a Non-Linear one reaches 773.43 MPa. This discrepancy is significant and represents an increment of 121% if Linear material is considered. While referring to the maximum displacement in a Linear single unit cell is 1.469e-1 mm, and in a Non-Linear one, it is 7.255e-1 mm, so the discrepancy is enormous. The increment is 393% if Non-Linear material is considered.

In concluding this second analysis about the Linear behavior, it is evident how considering Non-Linear material or Linear material is entirely different, so a Non-Linear material must be regarded to better determine the solid equivalent characteristics.

3.3. Analysis approach

The previous paragraph specified that Hypermesh is used to simulate tests to identify the equivalent characteristics of lattice structure and verify them on equivalent solid. It is a FE software belonging to the Altair family, and it presents a limit: it cannot run Non-Linear analysis considering anisotropy material.

The importance of these two aspects is fundamental to defining a method to approach the problem of lattice structural analysis. Regarding this, a simplification is done: Non-Linear anisotropy analysis is thought of as a linear problem. First, the anisotropy aspect is considered alone to determine the equivalent solid characteristics. So Linear anisotropy analyses are run, and the applied load must not be high to realize a plastic deformation. The Non-Linear aspect is studied second to obtain equivalent yielding stress, so a Non-Linear isotropy analysis is run.

After treating these phenomena individually, thanks to superposition is possible to have a global vision of the problem.

This methodology is a simplification of the real problem.

3.3.1.Software material definition

Starting from material information provided by the powder's seller, it is evident how a component realized through L-PBF, and SS316L powder has anisotropy characteristics. In particular, Young's moduli in the plane are vastly bigger than out of plane one.

To treat this type of material, Hypermesh offers two possibilities: MAT9ORT and MAT9.

3.3.1.1. MAT9ORT: Fast and cheap approach

At the beginning of the test campaign, MAT9ORT is chosen. It only requests Young's moduli, Poisson's coefficients, and Shear's moduli. Two of them must be provided to determine material characteristics. So Young's moduli and Poisson's coefficients are defined, while Hypermesh automatically evaluates the third one.

This approach is selected because it permits facing the problem simply and cheaply. It is a simplification of the stiffness matrix. This solution is adopted as the first choice because, from a company perspective, it represents the better solution to solve the problem to reduce time analysis and costs.

The second point to consider is related to constraints application. There are two possibilities: isostatic constraints and elastic constraints.

3.3.1.1.1. Isostatic constraints

This constraint application permits free displacement in the plane, avoiding the "barrel" effect and rotations, so only sliding along the reference system's axis is possible.

The implementation of this method includes a particular scheme where the nodes are located in an orthogonal reference system:

- One node has all degrees of freedom locked, and it is in a vertex base (A) (it is sufficient to lock only translation degrees of freedom because rotations are locked as a consequence)
- One node has only two degrees of freedom locked to permit sliding in one plane direction (B)
- One node has only two degrees of freedom locked to permit sliding in the other plane direction (C)

To create practical isostatic constraints, the distance between nodes A – B e A – C must be more noticeable as possible.

In the following image is reported this constraint scheme which is adopted on a cube to display this condition easily:
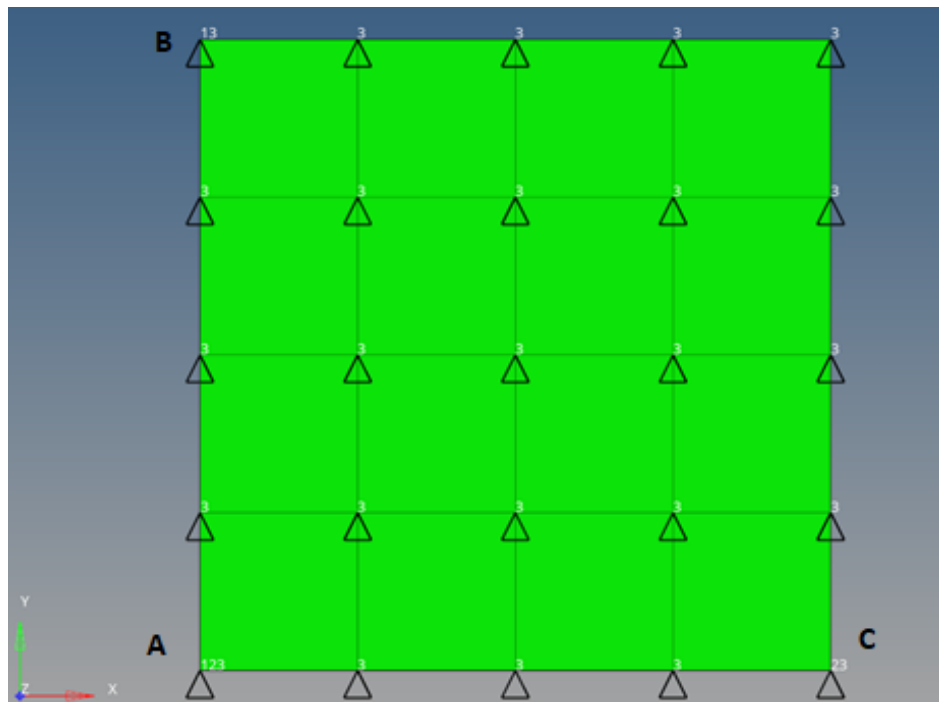
Figure 54 Degree of freedom scheme for isostatic constraints

These constraints are applied to a simple unit rhombic dodecahedron cell, and compression and shear tests are done.

The equivalent moduli are calculated, but the deformation curve is not like the real one. Indeed it is too markable near the application load and constrained areas.

This feature is justified by the presence of external struts, which are less stiff than the others, so displacement in the load direction is excessively amplified.

Regarding this result, it is necessary to reconsider the application of constraints and change type to find more compliance with the deformed natural structure. Following this idea, the elastic ones are selected.

3.3.1.1.2.   Elastic constraints

The second solution implemented is elastic constraints, which are applied because unit cells in a component are placed next to the others, so strut displacement is limited by an equal and opposite displacement of the near cell. According to this idea, all nodes' base degrees of freedom are locked to delete all possibilities of sliding. Using this type of constraint, the "barrel" effect is shown, and this behavior is more similar to the real one.

In the following image is reported this constraint scheme which is adopted on a cube to display this condition easily:
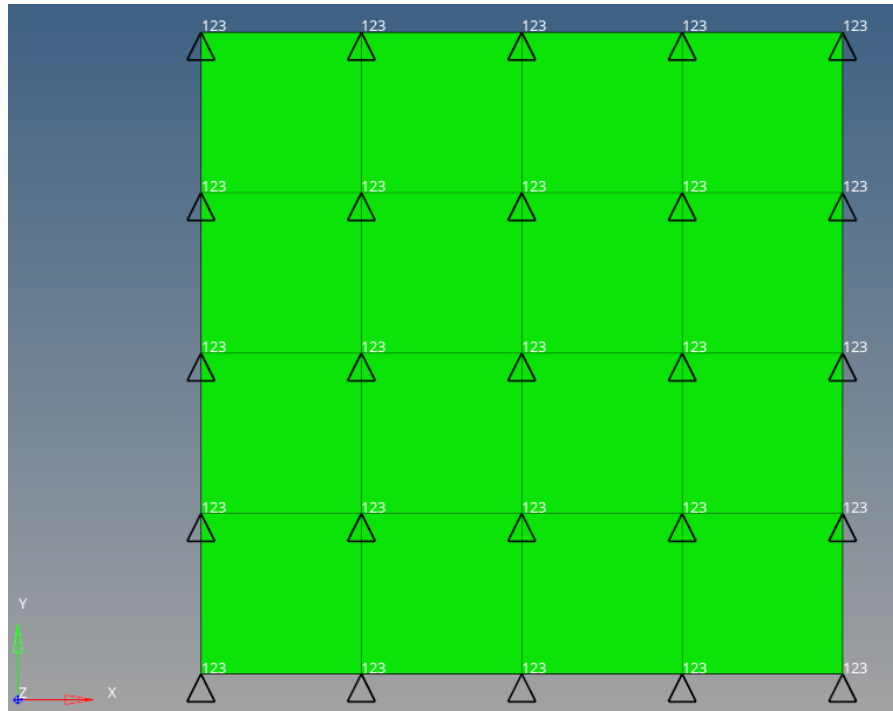
Figure 55 Degrees of freedom scheme of elastic constraints

At this point, a test campaign is started, and compression and shear load are applied to the single unit cell to define equivalent moduli.

It is essential to explain how moduli are evaluated. There are two types of moduli to be calculated: Young's moduli and Shear's moduli.

A compression test determines the first one: the unit cell is loaded by force applied through an RBE2. This rigid element connects a master node with slaves nodes. In the master node is imposed a constraint that permits displacement only in the force application direction, so the force is redistributed to all slaves node considering their different stiffness. According to this, displacement of the master node is considered like the equivalent one.

In the following image, a sketch is shown:
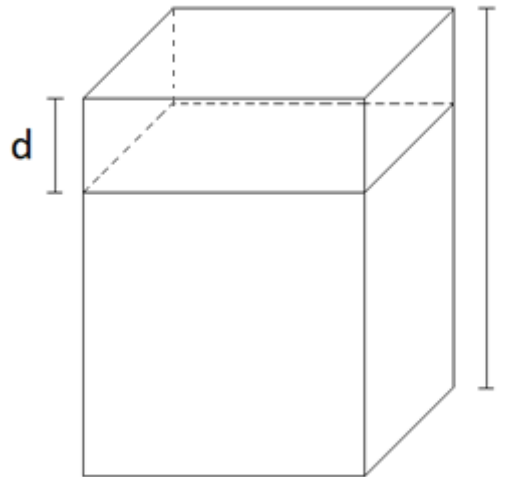
Figure 56 Compression distortion

Young's modulus is calculated using the Hooke's law:

$$\sigma = E\epsilon \rightarrow E = \frac{\sigma}{\epsilon}$$

$$\sigma = \frac{F}{A}$$

$$\epsilon = \frac{d}{l}$$

Where:

- σ is the stress value, and it is defined as the ratio between applied force and application area [MPa]
- E is Young's modulus [MPa]
- ε is the strain value, and it is defined as the ratio between displacement and initial length

The second one is determined with a shear test. It is essential to underline that this simplifies the real because it simulates pure shear stress, but usually, a shear load produces a bending moment too.

To better evaluate the shear's modulus, the displacement along the loading direction is attributed to the external node of the sample.

The sketch below reported shows how shear's modulus is calculated:
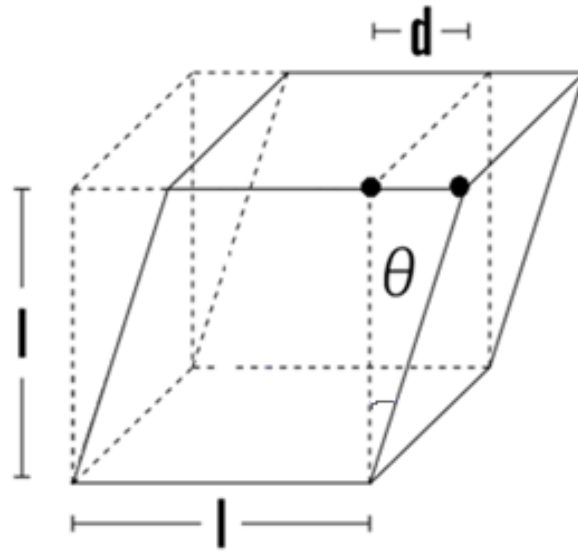
Figure 57 Shear distortion

To estimate this modulus is assumed a linear dependence between stress and angle formed by the deformed structure and the original one:

$$\tau = G\theta \;\rightarrow\; G = \frac{\tau}{\theta}$$

$$\tau = \frac{F}{A}$$

$$\theta = \arctan\left(\frac{d}{l}\right) \cdot \frac{\pi}{180}$$

Where:

- τ is the stress value, and it is defined as the ratio between applied force and application area [MPa]
- G is Shear's modulus [MPa]
- ϑ is the angle formed by the deformed structure and the original one [rad]

Constraints application produces less displacement compared to the previous one. Indeed, struts close to constraints and loads are stiffer than before, so their deformation is limited. This solution seems to produce better and more realistic results for compression moduli.

Shear's modulus creates an unrealistic displacement producing an angle's value very close to 90 degrees. According to this, the conclusion seems that the unit cell hasn't shear resistance to this type of loading.

Similar results are expected because this unit cell is usually used as filler into panels, so they are more resistant to compression loading instead of shear ones.

Regarding the simulation, doubts emerged about the reliability of the results because displacements are unrealistic, so control on the analysis output file is done.

This file is generated automatically at the end of the analysis. It contains much information about the simulation: there are some sections where warnings and possible errors are reported, other parts show a summary of geometry and elements, and the last one displays forces and moments applied, support reactions, and parameters about the reliability of the analysis. These parameters are "compliance" and "epsilon".

The first one is a direct measure of stiffness for a structure with an applied displacement constant, and it is calculated using the following relationship:

$$C = \frac{1}{2}u^T f$$

Where u is displacement and f is the applied force ($f = kx$).

The second one is the ratio of the work done by the residual forces to work done by the applied forces, and it is called the residual strain energy ratio. It is a relevant parameter because it provides feedback about the correctness of the analysis. It should be a small value, around 10^{-10} or 10^{-13}. It states if small deflections theory is respected and so if simulation results are reliable. In the determination analysis of shear's modulus, the epsilon parameter reaches values around 10^{-3} and 10^{-4}, so the results are incorrect and useless for evaluating equivalent moduli.

At the end of this paragraph, it is discovered that the material software definition is wrong and cannot correctly describe the lattice structure's behavior. This problem is generated by the complexity of the rhombic dodecahedron unit cell geometry. This simple approach in the software material definition must be changed to correctly evaluate moduli.

3.3.1.2. MAT9: Matrix approach

The geometrical complexity imposes using a different software material, and MAT9 is selected. Its characterization is more complicated than the previous one because it faces the analysis in a matrix way, so all 36 matrix terms are requested.

Short research is conducted about this material because the powder doesn't present isotropic characteristics, and so the matrix terms definition isn't standard.

At the end of the research, this material is defined as a transversally isotropic one. Indeed, it is a variation of anisotropic material where there is an elastic rotational axis and a symmetrical elastic plane, all directions, which belong to this plane or planes parallel to this one, are equivalent, referring to elastic properties. This material shows identical Young's moduli in two directions ($E = E_x = E_y$), while the third one is different ($E' = E_z$) [72].

Regarding this material, Hooke's law becomes the following:

$$
\begin{bmatrix} \epsilon_x \\ \epsilon_y \\ \epsilon_z \\ \gamma_{xy} \\ \gamma_{yz} \\ \gamma_{xz} \end{bmatrix} =
\begin{bmatrix}
\dfrac{1}{E} & -\dfrac{v}{E} & -\dfrac{v'}{E'} & 0 & 0 & 0 \\
-\dfrac{v}{E} & \dfrac{1}{E} & -\dfrac{v'}{E'} & 0 & 0 & 0 \\
-\dfrac{v'}{E'} & \dfrac{v'}{E'} & \dfrac{1}{E'} & 0 & 0 & 0 \\
0 & 0 & 0 & \dfrac{1}{G} & 0 & 0 \\
0 & 0 & 0 & 0 & \dfrac{1}{G'} & 0 \\
0 & 0 & 0 & 0 & 0 & \dfrac{1}{G'}
\end{bmatrix}
\begin{bmatrix} \sigma_x \\ \sigma_y \\ \sigma_z \\ \tau_{xy} \\ \tau_{yz} \\ \tau_{xz} \end{bmatrix}
$$

In the relation, there are different parameters:
-   ε is an axial strain
-   γ is the angle created by shear stress
-   E is Young's modulus
-   v is Poisson's coefficient, and it is assumed to be the same in all three-plane considered and equal to 0.33
-   G is Shear's modulus
-   σ is the axial stress
-   τ is the shear stress

In particular:
-   $E = E_x = E_y$
-   $E' = E_z$
-   $G = \dfrac{E}{2(1+v)}$
-   $G' = \dfrac{EE'}{E(1+2v')+E'}$
-   $\dfrac{v_{12}}{E_{11}} = \dfrac{v_{21}}{E_{22}}$
-   $\dfrac{v_{23}}{E_{22}} = \dfrac{v_{32}}{E_{33}}$
-   $\dfrac{v_{31}}{E_{33}} = \dfrac{v_{13}}{E11}$

Referring to these results and powder characteristics, the compliance matrix is calculated, and it is reported:

$$\begin{bmatrix} 4.18e-6 & -1.38e-6 & -1.85e-6 & 0 & 0 & 0 \\ -1.38e-6 & 4.18e-6 & -1.85e-6 & 0 & 0 & 0 \\ -1.85e-6 & -1.85e-6 & 5.62e-6 & 0 & 0 & 0 \\ 0 & 0 & 0 & 1.11e-5 & 0 & 0 \\ 0 & 0 & 0 & 0 & 1.35e-5 & 0 \\ 0 & 0 & 0 & 0 & 0 & 1.35e-5 \end{bmatrix}$$

MAT9 function requests a stiffness matrix, so the inverse one is calculated using Matlab starting from the compliance matrix. The following is inserted in Hypermesh to define software material correctly:

$$\begin{bmatrix} 406355.04 & 22665.80 & 208893.58 & 0 & 0 & 0 \\ 226655.80 & 406355.04 & 208893.58 & 0 & 0 & 0 \\ 208893.58 & 208893.58 & 315869.76 & 0 & 0 & 0 \\ 0 & 0 & 0 & 89849.62 & 0 & 0 \\ 0 & 0 & 0 & 0 & 74019.56 & 0 \\ 0 & 0 & 0 & 0 & 0 & 74019.56 \end{bmatrix}$$

3.3.2. Determination of equivalent Young's moduli and Shear's moduli

This part of the work represents the thesis' core. Indeed, some ways are followed to determine the correct equivalent moduli. A simplification is done because not all matrix terms are evaluated, but only diagonal ones.

In particular, the initial idea is to define the volume occupied by only one single unit cell as the equivalent solid. The results suggest this solid isn't suitable to persecute the goal, so two different ways are followed. First, a dimensional study is done, and then a shape study is conducted about the equivalent solid.

In the following paragraphs, more details are provided about each hypothesis thought, and obtained results are shown to make and justify conclusions.

3.3.2.1. Equivalent solid: Cube

3.3.2.1.1. Single unit cell

At the beginning of the thesis, a rhombic dodecahedron unit cell is selected as an equivalent solid because the idea is to define its properties and then translate them in all three directions to reduce the number of nodes valid to describe lattice structure behavior.

Regarding the target of the thesis to reduce time and analysis cost, advantages are evident to pass from a unit cell formed by 17425 CTETRA elements and 5059 nodes to a cubic volume formed by only one CHEXA element with 8 nodes. This is the justification for the volume choice. Compression and shear tests are conducted on a rhombic dodecahedron cell defined as MAT9 with elastic constraints.

Three compression and three shear tests are realized to determine diagonal matrix terms. In the pictures reported below, there are tests:
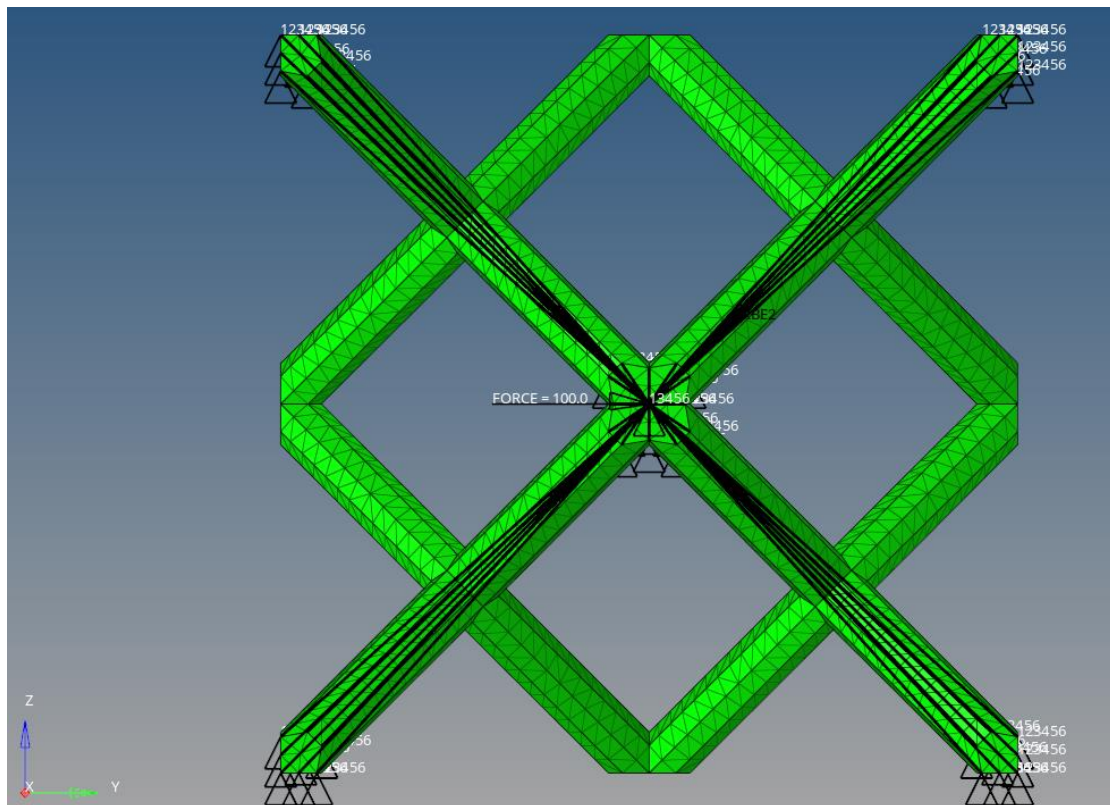
Figure 58 Determination of XY Shear's modulus
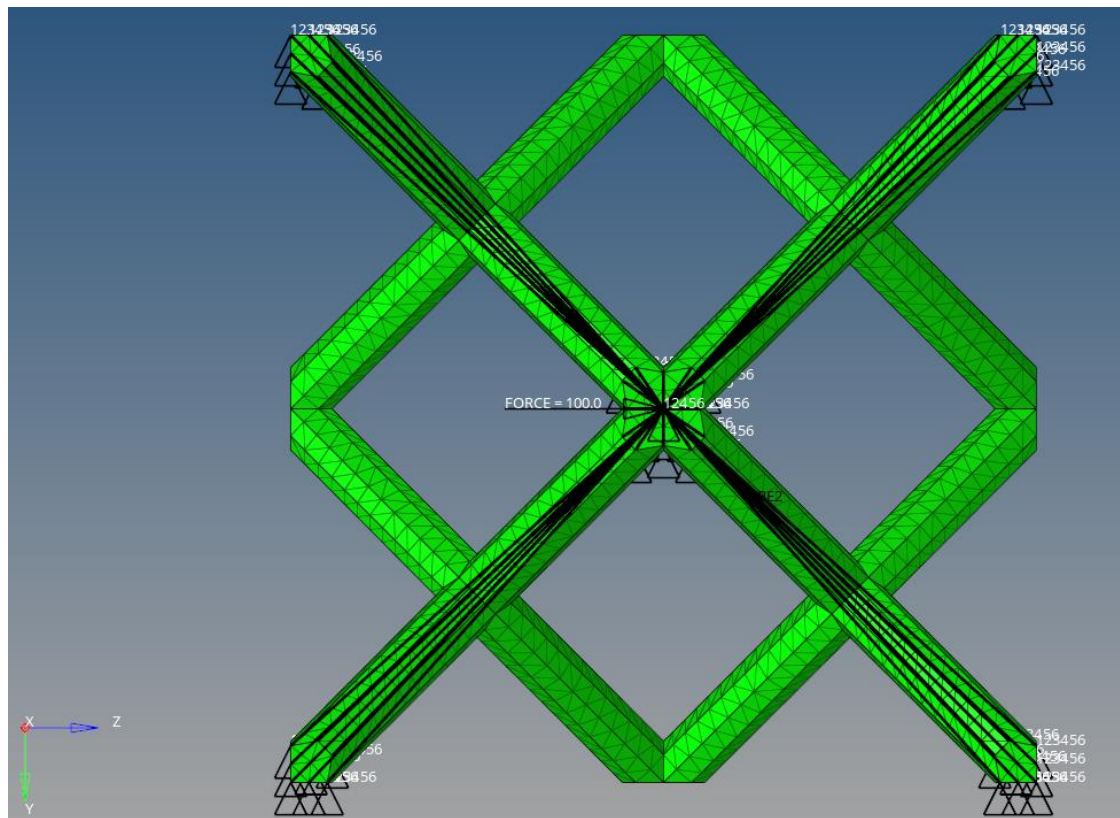
Figure 59 Determination of XZ Shear's modulus
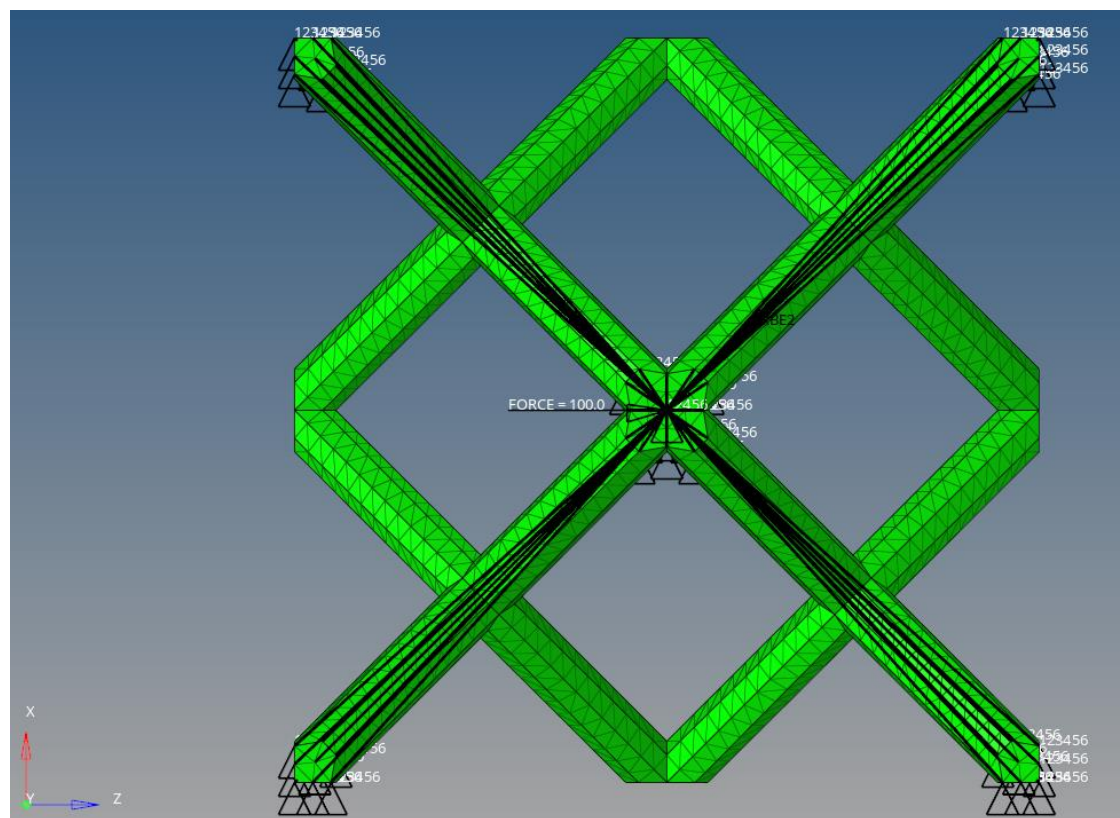
Figure 60 Determination of YZ Shear's modulus
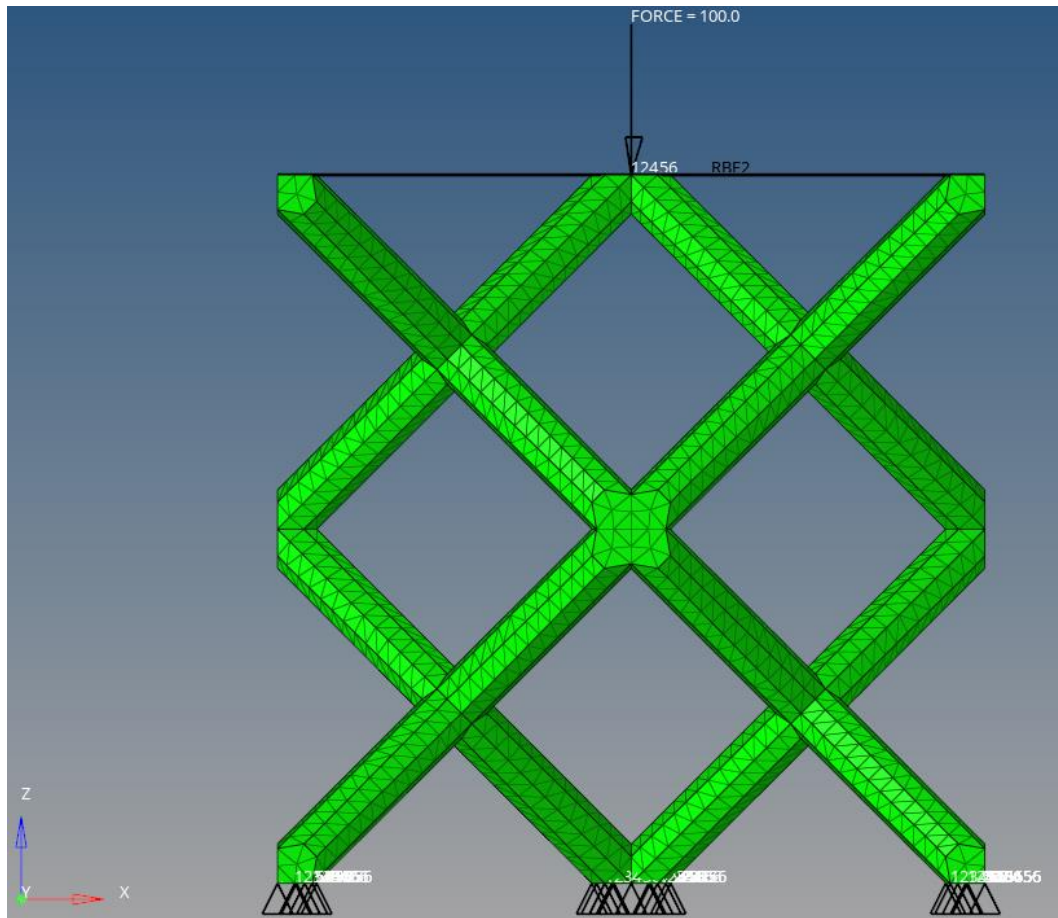
Figure 61 Determination of Z direction Young's modulus
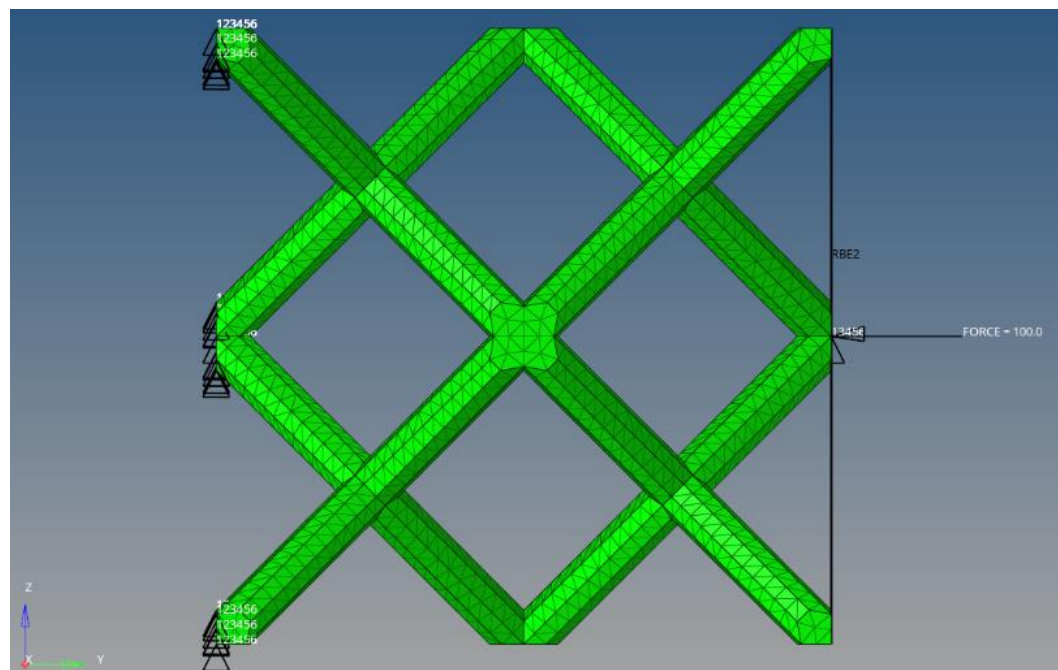
Figure 62 Determination of Y direction Young's modulus
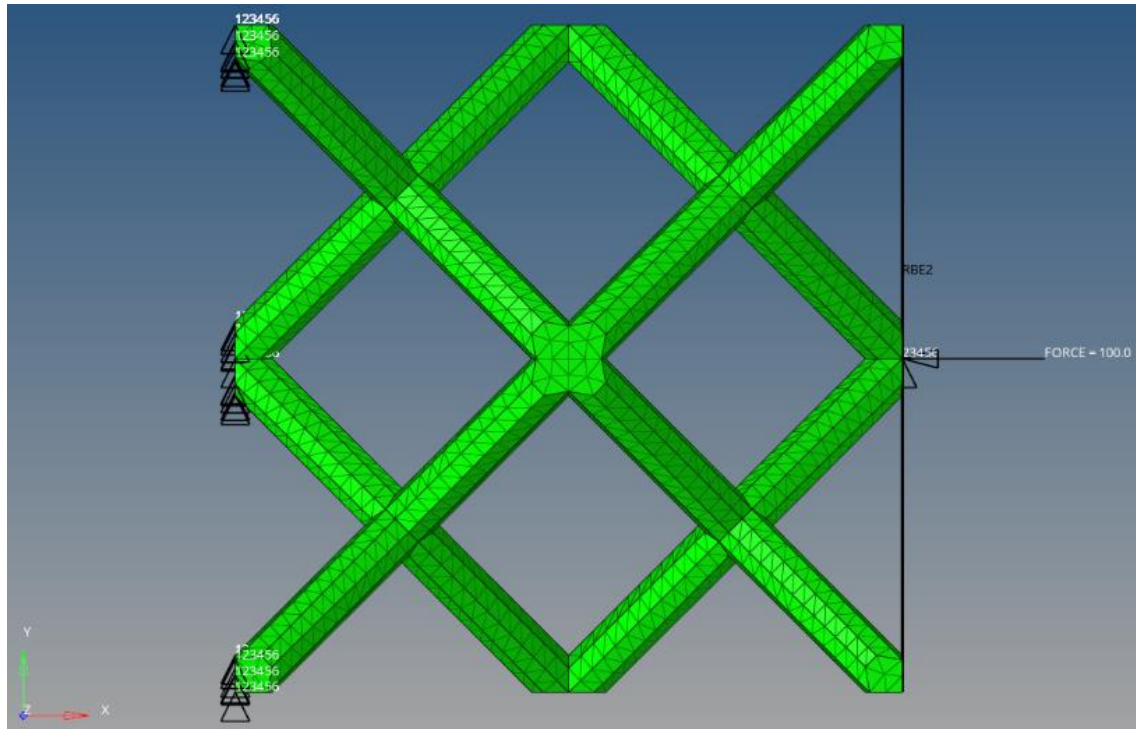
Figure 63 Determination of X direction Young's modulus

The applied load is chosen equal to 100 N. The previous tests define this load's entity. Indeed this stress doesn't create a plastic strain, so it is possible to determine the slope of the elastic segment of the stress-strain curve, which is the elastic moduli. The application load area of a unit cell must be the same as the equivalent solid one. The rhombic dodecahedron unit cell is inscribed into a cube whose edge is 10 mm long, so the area is 100 mm2. According to these values, the equivalent stress parameter is 1 MPa.

Test results are reported in the following table:

Table 7 Single unit cell equivalent moduli

Z		XY	
σ_z [MPa]	1	τ_{xy} [MPa]	1
ϵ_z	1.60E-03	γ_{xy}	3.59E-03
E_z [MPa]	623.72	G_{xy} [MPa]	278.56
X		YZ	
σ_x [MPa]	1	τ_{yz} [MPa]	1
ϵ_x	1.56E-03	γ_{yz}	3.68E-03
E_x[MPa]	640.25	G_{yz} [MPa]	271.94

Y		XZ	
σ_y [MPa]	1	τ_{xz} [MPa]	1
ϵ_y	1.53E-03	γ_{xz}	3.69E-03
E_y [MPa]	655.14	G_{xz} [MPa]	270.89

Considering geometry and powder characteristics, Young's moduli in X and Y directions must be the same, while Shear's one in XZ and YZ planes must be identical. From the simulation results, these constants seem to be different. Still, the discrepancy can be attributed to solver approximations and to not perfect symmetry between elements during the deformation along axis directions.

The smallest one is selected to evaluate equivalent moduli better because stress is lower in lattice structure if the strain is the same.

The table below shows equivalent moduli chosen to define the stiffness matrix:

Table 8 Single unit cell selected moduli

Moduli	Moduli selected
Ex [MPa]	640.25
Ey [MPa]	640.25
Ez [MPa]	623.72
Gxy [MPa]	278.56
Gxz [MPa]	270.89
Gyz [MPa]	270.89

The next step consists of the equivalent moduli validation. These moduli are used to define an equivalent material to persecute this goal, so they are put into a MAT9. Successively a solid cube is created with this equivalent material.

Some tests are done on the solid applying compression (Z direction) and shear (XZ plane) loads to calculate the Young's and Shear's moduli and to compare them with the reticular one. These two types of loads are selected because they represent all the others; if they are incorrect, the others are too.

It is crucial to verify if moduli are mesh independent because this permits to state that they are the correct equivalent moduli. To demonstrate this condition cube has meshed with an increasing number of elements: 1, 3, 5, and 10.

In the following are reported simulation results both graphically and numerically:
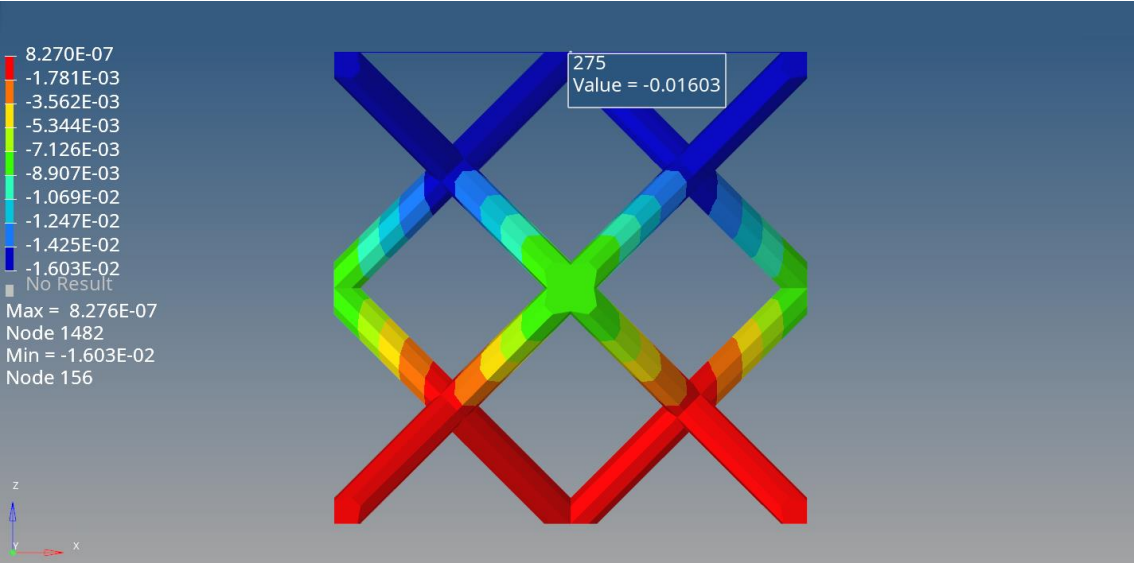
Figure 64 Reticular component - Compression Z direction

Figure 65 Equivalent solid - Compression Z direction

Figure 66 Reticular component - Shear XZ plane

Figure 67 Equivalent solid - Shear XZ plane

Table 9 Single unit cell: comparison between reticular component and equivalent solids

Compression Z	Ret. Component	Eq. Solid (1)	Eq. Solid (3)	Eq. Solid (5)	Eq. Solid (10)
σ_z [MPa]	1	1	1	1	1
Displacement [mm]	1.60E-02	1.60E-02	1.60E-02	1.60E-02	1.60E-02
ϵ_z	1.60E-03	1.60E-03	1.60E-03	1.60E-03	1.60E-03
E_z [MPa]	623.72	623.72	623.72	623.72	623.72
Discrepancy [%]	0	0	0	0	0

Shear XZ	Ret. Component	Eq. Solid (1)	Eq. Solid (3)	Eq. Solid (5)	Eq. Solid (10)
τ_{xz} [MPa]	1	1	1	1	1
Displacement [mm]	3.69E-02	3.69E-02	5.37E-02	5.67E-02	5.82E-02
γ_{xz} [rad]	3.69E-03	3.69E-03	5.37E-03	5.67E-03	5.82E-03
G_{xz} [MPa]	270.90	270.89	186.12	176.26	171.69
Discrepancy [%]	0	1.30E-03	31.29	34.93	36.62

In the above tables, the discrepancy values are calculated with respect to the reticular component using this relation:

$$discrepancy = \left(\frac{Ret.Component - Eq.Solid}{Ret.Component} \right) \cdot 100$$

It is essential to underline that an equivalent solid composed of only one element presents the same moduli as the reticular component. This is due to the moduli definition itself. Indeed, compression's and shear's moduli are calculated without considering the deformation in the middle of the unit cell. Still, only the upper and lower surface are considered, so the "barrel" effect cannot influence the results.

While if the number of elements present in the solid increases, different considerations must be made about two different moduli:

- Young's modulus → In this case, the discrepancy referred to the reticular component stays constant, and convergence is reached soon, so the result is mesh independent. It is possible to state that equivalent moduli determined are correct

- Shear's modulus → In this case, the discrepancy increases when the element number grows. This can be justified because the structure becomes less stiff than using a single element, so the displacement along the force application direction increases. Referring to the mode to determine the angle and so the modulus, if the displacement increases, the modulus becomes smaller

At the end of this analysis, results suggest that more than a single rhombic dodecahedron unit cell is necessary to estimate the shear's equivalent moduli better and to consider the significant structure compliance.

3.3.2.1.2.   Cubic volume: 3x3x3 unit cell

In the previous step emerges the importance of the unit cells' number, which compose the equivalent solid. Following this idea, a component with 27 rhombic dodecahedron unit cells

(3x3x3) is made. This solid is composed of 478873 CTETRA elements and 855389 nodes, so the definition of an equivalent solid becomes fundamental to analyzing this case. For example, introducing a solid formed by 27 CHEXA elements with only 62 nodes represents a remarkable improvement in reducing time and costs.

The tests on this new component are executed as before, so compression and shear simulations are conducted.

In the following pictures are reported the scheme of loads and constraints:
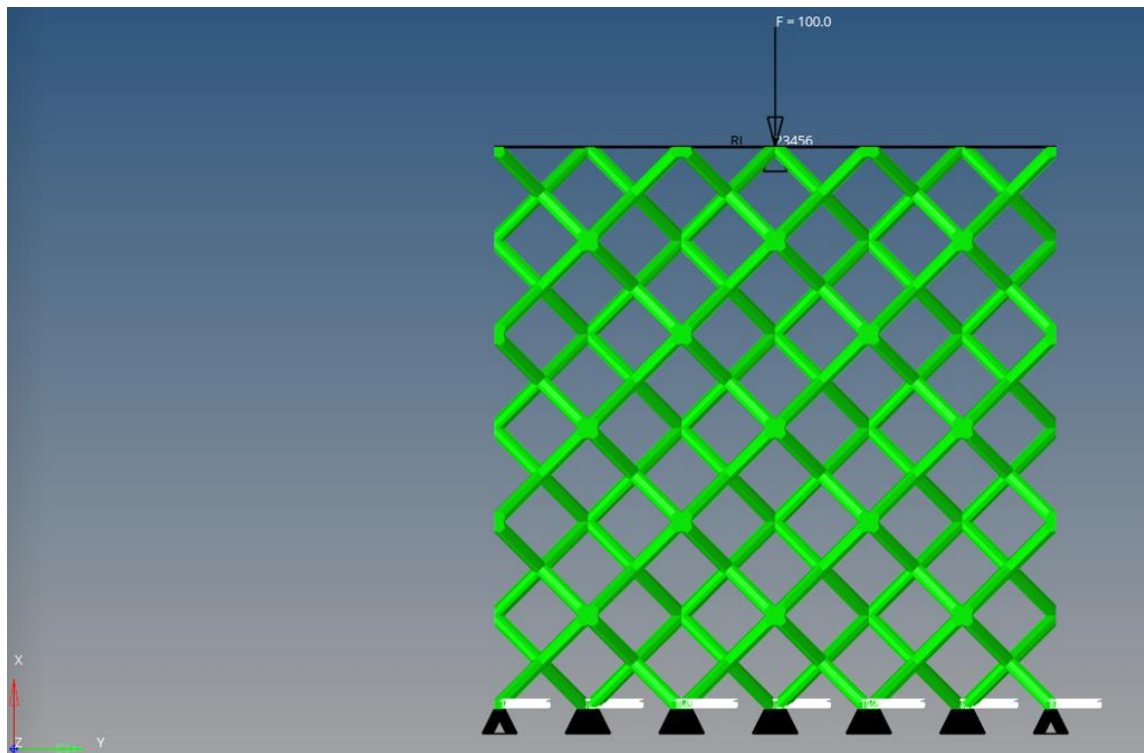
Figure 68 Determination of X direction Young's modulus
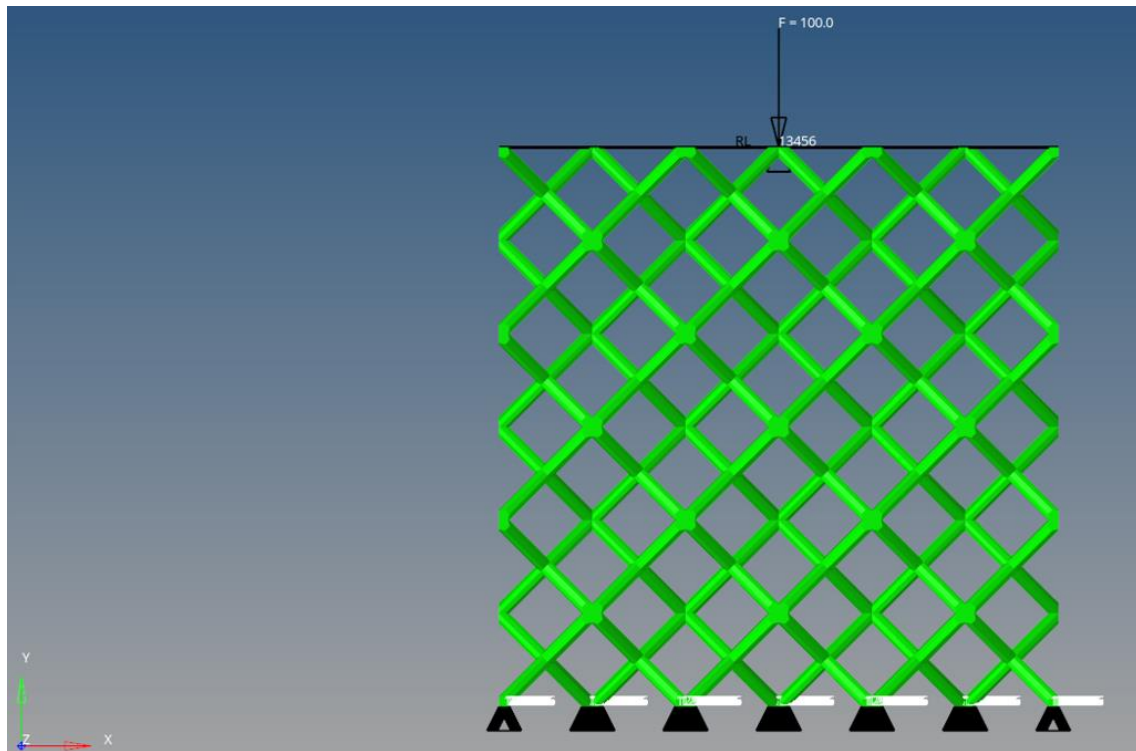
Figure 69 Determination of Y direction Young's modulus
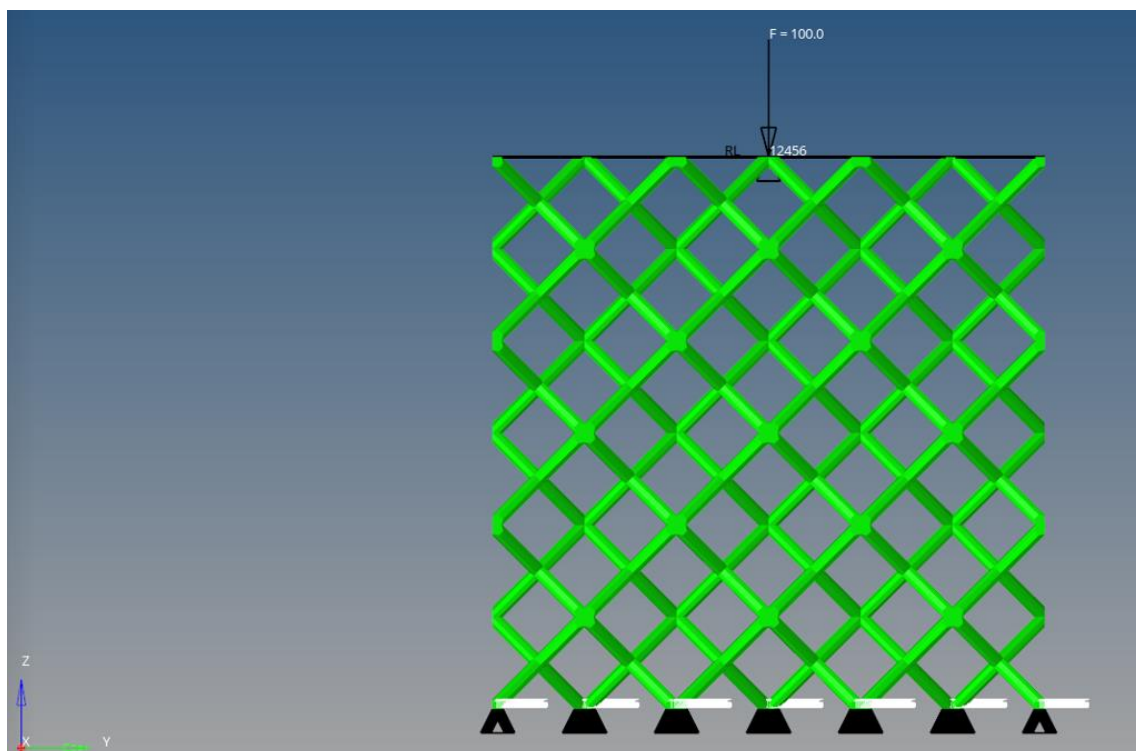
Figure 70 Determination of Z direction Young's modulus

Figure 71 Determination of XY Shear's modulus

Figure 72 Determination of YZ Shear's modulus

Figure 73 Determination of XZ Shear's modulus

The load is the same as the previous case and equal to 100 N, but the application area is 900 mm2, so the applied stress is around 0.11 MPa.

In the below table are shown the equivalent moduli obtained:

Table 11 Cubic volume (3x3x3 unit cells) equivalent moduli

Z		XY	
σ_z [MPa]	0.11	τ_{xy} [MPa]	0.11
ϵ_z	3.58E-04	γ_{xy} [rad]	8.18E-04
E_z [MPa]	309.95	G_{xy} [MPa]	135.77
X		YZ	
σ_x [MPa]	0.11	τ_{yz} [MPa]	0.11
ϵ_x	3.53E-04	γ_{yz} [rad]	8.27E-04
E_x [MPa]	314.68	G_{yz} [MPa]	134.37
Y		XZ	
σ_y [MPa]	0.11	τ_{xz} [MPa]	0.11
ϵ_y	3.51E-04	γ_{xz} [rad]	8.23E-04
E_y [MPa]	316.74	G_{xz} [MPa]	134.97

Young's moduli in X and Y directions are considered the same in the previous case considering geometry and powder characteristics. In contrast, Shear's moduli in XZ and YZ planes are defined as identical. From the simulation results, these constants seem to be different. Still, the discrepancy can be attributed to solver approximation and not perfectly symmetrically between elements during the deformation along axis directions.

The smallest one is selected to evaluate equivalent moduli better because stress is lower in lattice structure if the strain is the same.

The table below shows equivalent moduli chosen to define the stiffness matrix:

Table 12 Cubic volume (3x3x3 unit cells) selected equivalent moduli

Moduli	Moduli selected
Ex [MPa]	314.68
Ey [MPa]	314.68
Ez [MPa]	309.95
Gxy [MPa]	135.77
Gxz [MPa]	134.37
Gyz [MPa]	134.37

At this point of the analysis, verifying if the equivalent moduli are correct is necessary, so a validation occurs. These moduli are used to define an equivalent material, so they are put into a MAT9. Successively a solid cube is created and described with this equivalent material.

Like the unit cell, some tests are done on the solid applying compression (Z direction) and shear (XZ plane) loads to calculate the Young's and Shear's moduli and to compare them with the reticular one. These two types of loads are selected because they represent each other; if they are incorrect, the others are too.

It is essential to verify if moduli are mesh independent because this permits to state that they are correct equivalent moduli. To confirm this condition cube is meshed with an increasing number of elements: 1, 5, 10, and 15.

In the following, simulation results are reported both graphically and numerically:
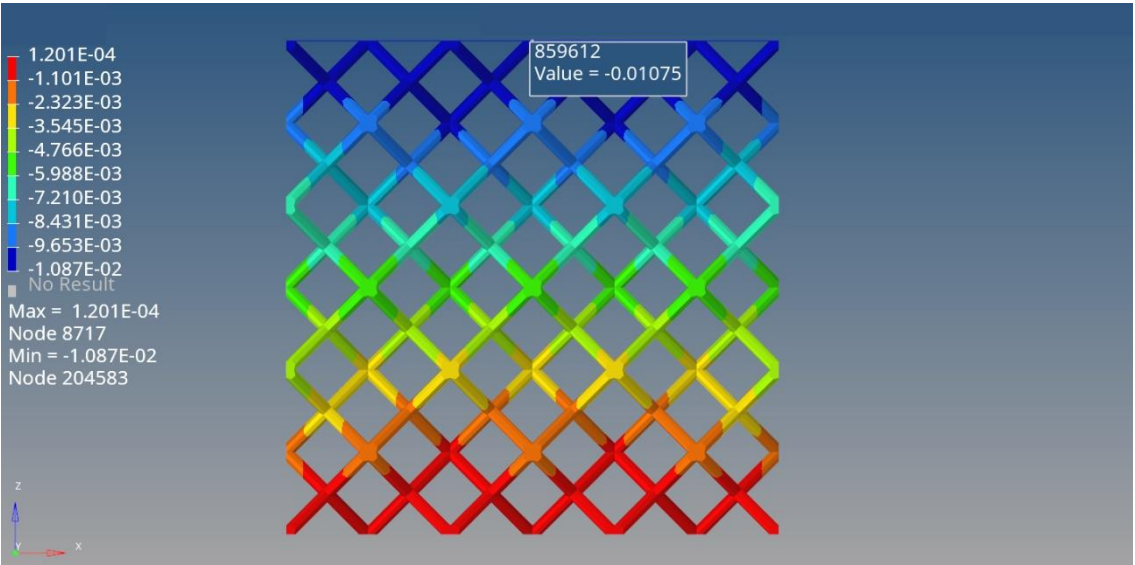
Figure 74 Reticular component - Compression Z direction
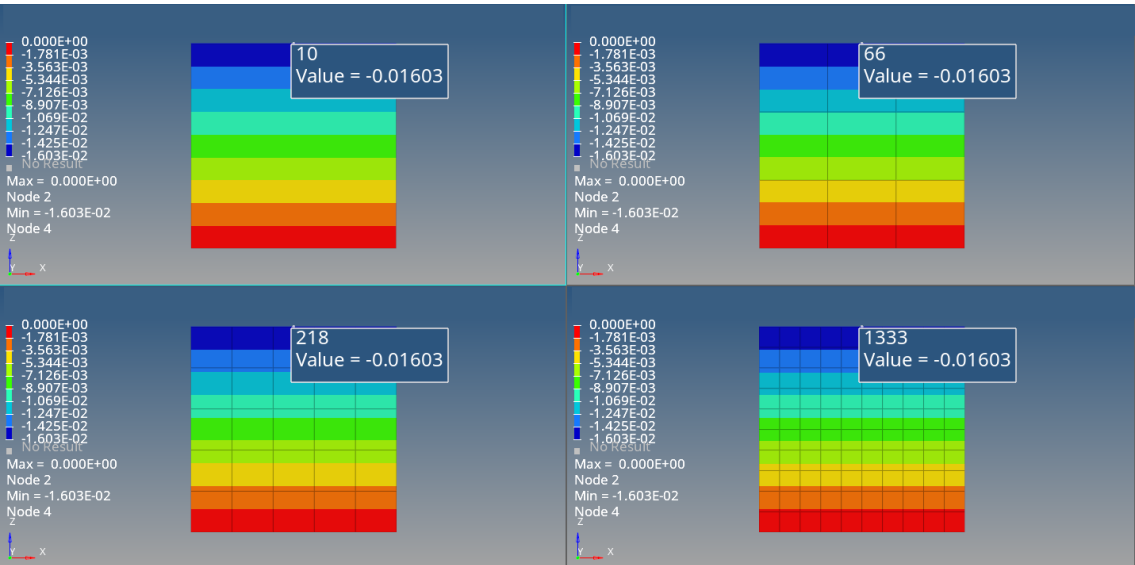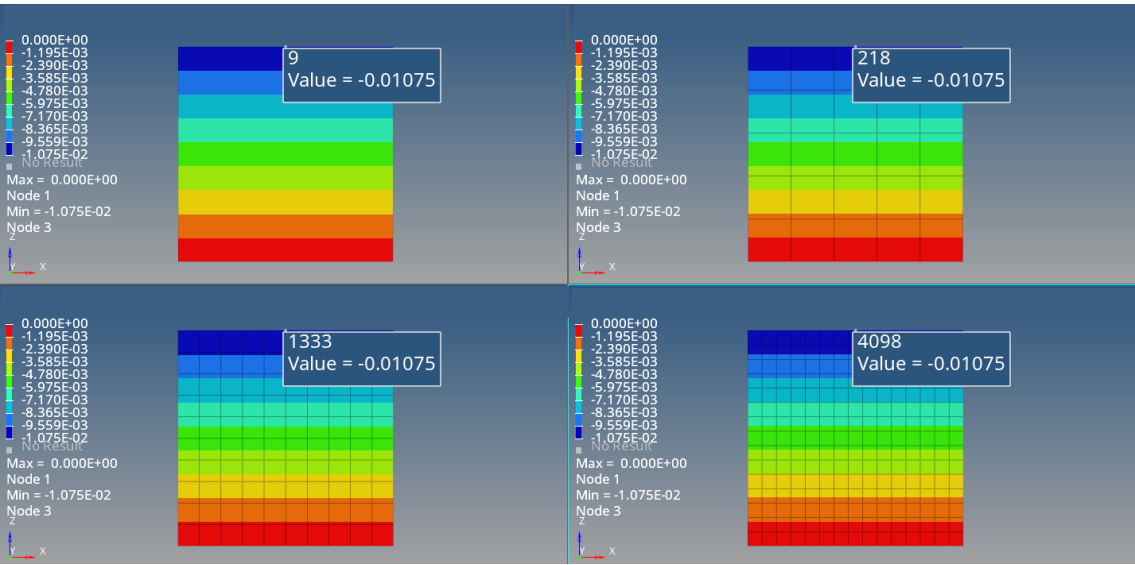

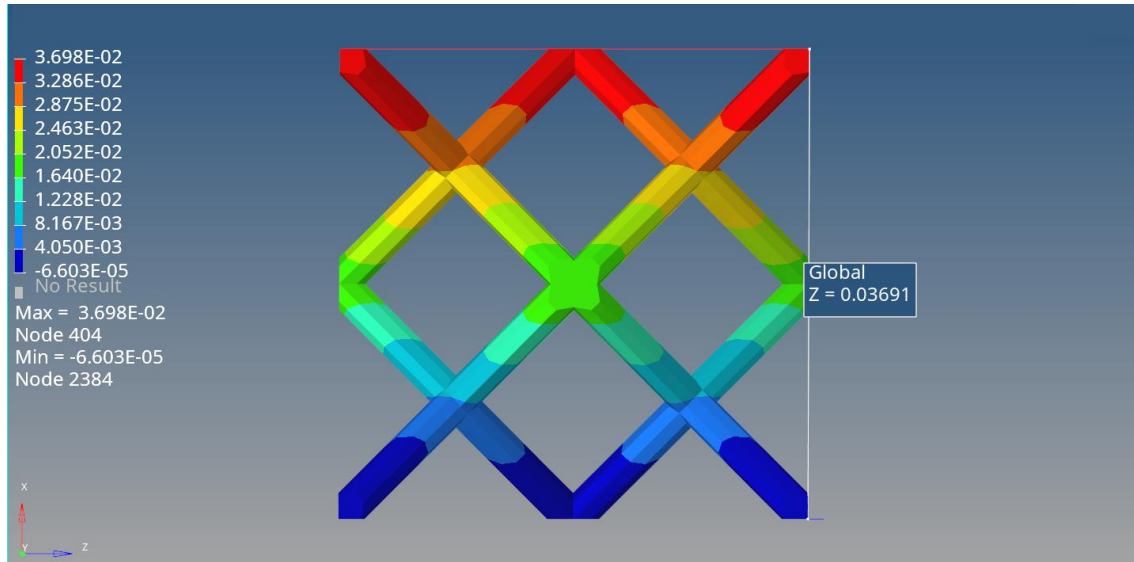*Figure 75 Equivalent solid - Compression Z direction*
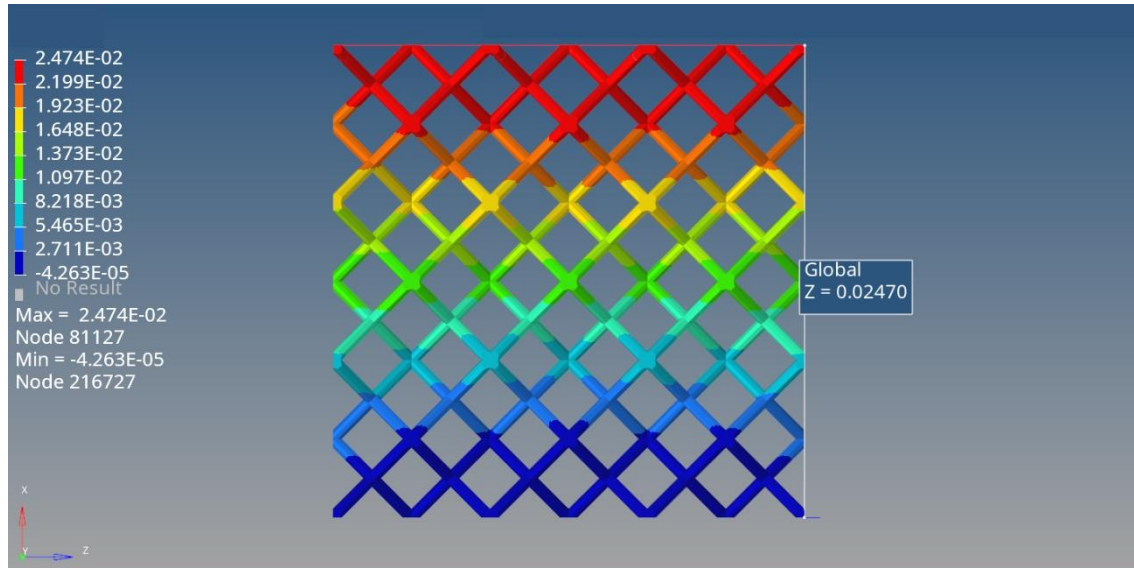
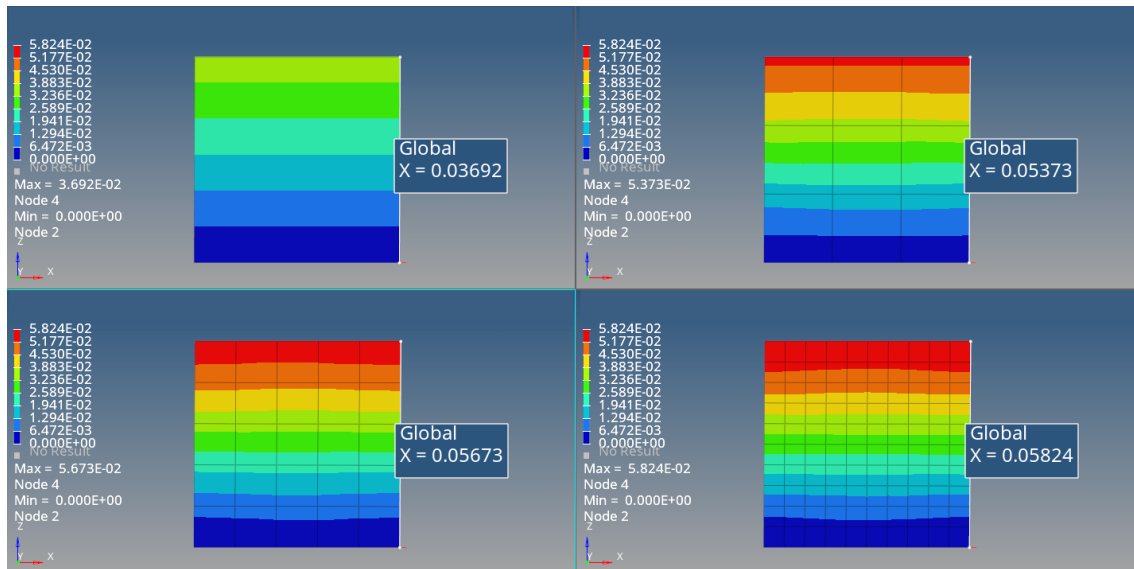*Figure 76 Reticular component - Shear XZ plane*
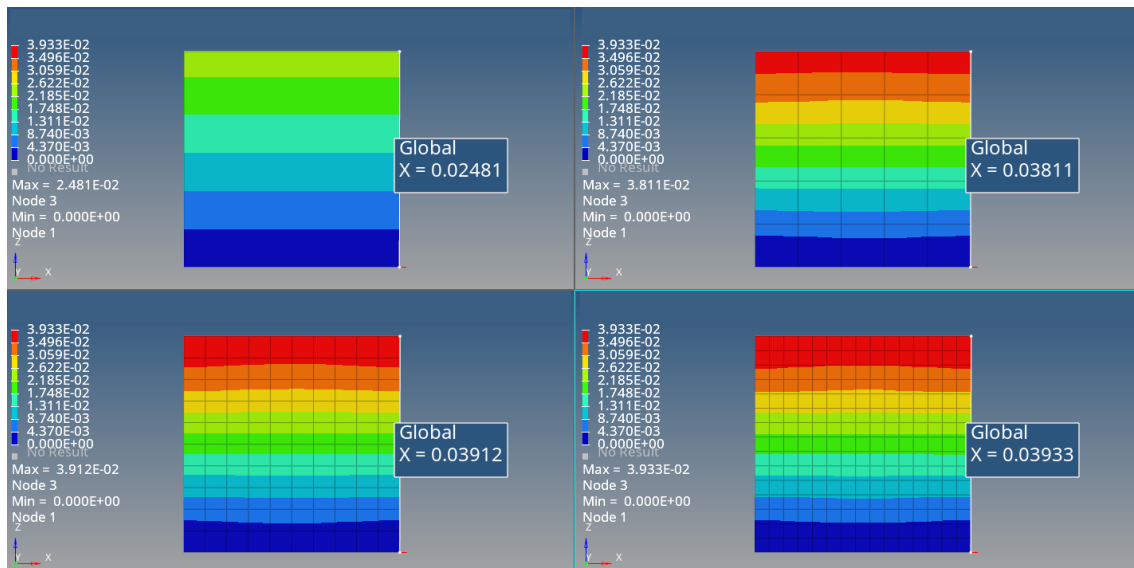
Figure 77 Equivalent solid - Shear XZ plane

Table 13 Cubic volume (3x3x3 unit cells): comparison between reticular component and equivalent solids

Compression Z	Ret. Component	Eq. Solid (1)	Eq. Solid (5)	Eq. Solid (10)	Eq. Solid (15)
σ_z [MPa]	0.11	0.11	0.11	0.11	0.11
Displacement [mm]	1.08E-02	1.08E-02	1.08E-02	1.08E-02	1.08E-02
ϵ_z	3.58E-04	3.58E-04	3.58E-04	3.58E-04	3.58E-04
E_z [MPa]	309.95	309.95	309.95	309.95	309.95
Discrepancy [%]	0	0	0	0	0

Table 14 Cubic volume (3x3x3 unit cells): comparison between reticular component and equivalent solids

Shear XZ	Ret. Component	Eq. Solid (1)	Eq. Solid (5)	Eq. Solid (10)	Eq. Solid (15)
τ_{xz} [MPa]	0.11	0.11	0.11	0.11	0.11
Displacement [mm]	2.47E-02	2.48E-02	3.81E-02	3.91E-02	3.93E-02
γ_{xz} [rad]	8.23E-04	8.27E-04	1.27E-03	1.30E-03	1.31E-03
G_{xz} [MPa]	134.97	134.37	87.47	85.21	84.75
Discrepancy [%]	0	0.45	35.19	36.87	37.21

In the above tables, the discrepancy values are calculated with respect to the reticular component using this relation:

$$discrepancy = \left(\frac{Ret.\,Component - Eq.\,Solid}{Ret.\,Component}\right) \cdot 100$$

It is essential to underline that an equivalent solid composed of only one element presents the same Young's modulus as the reticular component. This result is due to the modulus definition itself; compression is calculated without considering the deformation in the middle of the reticular component, but only the upper and lower surface are considered, so the "barrel" effect cannot influence the results. In comparison, the shear's modulus presents a slight discrepancy starting from an equivalent solid composed of only one mesh element because there is a difference between the calculated shear's modulus of the reticular component (134.97 MPa) and the equivalent one in the XZ plane provided to the software (134.37 MPa). The user induces this error to consider the theory behind this type of geometry and the characteristic of a transversal isotropic material.

It is possible to note different considerations about two different types of moduli considering an increment of the number of elements in the solid:

- Young's modulus → The discrepancy referred to as the reticular component stays constant, and convergence is reached soon, making the result mesh independent. It is possible to state that equivalent moduli determined are correct. If a comparison between this modulus and the previous determined using only a single unit cell appears how they are different. This result can be explained considering the compliance, which is more significant in the component realized with 27 single unit cells. If compliance is paramount, the displacement grows, so Young's modulus becomes smaller.

  The difference between the two reticular components is around 50%.

This result shows that only a single unit cell isn't sufficient to evaluate the equivalent moduli better because its results are incorrect, and so the equivalent solid must be constituted by many single cells to obtain a result that is representative of the global lattice structure

- Shear's modulus → The discrepancy tends to increase when the element number grows. This result can be justified because the structure becomes less stiff than a single element, so the displacement along the force application direction increases. Referring to the mode to determine the angle and modulus, the modulus becomes smaller if the displacement increases.

  Comparing these results and single unit cells appears that shear's modulus decreases, and the difference is around 50%. This result is according to the consideration stated before about Young's modulus, so the number of elements that belongs to an equivalent solid must be more than a single one

At the end of this step, the object of the subsequent paragraphs is to understand the correct elements' number to determine equivalent moduli, which can be used to define an equivalent material that is representative of the entire lattice structure.

3.3.2.1.3. Cubic volume: 6x6x6 unit cell

The following paragraph underlines the importance of increasing the elements' number, which composes the equivalent solid. Following this concept, it is realized a reticular component with 216 rhombic dodecahedron unit cells (6x6x6). This solid is formed by 3830977 CTETRA elements and 6827708 nodes. Implementing an equivalent solid to this component primarily represents a valuable means to analyze a lattice structure. Indeed, considering this component, it is possible to shift focus from 6827708 to 343 nodes and from 3830977 CTETRA to 216 CHEXA elements, taking an enormous reduction in time and saving money.

For this component, the same tests are conducted as before.

In the following pictures are shown the scheme of loads and constraints:
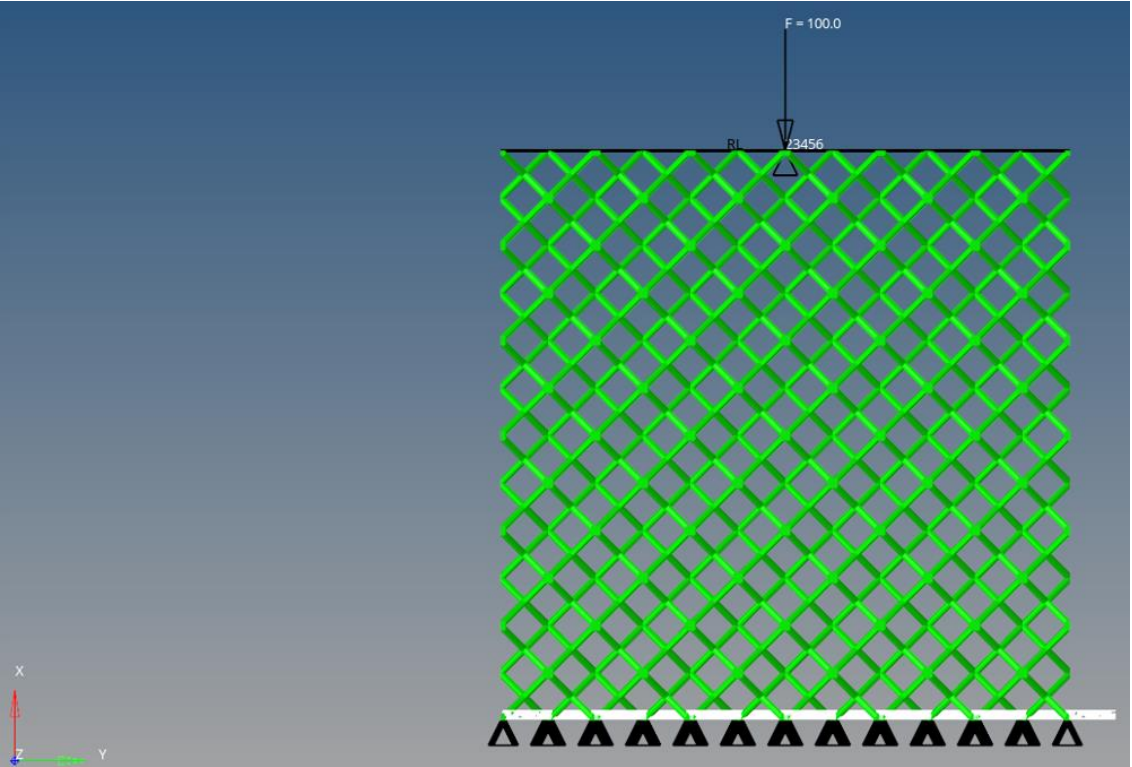
Figure 78 Determination of X direction Young's modulus
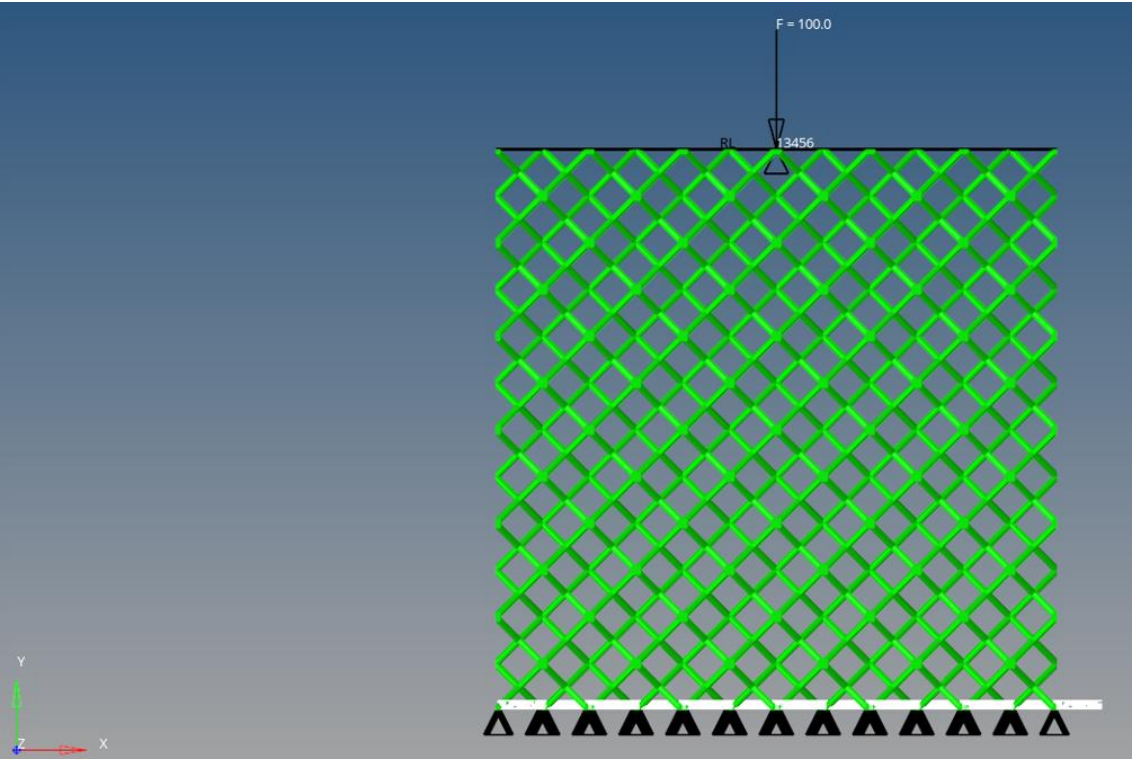
Figure 79 Determination of Y direction Young's modulus
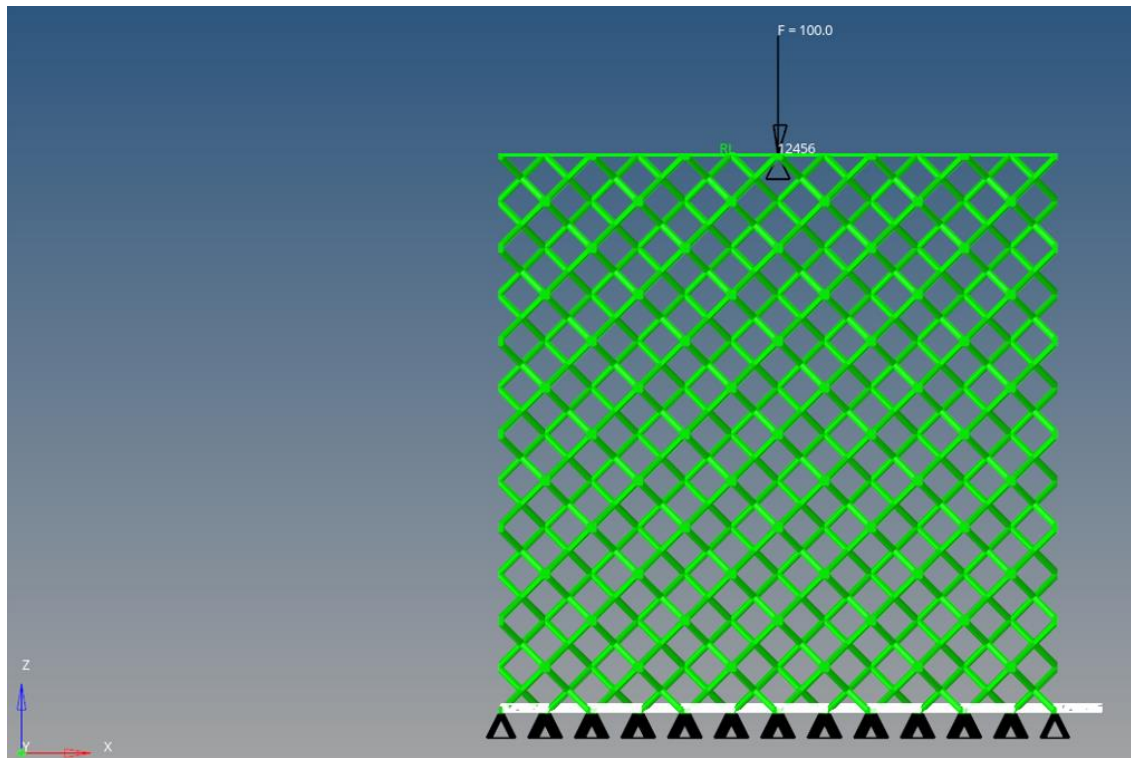
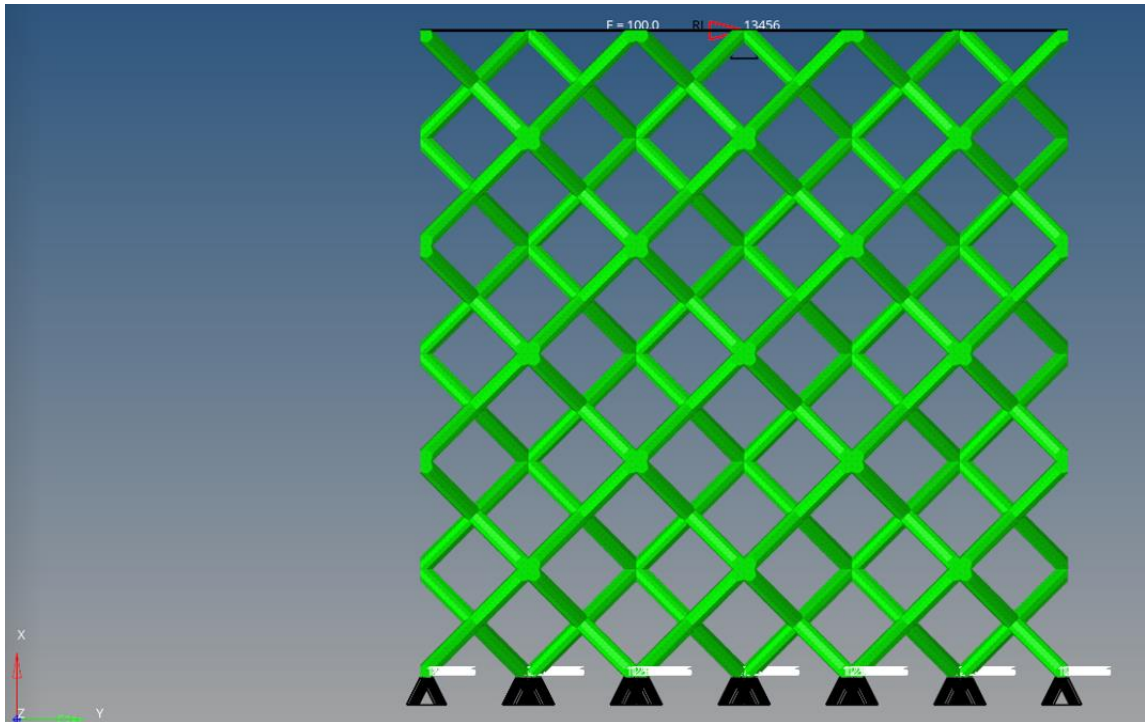*Figure 80 Determination of Z direction Young's modulus*
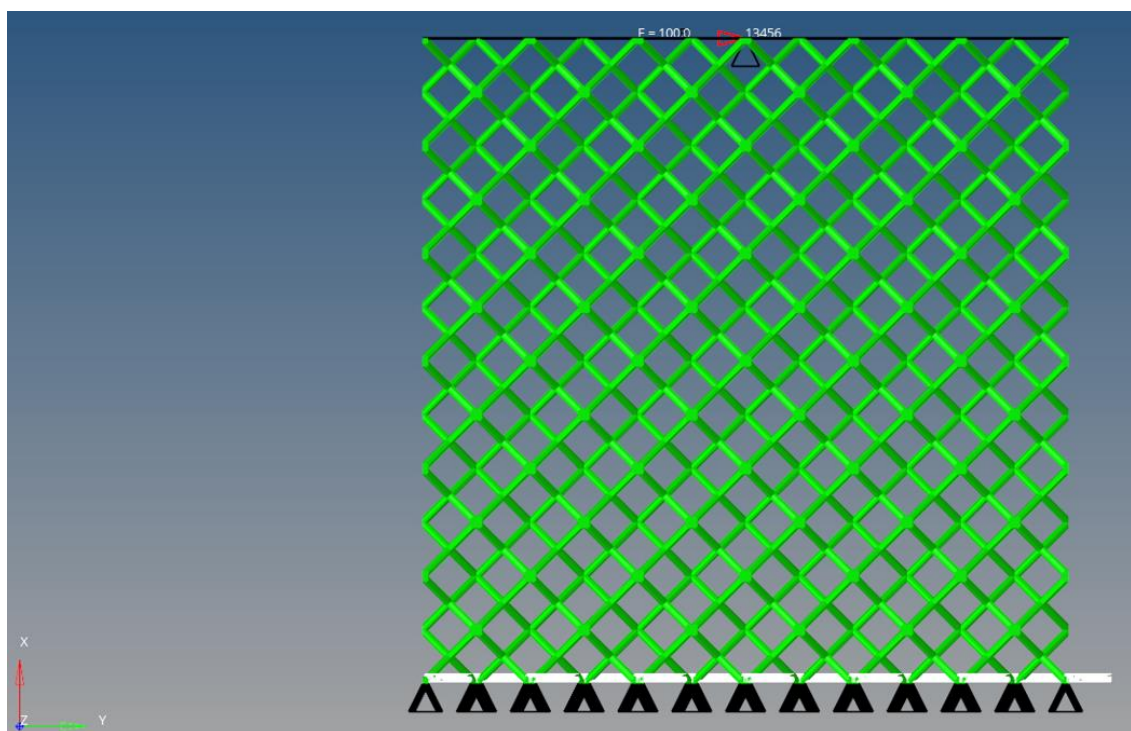
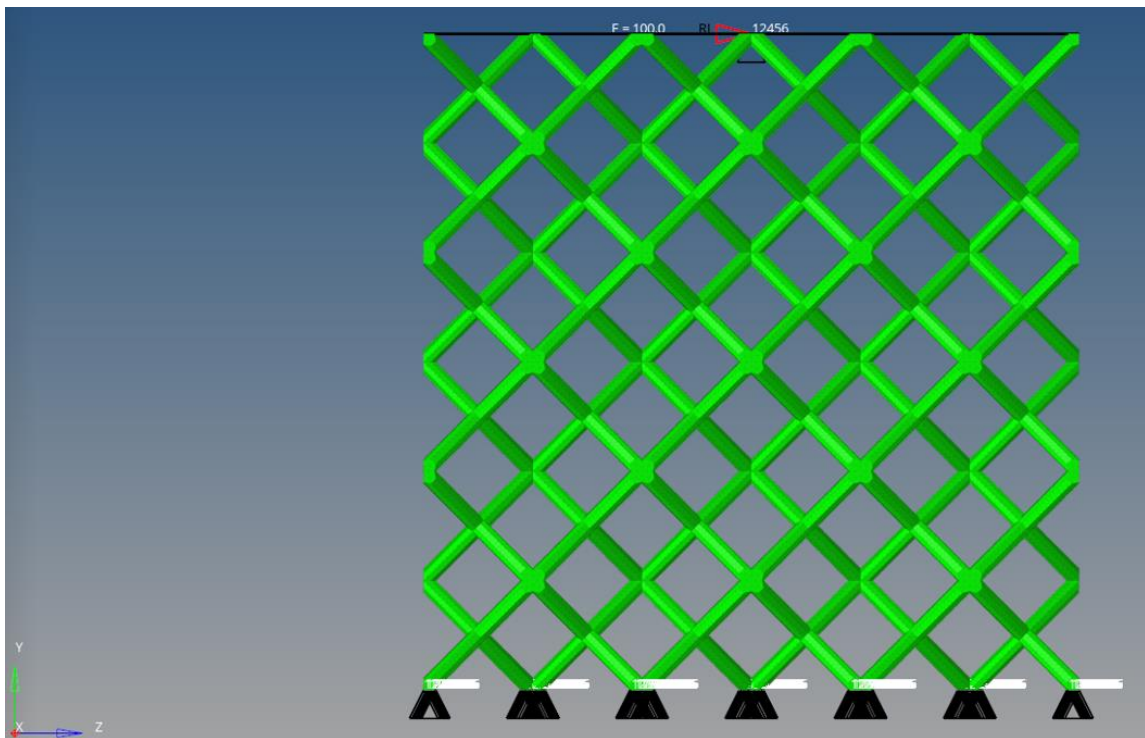*Figure 81 Determination of XY Shear's modulus*

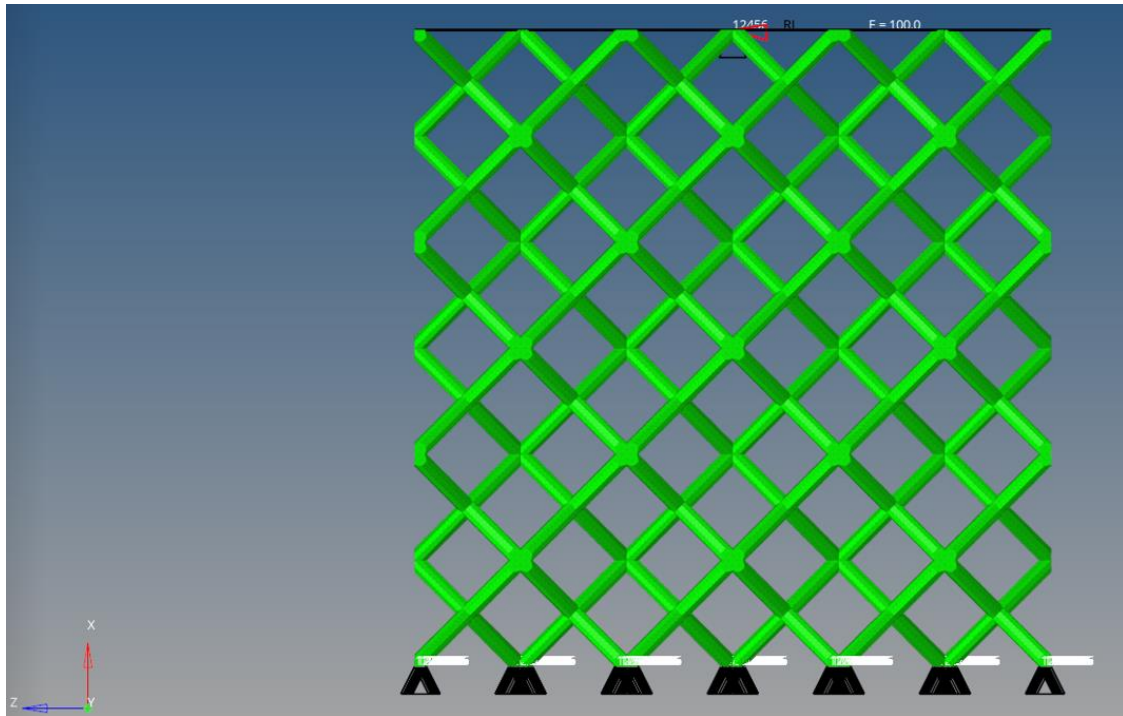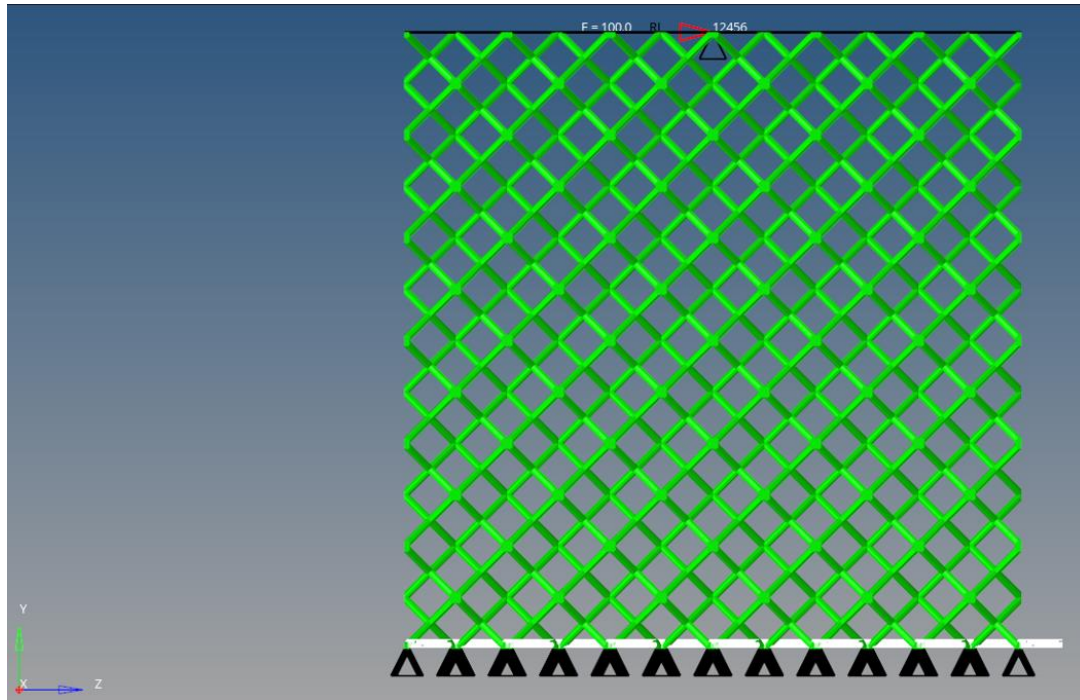*Figure 82 Determination of YZ Shear's modulus*
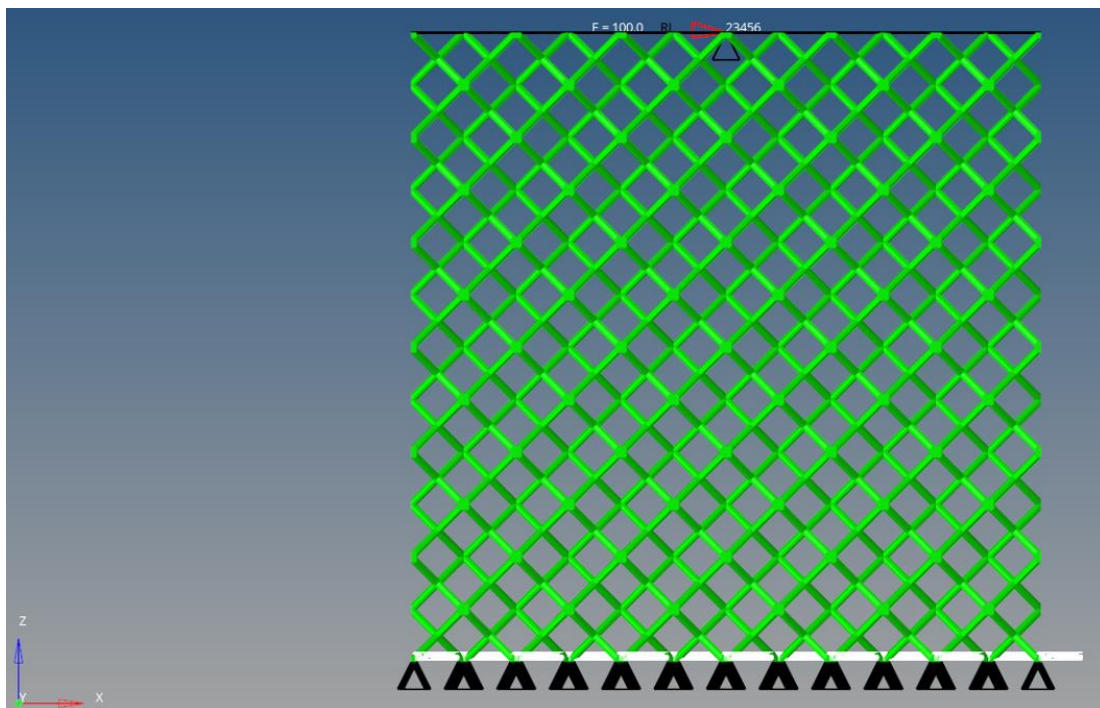
Figure 83 Determination of XZ Shear's modulus

The load is the same as the previous components and equal to 100 N, but the application area is 3600 mm², so the applied stress is around 0.0278 MPa.

In the below table are reported the equivalent moduli determined:

Table 15 Cubic volume (6x6x6 unit cells) equivalent moduli

X		XY	
σ_x [MPa]	0.028	τ_{xy} [MPa]	0.028
ϵ_x	9.34E-05	γ_{xy} [rad]	2.17E-04
E_x [MPa]	297.31	G_{xy} [MPa]	128.24
Y		XZ	
σ_y [MPa]	0.028	τ_{xz} [MPa]	0.028
ϵ_y	9.29E-05	γ_{xz} [rad]	2.19E-04
E_y [MPa]	299.07	G_{xz} [MPa]	126.90
Z		YZ	
σ_z [MPa]	0.028	τ_{yz} [MPa]	0.028
ϵ_z	9.44E-05	γ_{yz} [rad]	2.18E-04
E_z [MPa]	294.15	G_{yz} [MPa]	127.19

Young's moduli in X and Y directions are considered the same in the previous case considering geometry and powder characteristics. In contrast, Shear's moduli in XZ and YZ planes are defined identically. From the simulation results, these constants seem to be different. Still, the discrepancy can be attributed to solver approximation and not perfectly symmetrically between elements during the deformation along axis directions.

The smallest one is selected to evaluate equivalent moduli better because stress is lower in lattice structure if the strain is the same.

The table below shows equivalent moduli chosen to define the stiffness matrix:

Table 16 Cubic volume (6x6x6 unit cells) selected equivalent moduli

Moduli	Moduli selected
Ex [MPa]	297.31
Ey [MPa]	297.31
Ez [MPa]	294.15
Gxy [MPa]	128.24
Gxz [MPa]	126.90
Gyz [MPa]	126.90

At this point of the analysis, a validation of the equivalent moduli is necessary because these are discovered to be incorrect and mesh dependent in the previous steps. These moduli are used to define an equivalent material, so they are put into a MAT9. Successively a solid cube is created with this equivalent material.

Like the unit cell, some tests are done on the solid applying compression (Z direction) and shear (XZ plane) loads to calculate the Young's and Shear's moduli and to compare them with the reticular one. These two types of loads are selected because they are representative of each other, and if they are incorrect, the others are too.

It is crucial to verify if moduli are mesh independent because this permits to state that they are the correct equivalent moduli. To demonstrate this condition cube has meshed with an increasing number of elements: 1, 5, 10, and 15.

In the following are reported simulation results both graphically and numerically:
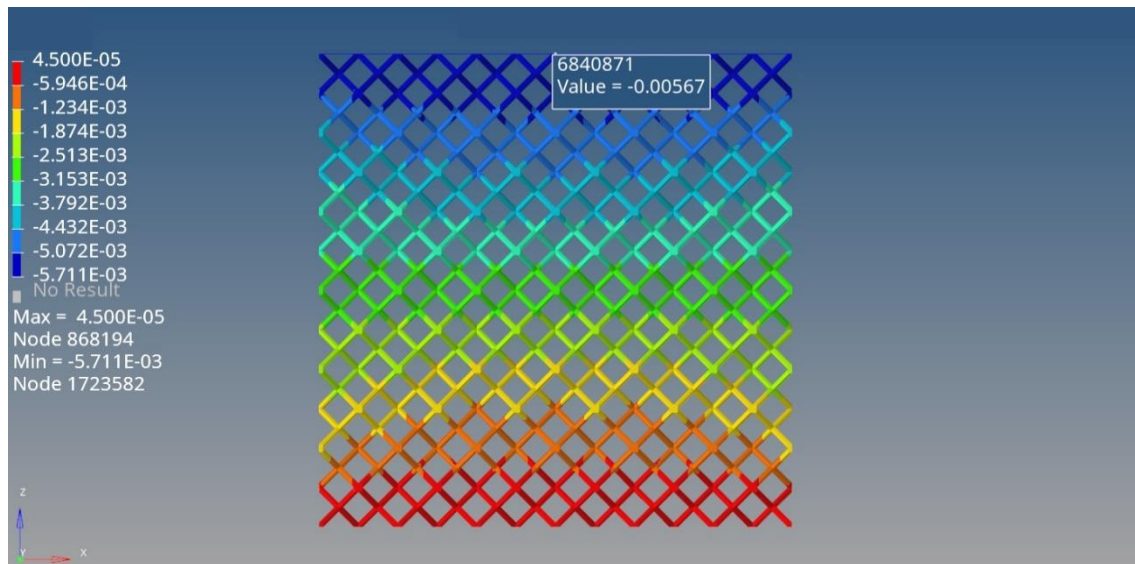
Figure 84 Reticular component - Compression Z direction
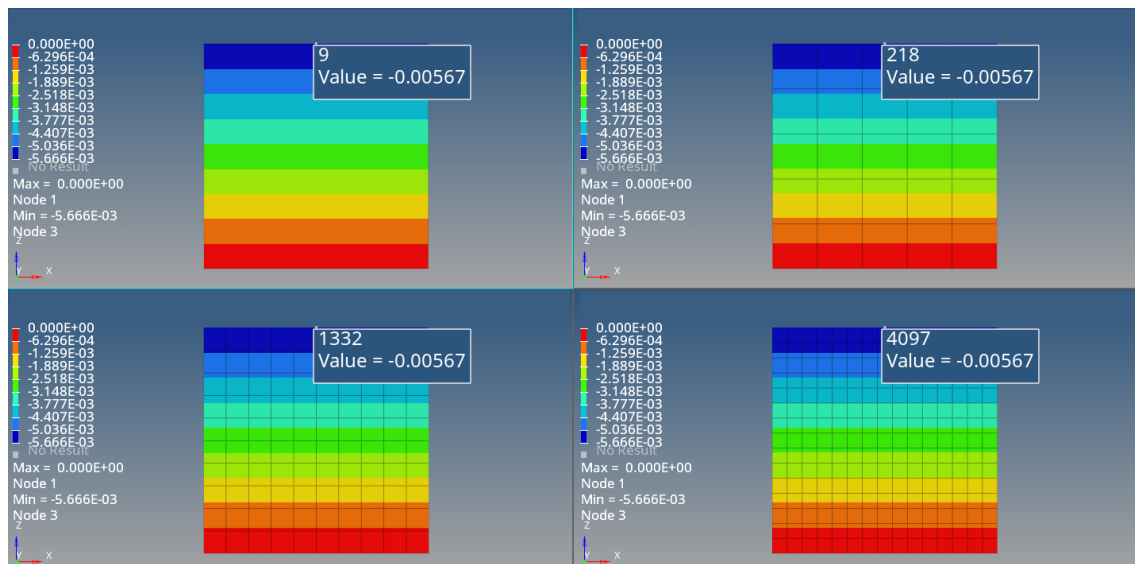
Figure 85 Equivalent solid - Compression Z direction
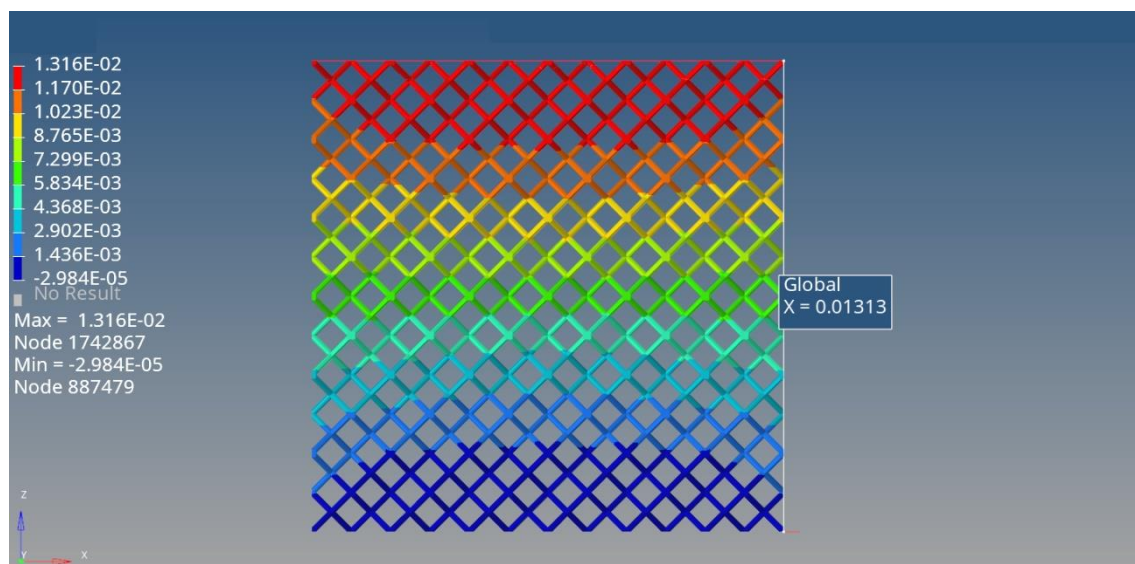
Figure 86 Reticular component - Shear XZ plane
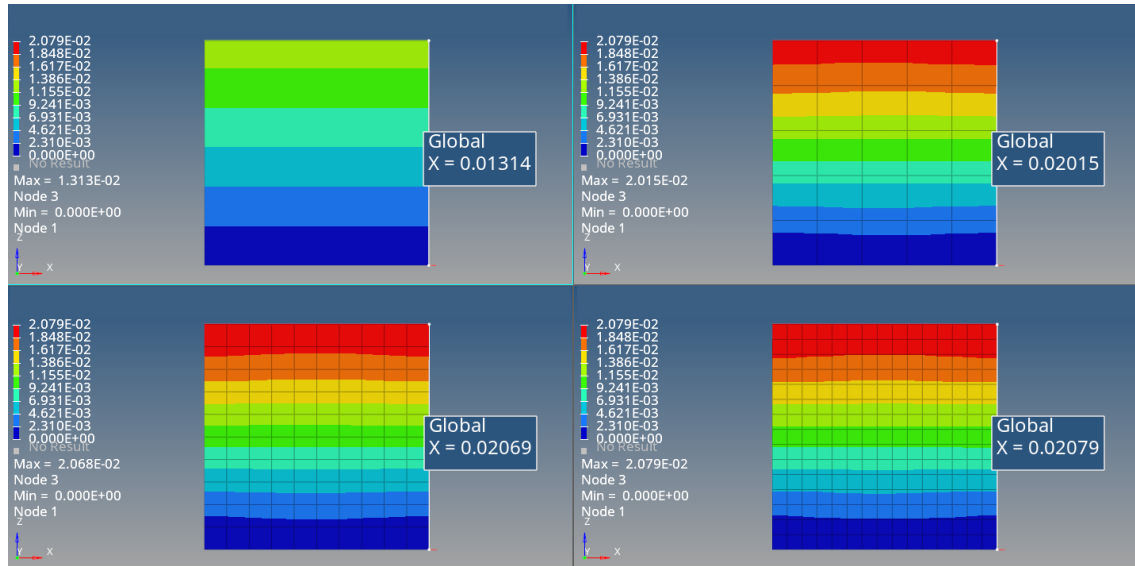
Figure 87 Equivalent solid - Shear XZ plane

Table 17 Cubic volume (6x6x6 unit cells): comparison between reticular component and equivalent solids

Compression Z	Ret. Component	Eq. Solid (1)	Eq. Solid (5)	Eq. Solid (10)	Eq. Solid (15)
σ_z [MPa]	0.028	0.028	0.028	0.028	0.028
Displacement [mm]	5.66E-03	5.67E-03	5.67E-03	5.67E-03	5.67E-03
ϵ_z	9.43E-05	9.44E-05	9.44E-05	9.44E-05	9.44E-05
E_z [MPa]	294.15	294.15	294.15	294.15	294.15
Discrepancy [%]	0	-5.51E-04	-5.51E-04	-5.51E-04	-5.51E-04

Table 18 Cubic volume (6x6x6 unit cells): comparison between reticular component and equivalent solids

Shear XZ	Ret. Component	Eq. Solid (1)	Eq. Solid (5)	Eq. Solid (10)	Eq. Solid (15)
τ_{xz} [MPa]	0.028	0.028	0.028	0.028	0.028
Displacement [mm]	1.31E-02	1.31E-02	2.01E-02	2.07E-02	2.08E-02
γ_{xz} [rad]	2.19E-04	2.19E-04	3.36E-04	3.45E-04	3.47E-04
G_{xz} [MPa]	126.90	126.88	82.72	80.57	80.15
Discrepancy [%]	0.00	0.01	34.82	36.51	36.84

In the above tables, the discrepancy values are calculated with respect to the reticular component using this relation:

$$discrepancy = \left(\frac{Ret.Component - Eq.Solid}{Ret.Component} \right) \cdot 100$$

Opposite to the previous cases, it is essential to underline that an equivalent solid composed of only one element presents a short discrepancy in Young's modulus with respect reticular component. This result occurs because a rhombic dodecahedron unit cell translation creates the reticular component along three reference axes. This single cell isn't ideally 10x10x10 mm, so when the unit cells' number grows in the reticular component, this short discrepancy is propagated. So the dimensions are different concerning the equivalent, which is created as a single block and is 60x60x60 mm. Moreover, the discrepancy is around 10-4, which is negligible. It is possible to note different considerations about two different types of moduli considering an increasing the number of elements in the solid:

- Young's modulus → The discrepancy referred to as the reticular component stays constant, and convergence is reached soon, making the result mesh independent. It is possible to state that equivalent moduli determined are correct. Another feature to underline is the variation concerning Young's modulus evaluated in a component composed of 27 unit cells: the previous value is 309.95 MPa, while the actual one is 294.15 MPa. This variation is caused by the increase of cells in the thickness of equivalent solid, which permits better evaluation of the compression, introducing more compliance in the structure. Regarding this result, Young's modulus variation is around 5.09%, and so the improvement in the equivalent modulus definition is negligible. Indeed, it must be remembered that if the analysis elements increase, time and costs grow exponentially. For example, to run this type of analysis using 27 or 216 unit cells, time increases significantly: from 00:03:05 to 01:28:44.

This result states that to evaluate equivalent Young's moduli correctly is sufficient a reticular component, the sample, formed by at least 3 unit single cells in the thickness. This conclusion permits obtaining a reasonable estimation of equivalent moduli without causing a waste of time and high computational cost.

To reinforce this conclusion are shown element stresses distributions in both component 27 and component 216 unit cells:
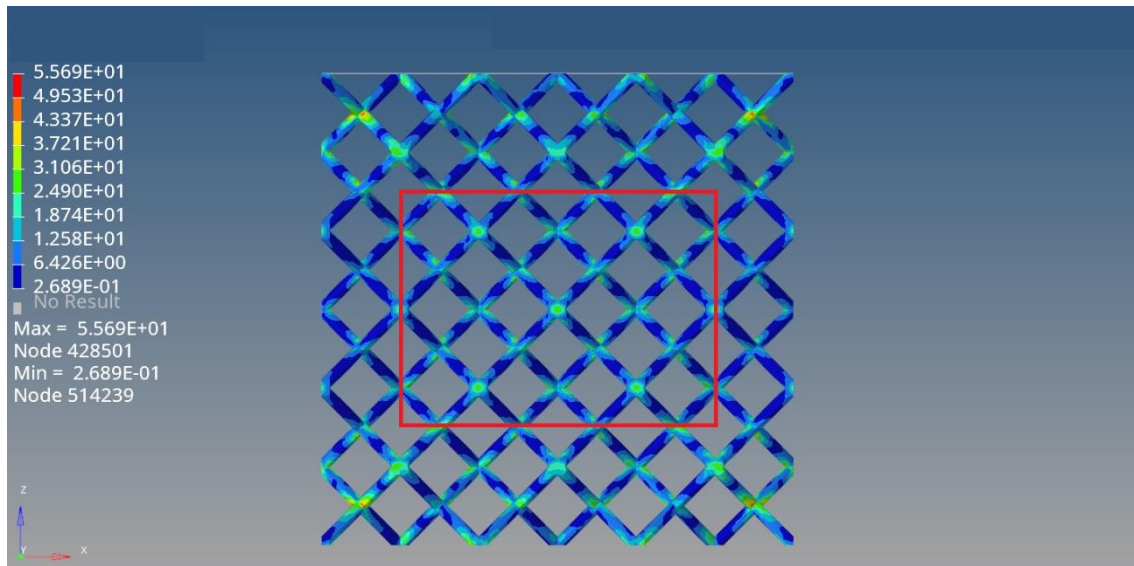
Figure 88 Element stresses detail of component composed by 27 unit cells
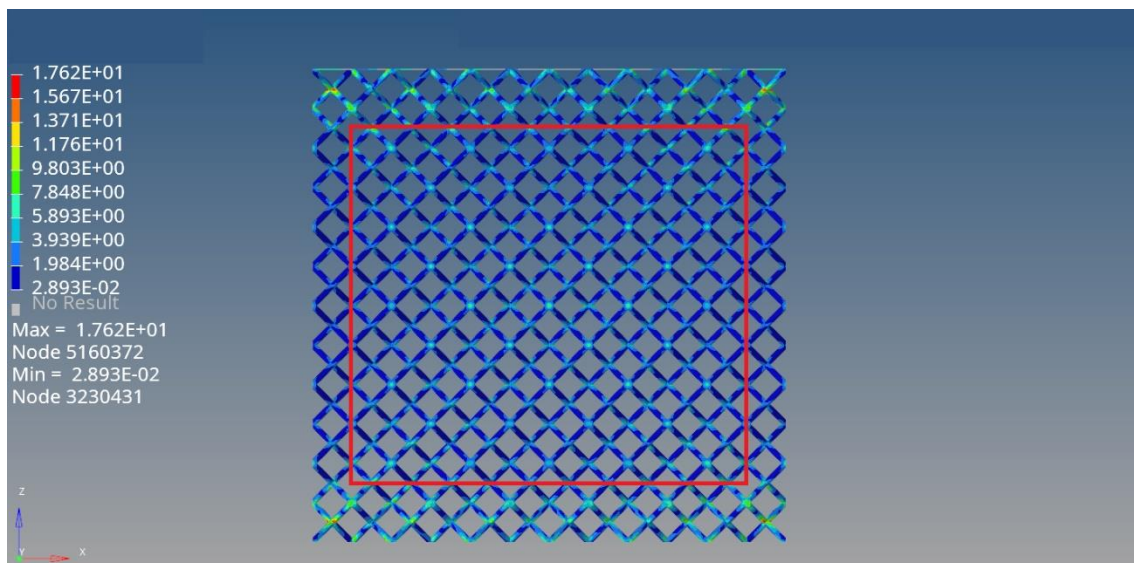
Figure 89 Element stresses detail of component composed by 216 unit cells

In the pictures, areas are squared to underline how the boundary conditions are relevant only for the unit cell close to the upper and lower surfaces. This zone can be quantified as ¾ of a single unit cell, so the choice of using 3 unit cells in the thickness is justified because the effects of the boundary conditions are mitigated

- Shear's modulus → The discrepancy tends to increase when the elements' number grows. This result can be justified because the structure becomes less stiff than a single element, so the displacement along the force application direction increases. Referring to the mode to determine the angle and modulus, the modulus becomes smaller if the displacement increases.

  Comparing this result with the component 27 unit cell one, it is primarily increased because compliance is grown significantly, and a more considerable thickness is similar to a lever arm in a bending moment. Regarding this, another consideration must be done: the constraints and load application create a pure shear, but in reality, this makes a bending moment. So the shear's moduli obtained by a component of 6x6x6 unit cells are incorrect

At the end of this step, many conclusions are stated:

- Young's moduli can be determined using at least 3 unit cells in the thickness of the reticular component
- Shear's moduli produce many problems if a cubic equivalent volume is considered and the convergence isn't reached

According to this conclusion, something must be changed to determine these equivalent moduli.

3.3.2.2. Equivalent solid: Plate

It is evident how a cubic equivalent volume cannot be used to persecute the thesis' target because it presents many problems related to Shear's moduli.

Considering the thickness effect and the load applied, which is a pure shear, the idea is to shift the concept of equivalent solid from a cube to a plate. It is important that the equivalent solid must be the same to determine Young's moduli and evaluate Shear's ones. So the thickness is fixed to 3 unit cells, while some studies are conducted on the other two solid's dimensions to correctly estimate the unit cell's number.

3.3.2.2.1. Plate volume: Dimensional study

First, this type of study is limited by the software's computational power because if the number of unit cells grows, nodes and elements vastly increase, and the solver doesn't conclude analysis because they are too expensive and allocated memory is insufficient.

To define the other two equivalent solid dimensions (length and depth), only shear load is considered because this kind of load generates problems in the moduli determination. While Young's modulus is stated before that, a thickness of 3 unit cells is necessary to evaluate the moduli correctly.

According to the idea of using a plate as equivalent volume, the first analysis regards a reticular component composed of 216 unit cells. It presents 12 unit cells located along the length of component (a), 6 unit cells situated along the depth of component (b), and 3 unit cells disposed along the height (c).

This volume is composed of 3830977 CTETRA elements and 6830219 nodes.

The following picture reports a scheme to understand this equivalent volume definition and the next ones better:
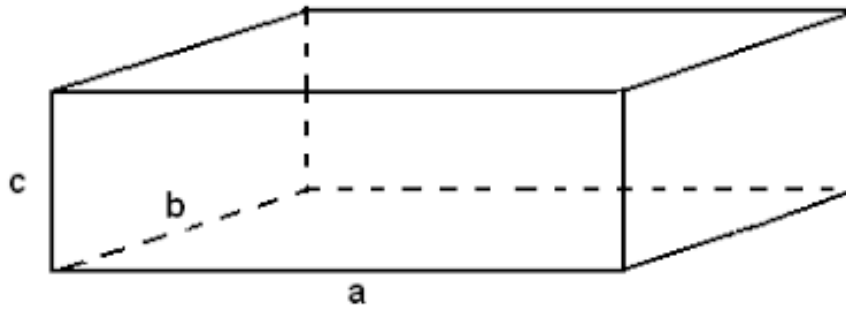
Figure 90 Scheme of plate dimensions

In the beginning, the reticular component is created and defined by MAT9 using the powder stiffness matrix as in the previous cases. Successively the shear's load is applied, and the modulus is estimated.

In the second part, the validation consists of meshing the equivalent solid in different ways to understand the shape and dimension of mesh elements, which permits the production of a result that is coherent with the reticular one.

Results obtained by analysis are reported numerically and graphically below:

Table 19 Plate volume: First analysis

	Ret. Component	Eq. Solid (1)	Eq. Solid (5h)	Eq. Solid (10Lx6Dx5H)
τ_{xz} [MPa]	0.014	0.014	0.014	0.014
Displacement [mm]	2.14E-03	2.14E-03	2.23E-03	2.38E-03
γ_{xz} [rad]	7.12E-05	7.15E-05	7.43E-05	7.93E-05
G_{xz} [MPa]	195.05	194.35	187.03	175.04
Discrepancy [%]	0.00	0.36	4.11	10.26
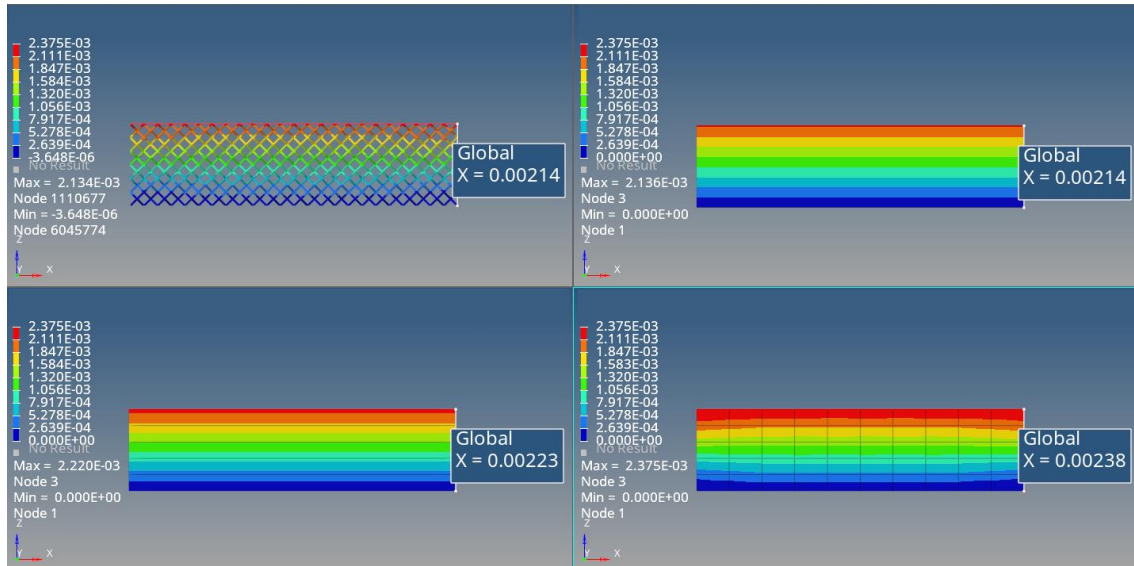
Figure 91 Shear XZ plane

Regarding the results of these simulations, it can be possible to state some considerations:

- When the mesh is composed of only one element, results are coincidence with the reticular component less than a short discrepancy due to the solver approximation
- When equivalent solid has meshed using 5 plate elements, results can be considered correct because the discrepancy produced is around 4.11%, and so it is acceptable
- When mesh's elements increase a lot (10x6x5), the simulation produces a not negligible error of around 10%

These results confirm that an equivalent solid must be similar to a plate, so some research is conducted to identify the correct shape and dimensions of the equivalent solid.

During this research is found a thesis work where a mechanical characterization of a sandwich panel is done [4]. This work presents how tests are correctly realized and samples' dimensions and shapes. According to this information, it is defined that the shear test sample must have a length of at least 12 times the thickness.

The second type of analysis is conducted on a reticular component composed of 324 rhombic dodecahedron unit cells. It has 36 unit cells in length (a), 3 unit cells in depth (b), and 3 unit cells in thickness (c). It is formed by 5645377 CTETRA elements and 1602446 nodes.

The simulation procedure is the same as in the previous cases: the reticular component is defined as MAT9 using the powder's stiffness matrix, and shear's modulus is evaluated. This modulus is attributed to the equivalent solid and tested.

In this case, the scope is to determine the correct shape, dimension, and the mesh's elements number to reach a mesh independent condition.

This part consists of four different steps which correspond to four different ways to generate elements:

1. Elements are created by dividing the equivalent solid with planes that are orthogonal to the YZ plane and parallel to the XY plane

2. Elements are created by dividing the equivalent solid with planes that are orthogonal to the XY plane and parallel to the YZ plane

3. Elements are created by dividing the equivalent solid with planes that are orthogonal to the XY plane and parallel to the XZ plane

4. Elements are created by mixing previous cases, varying the number of elements considered

In the following results are reported, and some considerations are made:

1. Elements are created by dividing the equivalent solid with planes that are orthogonal to the YZ plane and parallel to the XY plane:

Table 20 Plate volume: Second analysis

	Ret. Component	Eq. Solid (5H)	Eq. Solid (25H)
τ_{xz} [MPa]	0.093	0.093	0.093
Displacement [mm]	8.85E-03	8.91E-03	8.91E-03
γ_{xz} [rad]	2.95E-04	2.97E-04	2.97E-04
G_{xz} [MPa]	313.87	311.72	311.72
Discrepancy [%]	0.00	0.68	0.68
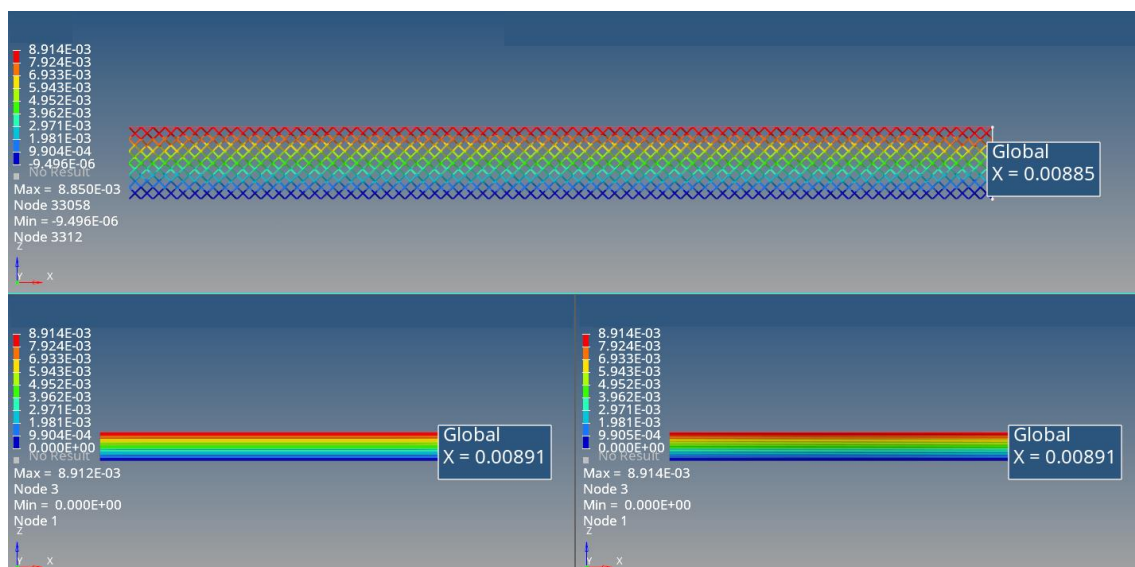
Figure 92 Shear XZ plane: Reticular component, Eq. Solid 5H, and Eq. Solid 25H

95

This first study determines the importance of having a plate element's mesh. Indeed, equivalent solid with 5 and 25 plates overlapped presents shear's moduli very close to the reticular component. The discrepancy is around 0.68%, so this result soon becomes mesh independent. This short difference is due to the number of elements in the equivalent solid thickness. If there are some elements in this area, the compliance of the solid grows, so a more significant displacement is produced, decreasing the shear's modulus. But the considerable dimensions of elements and their plate shape permit obtaining the correct equivalent modulus.

These results indicate that the plate is the better solid to determine a correct shear's modulus. Indeed, when the plate's thickness is reduced (from 5H to 25H), the result is constant and close to the estimate. This conclusion follows the plate's definition: a solid where two dimensions are more significant than the third one.

2. Elements are created by dividing the equivalent solid with planes that are orthogonal to the XY plane and parallel to the YZ plane:

Table 21 Plate volume: Third analysis

	Ret. Component	Eq. Solid (5D)	Eq. Solid (25D)
τ_{xz} [MPa]	0.093	0.093	0.093
Displacement [mm]	8.85E-03	8.85E-03	8.85E-03
γ_{xz} [rad]	2.95E-04	2.95E-04	2.95E-04
G_{xz} [MPa]	313.87	313.87	313.87
Discrepancy [%]	0.00	0.00	0.00
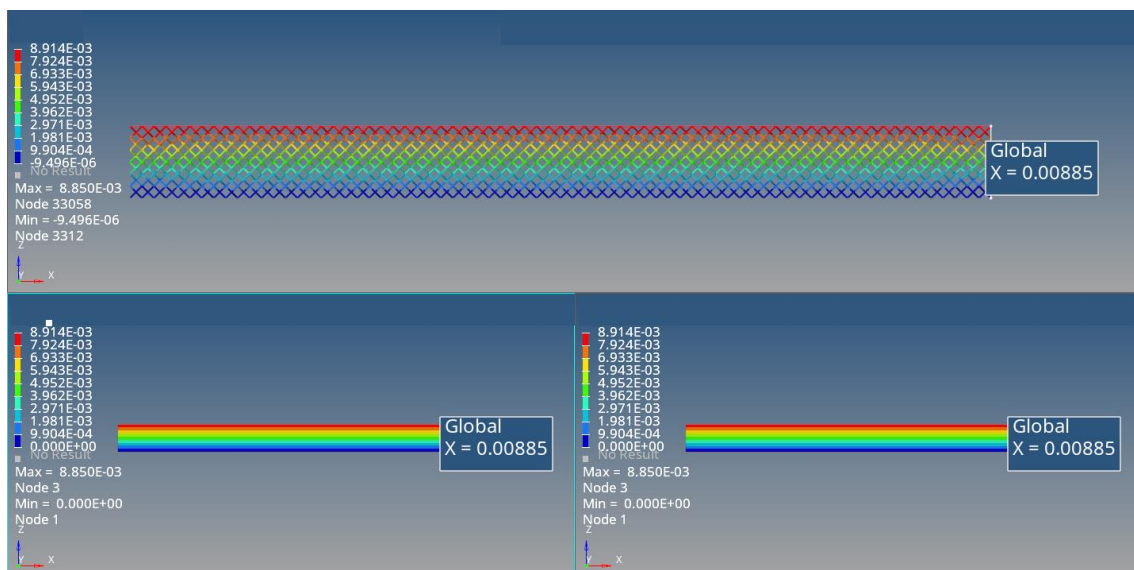
Figure 93 Shear XZ plane: Reticular component, Eq. Solid 5D, and Eq. Solid 25D

The second point follows the same idea as the previous one. Regarding the results in the table, it is evident that having elements mesh with a plate's shape is essential to evaluate the shear's modulus better. Indeed, an equivalent solid with 5 and 25 plates side by side presents shear's moduli the same as the reticular component one. This result is significant because mesh independence will be reached soon. This behavior is justified by the presence of only one element along the height of the equivalent solid. The results are coincident because the way to determine the equivalent modulus of the reticular component includes only one element along the height.

3. Elements are created by dividing the equivalent solid with planes that are orthogonal to the XY plane and parallel to the XZ plane:

Table 22 Plate volume: Fourth analysis

	Ret. Component	Eq. Solid (5L)	Eq. Solid (25L)
τ_{xz} [MPa]	0.093	0.093	0.093
Displacement [mm]	8.85E-03	8.85E-03	8.85E-03
γ_{xz} [rad]	2.95E-04	2.95E-04	2.95E-04
G_{xz} [MPa]	313.87	313.87	313.87
Discrepancy [%]	0.00	0.00	0.00
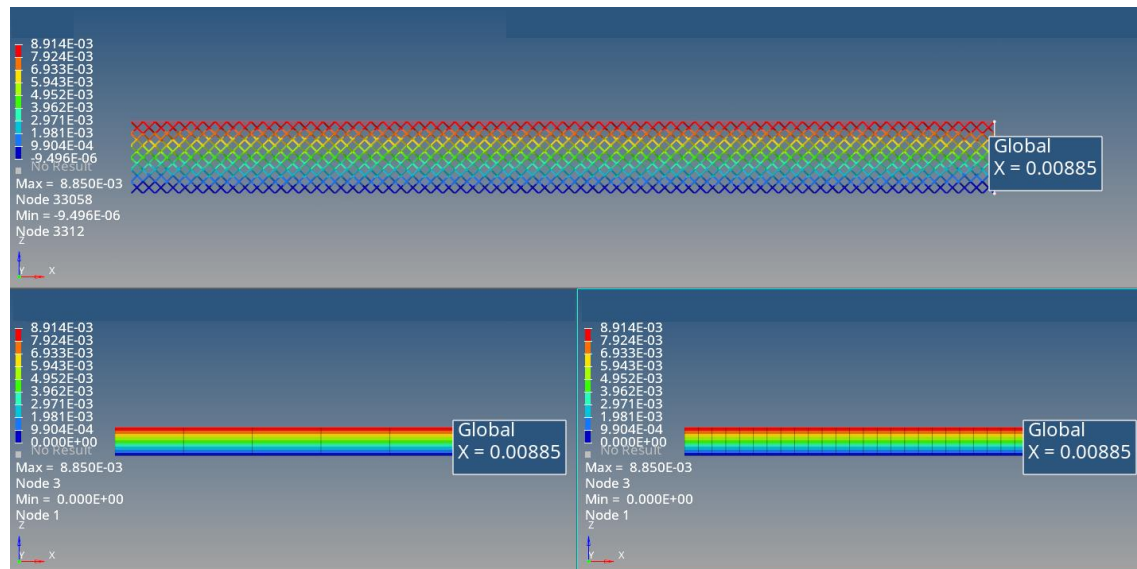
Figure 94 Shear XZ plane: Reticular component, Eq. Solid 5L, and Eq. Solid 25L

The third point follows the same idea as the previous ones. Regarding the results, it is evident the importance of having a plate element's mesh to evaluate the shear's modulus better. Indeed,

an equivalent solid with 5 and 25 plates side by side presents shear's moduli the same as the reticular component one. This result is significant because mesh independence is reached soon. This behavior is justified by the presence of only one element along the equivalent solid's height as in the previous case. The results are coincident because the way to determine the equivalent modulus of the reticular component includes only one element along the height.

4. Elements are created by mixing previous cases, varying the number of elements considered

Table 23 Plate volume: Fifth analysis

	Ret. Component	Eq. Solid (5Hx5L)	Eq. Solid (36Lx3Dx3H)	Eq. Solid (60Lx5Dx7H)
τ_{xz} [MPa]	0.093	0.093	0.093	0.093
Displacement [mm]	8.85E-03	9.00E-03	9.25E-03	9.28E-03
γ_{xz} [rad]	2.95E-04	3.00E-04	3.08E-04	3.09E-04
G_{xz} [MPa]	313.87	308.55	300.40	299.42
Discrepancy [%]	0.00	1.69	4.29	4.61
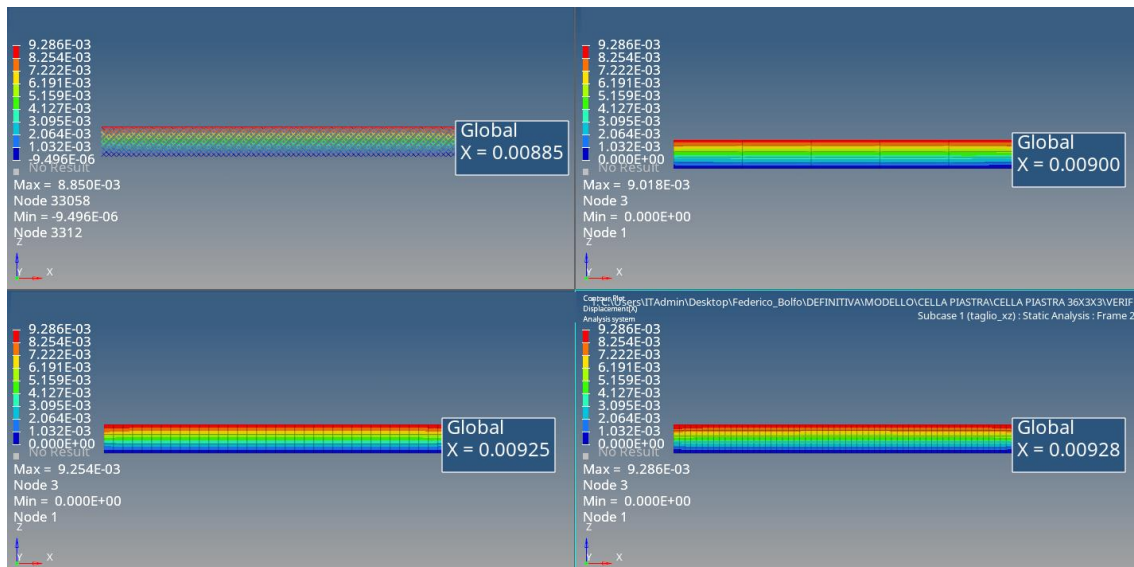
Figure 95 Shear XZ plane: Reticular component, Eq. Solid 5Hx5L, Eq. Solid 36Lx3Dx3H, and Eq. solid 60Lx5Dx7H

The first three studies suggest that elements on the thickness largely influenced the convergence of the solution, and they underline that the equivalent modulus determined is incorrect.

This last point of the study is involved mixing the previous cases, and the results confirm this trend.

Regarding the shear's modulus, it is possible to state different conclusions:

- Eq. Solid 5Hx5L → If it is compared with the first case, the dimensions of the elements are changed. The element's shape is a plate shorter than before, so the boundary effects are amplified, incrementing the discrepancy from 0.68% to 1.69%. This result suggests that the elements' dimensions and shape must be defined to mesh the equivalent solid correctly

- Eq. Solid 36Lx3Dx3H → Regarding the previous results, the idea to mesh the equivalent solid with an elements number equal to the rhombic dodecahedron unit cell is followed, and the result shows a discrepancy not very high and around 4.29%, this is acceptable

- Eq. Solid 60Lx5Dx7H → The consciousness of the result obtained above the number of elements is increased, and it is possible to underline how the discrepancy remains more or less constant, so the result is acceptable. In conclusion, it is discovered that using a number of elements paired with the number of unit cells produces a valuable result and a slight discrepancy compared to the expected one

At the end of this paragraph, some conclusions are defined: the equivalent solid to consider in evaluating the equivalent moduli of a lattice structure is a plate whose dimensions are determined by the ratio between length and thickness, which must be at least 12 times. Moreover, the number of elements in the equivalent solid must amount to the same number of unit cells because tests demonstrate that this solution permits correctly describing the trends of the reticular structure. Suppose the elements in the equivalent solid are more conspicuous. In that case, the results aren't different from the previous one, but the number of nodes and time to solve the simulation increase.

3.3.2.2.2. Boundary conditions study

In the previous paragraph, some conclusions are reached: the equivalent shear's modulus determined on the reticular component, and the equivalent solid one is different and sensitive to the reticular component dimensions. This result instills doubts about the boundary conditions.

Indeed, suppose the reticular component dimension represents the entire lattice structure to determine the equivalent moduli, and the number of elements is correct to predict the equivalent solid's behavior. In that case, the only aspect of studying is the boundary conditions. According to this, the goal of the paragraph is to determine the correct way to introduce constraints and applied load on the reticular component.

The study is divided into many types of analysis because two ways to impose constraints and two ways to introduce loads are considered. It is fundamental to underline that these application schemes must be suitable for an isotropic and anisotropic material.

This aspect becomes relevant considering the software limits regarding the Non-Linear analysis, which run only with isotropic material, and so to evaluate this behavior, a MAT1 is used. While equivalent moduli are determined considering a Linear analysis, an anisotropic material MAT9 is used.

Some experimental dates regarding lattice structure are necessary to determine the correct application scheme. This working thesis doesn't provide experimental tests, so these dates aren't suitable.

The importance of the definition application scheme is fundamental to define a methodology better to analyze a lattice structure, so another way must be found.

The idea is to create an equivalent solid constituted by aluminium whose dimensions are 360x60x30 mm. These sizes respect all conditions previously defined. The depth is double necessary. Still, the scope is to create a solid as close to a plate as possible, respecting the computational software's limits.

The aluminium choice is influenced by the knowledge of its Young's modulus (70000 MPa) and Poisson's coefficient (0.33). The relationship between Young's modulus, Poisson's coefficient, and Shear's modulus is known, so it is possible to define MAT1 and MAT9 materials to attribute to the simulation's sample.

Using a knowing material permits to compare the simulation results with the real ones and verify their correctness.

The test's procedure is opposite to the previous one because it starts from an equivalent solid and determines the equivalent moduli. Successively it is compared to the reticular one.

Following this strategy, an application scheme for loads and constraints is defined.

This study considers only compression in the Z direction and shear XZ plane; they are representative of all loads type, and so their results permit to state general conclusions.

During this part of the thesis, the way to evaluate the displacement caused by the shear load is changed because previous results suggest that the displacement of an external node is more significant than the displacement of the force application node. This effect is due to boundary conditions that predominantly affect the result and because compliance is stronger in that area.

In the following picture, the new approach is graphically reported:
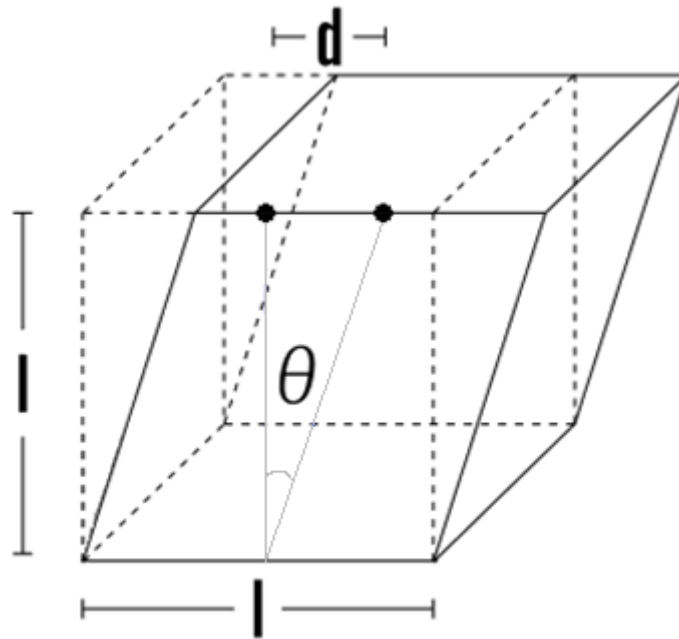
Figure 96 Shear's modulus determination: New methodology

In contrast, the displacement caused by compression load is evaluated regarding the central node of the upper surface or the applied load node to delete the boundary condition influence. The boundary conditions study is divided into 4 parties:

1. Isostatic constraints and pressure load
2. Isostatic constraints and force load
3. Elastic constraints and pressure load
4. Elastic constraints and force load

In the following, each part is deepened to show the application scheme, results better and to state conclusions:

1. Isostatic constraints and pressure load:

Below two pictures show the scheme of loads and constraints application:
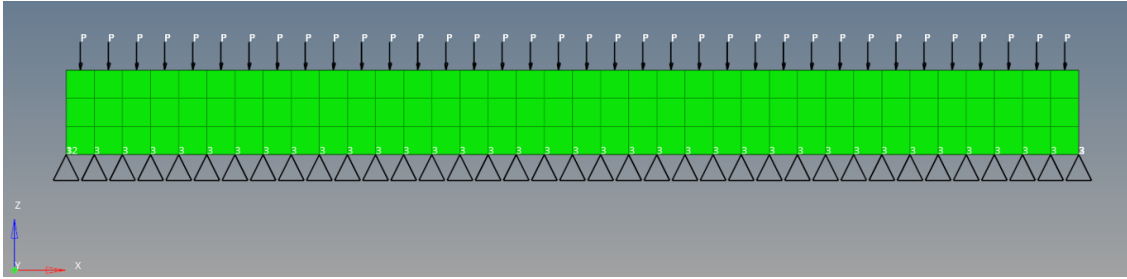
Figure 97 Compression Z: Isostatic constraints + Pressure load

Figure 98 Shear XZ: Isostatic constraints + Pressure load

The table summarizes the results of the simulation considering isotropic and anisotropic material loaded with compression and shear load:

Table 24 Constraints and applied load study

ISOSTATIC CONSTRAINTS + PRESSURE	MAT1		MAT9	
COMPRESSION Z	Eq. Solid (1)	Eq. Solid (36x6x3)	Eq. Solid (1)	Eq. Solid (36x6x3)
σ_z [MPa]	1000	1000	1000	1000
ϵ_z	1.43E-02	1.43E-02	1.43E-02	1.43E-02
E_z [MPa]	70000.00	70000.00	70000.00	70000.00
Discrepancy [%]	9.87E-07	9.87E-07	9.87E-07	9.87E-07
SHEAR XZ	Eq. Solid (1)	Eq. Solid (36x6x3)	Eq. Solid (1)	Eq. Solid (36x6x3)
τ_{xz} [MPa]				
γ_{xz} [rad]				
G_{xz} [MPa]				
Discrepancy [%]				

102

This way of applying loads and constraints generates the correct results of compression considering both an isotropic and an anisotropic material, and the results converge using one or more elements to mesh the volume. The short discrepancy is negligible and can be attributed to solver approximations.

Regarding the shear, some problems emerge because boundary conditions create a deformed volume, not coherent with the real one, so these results aren't considered to evaluate the shear's modulus.

In the pictures are reported volumes deformed:
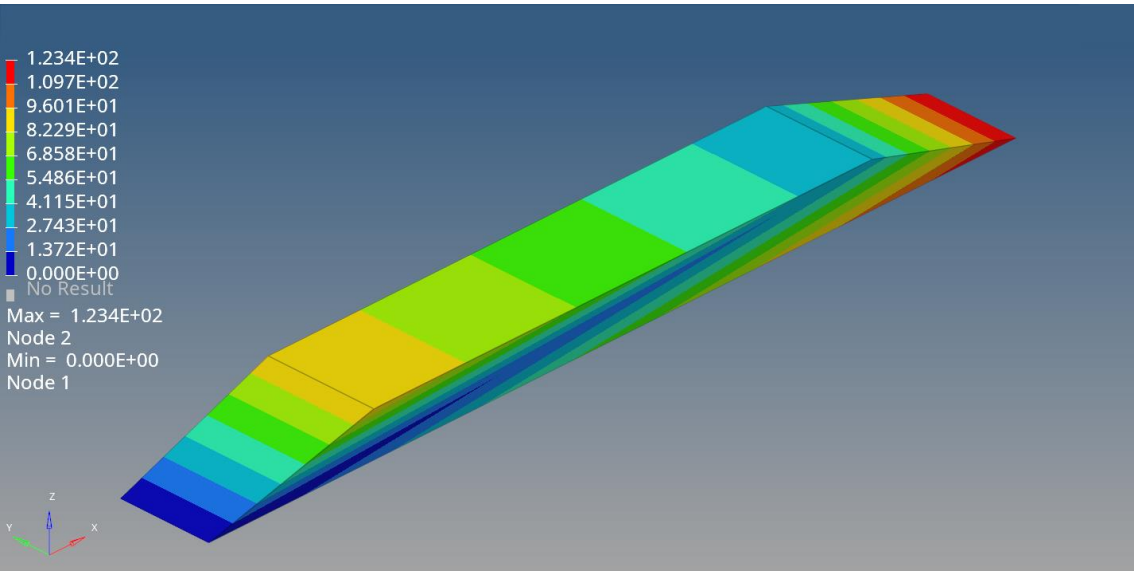
Figure 99 Shear XZ: Incorrect deformation (Eq. Solid (1))

Figure 100 Shear XZ: Incorrect deformation (Eq. Solid (36x6x3))

Considering an isotropic or an anisotropic material is the same in terms of deformed volume. If a comparison between the volume composed of only one element and the volume consisting of many elements is made, the differences are evident. Regarding the first one, the deformation is affected mainly by the effects of isostatic constraints because the volume has the freedom to slide on the plane. So the lower surface moves more than the upper one. These different displacements create a deformed structure like in the picture, so it is useless to determine the correct shear's modulus.

The behavior is more different than before, considering the second one. In this case, the freedom imposed by constraints permits the node situated along the Y axis to slide in the negative Y direction and go through the node located in the reference system's origin. This movement generates the deformed structure shown in the picture above, so it is impossible to use it to determine the correct shear's modulus.

2. Isostatic constraints and force load:

Below two pictures show the scheme of loads and constraints application:
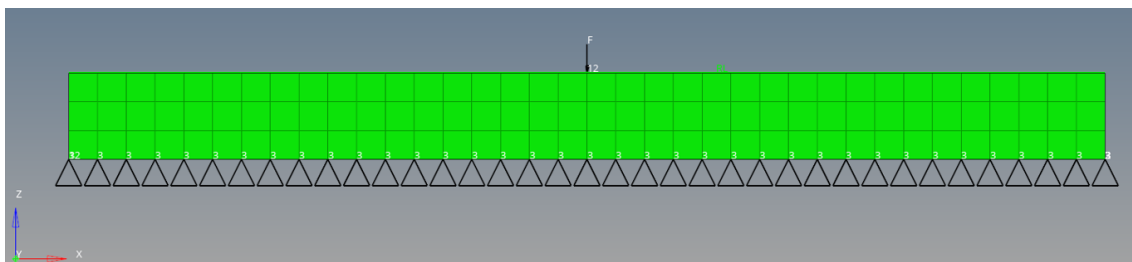
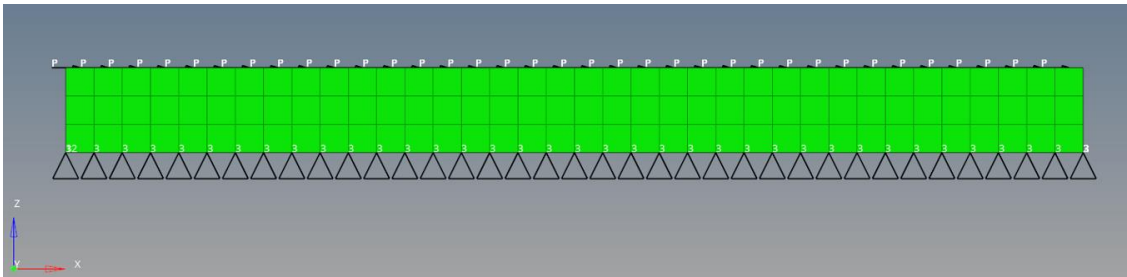*Figure 101 Compression Z: Isostatic constraints + Force load*
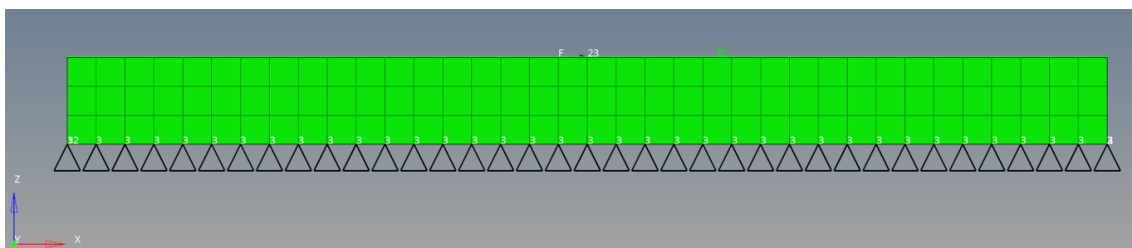
Figure 102 Shear XZ: Isostatic constraints + Force load

The table summarizes the results of the simulation considering isotropic and anisotropic material loaded with compression and shear load:

Table 25 Constraints and applied load study

ISOSTATIC CONSTRAINTS + FORCE	MAT1		MAT9	
COMPRESSION Z	Eq. Solid (1)	Eq. Solid (36x6x3)	Eq. Solid (1)	Eq. Solid (36x6x3)
σ_z [MPa]			0.046	0.046
ϵ_z			6.61E-07	6.61E-07
E_z [MPa			69999.89	69999.89
Discrepancy [%]			1.52E-04	1.52E-04
SHEAR XZ	Eq. Solid (1)	Eq. Solid (36x6x3)	Eq. Solid (1)	Eq. Solid (36x6x3)
τ_{xz} [MPa]				
γ_{xz} [MPa]				
G_{xz} [MPa]				
Discrepancy [%]				

This way of applying loads and constraints generates the correct results of compression considering only an anisotropic material and the results are convergent using one or more elements to mesh the volume. The short discrepancy is negligible and can be attributed to solver approximations. If compression of an isotropic volume is considered, the deformed structure is incorrect regarding the real one, so it is not used to define the modulus.

Regarding the shear, some problems emerge because boundary conditions create a deformation volume, not coherence with the real one, so these results aren't considered to evaluate the shear's modulus.

In the pictures are reported volume deformed:
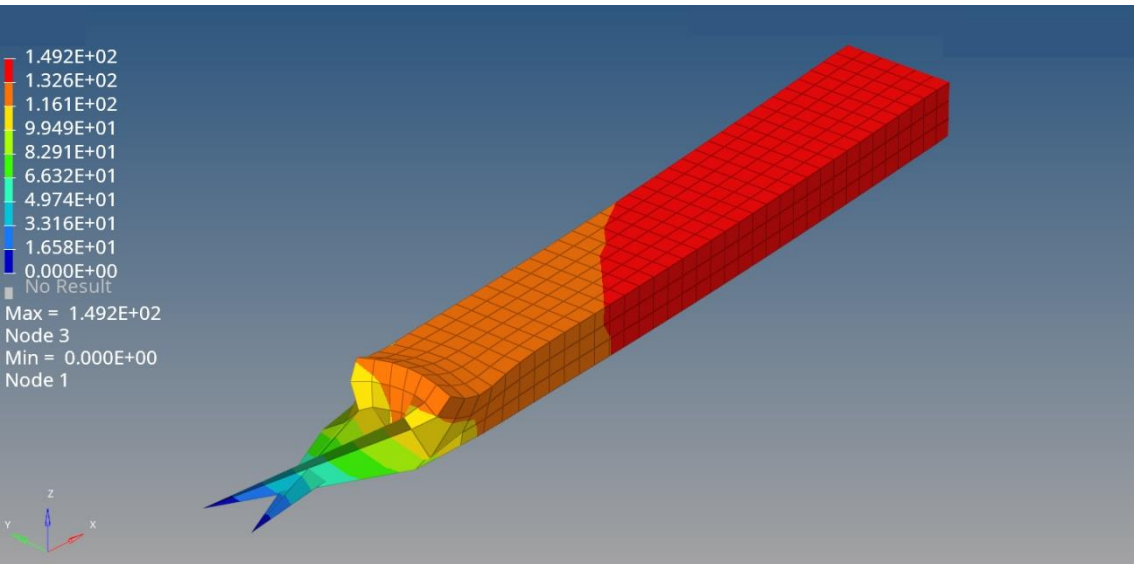

Figure 103 Compression Z: Incorrect deformation (x1000000) (Eq. Solid (1))

Figure 104 Compression Z: Incorrect deformation (x500000) (Eq. Solid (36x6x3))
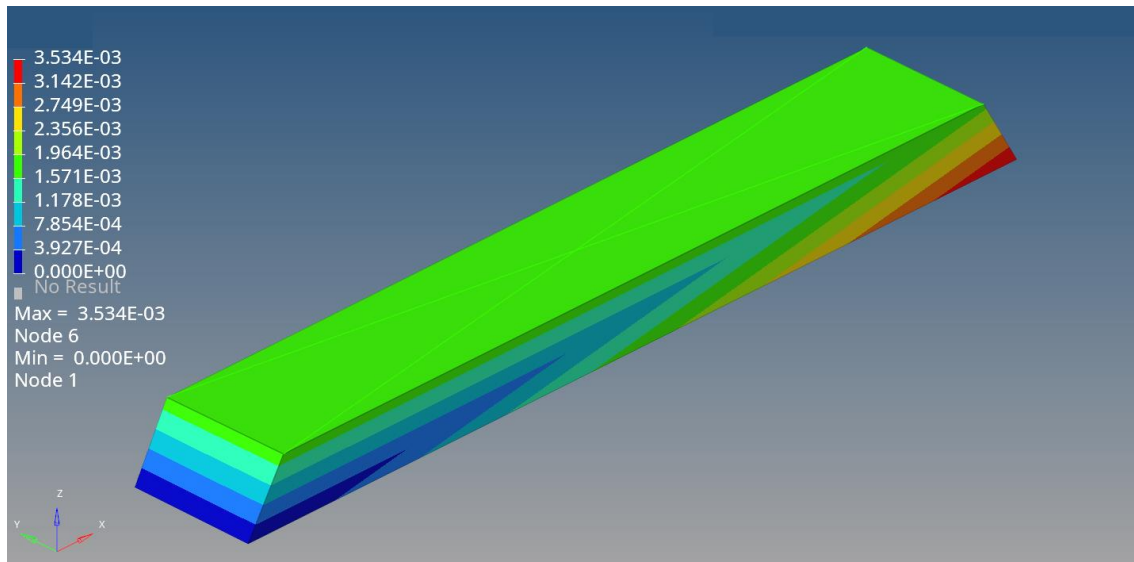
Figure 105 Shear XZ: Incorrect deformation (x10000) (Eq. Solid (1))
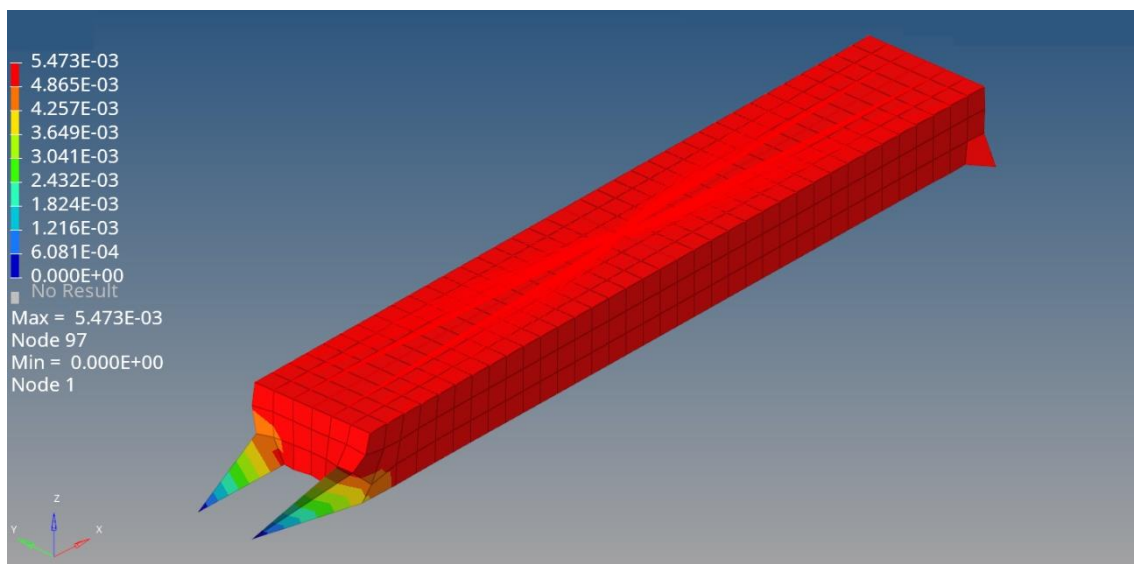
Figure 106 Shear XZ: Incorrect deformation (x10000) (Eq. Solid 36x6x3))

In this case, some considerations must be made. First of all, it is essential to underline that force is applied using a rigid element (RBE2) which imposes all slaves nodes to have the same behavior as the master one. The master node presents a constraint that permits only the displacement in the Z direction, so other degrees of freedom are locked.

Regarding the compression of an isotropic material meshed with only one element, the deformed structure has a shape different from the real one. Indeed RBE2 presence doesn't permit the upper surface to deform itself, and the isostatic constraints allow the lower one to slide along the Y and X axis. The result is that displacement in the Z direction on the reference

107

system's origin is more significant than the extremal node located along the Y axis. According to the deformed structure, this cannot be used to determine Young's modulus correctly.

The result is just a bit different regarding the compression of an isotropic volume meshed with many elements. It is due to the presence of many elements along the volume's height that increases the structure's compliance and origins the "barrel" effect. This way of applying boundary conditions seems to create a correct deformed structure, but if it is better analyzed, it isn't conformed to the real one.

Regarding the shear load applied to a volume meshed using only an element, the deformation is affected mainly by the effects of isostatic constraints because the volume has the freedom to slide on the plane. So the lower surface moves more than the upper one. These different displacements create a deformed structure like in the picture, so it is useless to determine the correct shear's modulus. Suppose a comparison is made between this result and the isostatic constraints and pressure load one; the difference is that the upper surface cannot be deformed following the load because RBE2 presence forbids displacements.

While if the volume has meshed using many elements, the deformed structure is the same as the isostatic constraints and pressure load one, but the RBE2 effects must be considered. So, this way of applying boundary conditions cannot be used to evaluate the modulus correctly.

3. Elastic constraints and pressure load:

Below two pictures show the scheme of loads and constraints application:
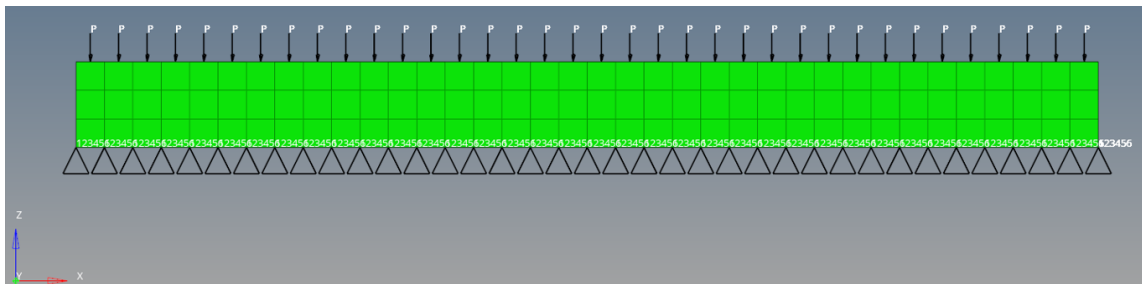
Figure 107 Compression Z: Elastic constraints + Pressure load
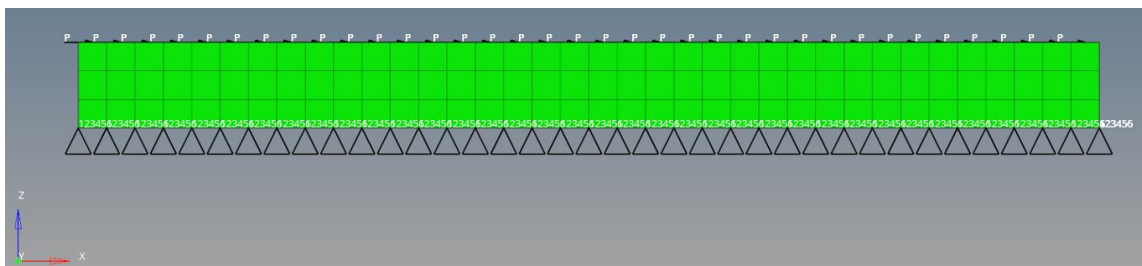
Figure 108 Shear XZ: Elastic constraints + Pressure load

The table summarizes the results of the simulation considering isotropic and anisotropic material loaded with compression and shear load:

Table 26 Constraints and applied load study

ELASTIC CONSTRAINTS + PRESSURE	MAT1		MAT9	
COMPRESSION Z	**Eq. Solid (1)**	**Eq. Solid (36x6x3)**	**Eq. Solid (1)**	**Eq. Solid (36x6x3)**
σ_z [MPa]			1000	1000
ϵ_z			1.43E-02	1.43E-02
E_z [MPa]			70000.00	70000.00
Discrepancy [%]			9.87E-07	9.87E-07
SHEAR XZ	**Eq. Solid (1)**	**Eq. Solid (36x6x3)**	**Eq. Solid (1)**	**Eq. Solid (36x6x3)**
τ_{xz} [MPa]		1000		1000
γ_{xz} [rad]		3.80E-02		3.80E-02
G_{xz} [MPa]		26286.25		26289.80
Discrepancy [%]		0.11		9.87E-02

This way of applying loads and constraints generates the correct results of compression considering only an anisotropic material and the results are convergent using one or more elements to mesh the volume. The short discrepancy is negligible and can be attributed to solver approximations. If the compression of an isotropic volume is considered, the deformed structure is incorrect from the real one, so it isn't used to define the modulus.

Regarding shear, problems emerge in both isotropic and anisotropic material when the volume has meshed with one element. These boundary conditions create a deformation volume, not coherent with the real one, so these results aren't considered to evaluate the shear's modulus.
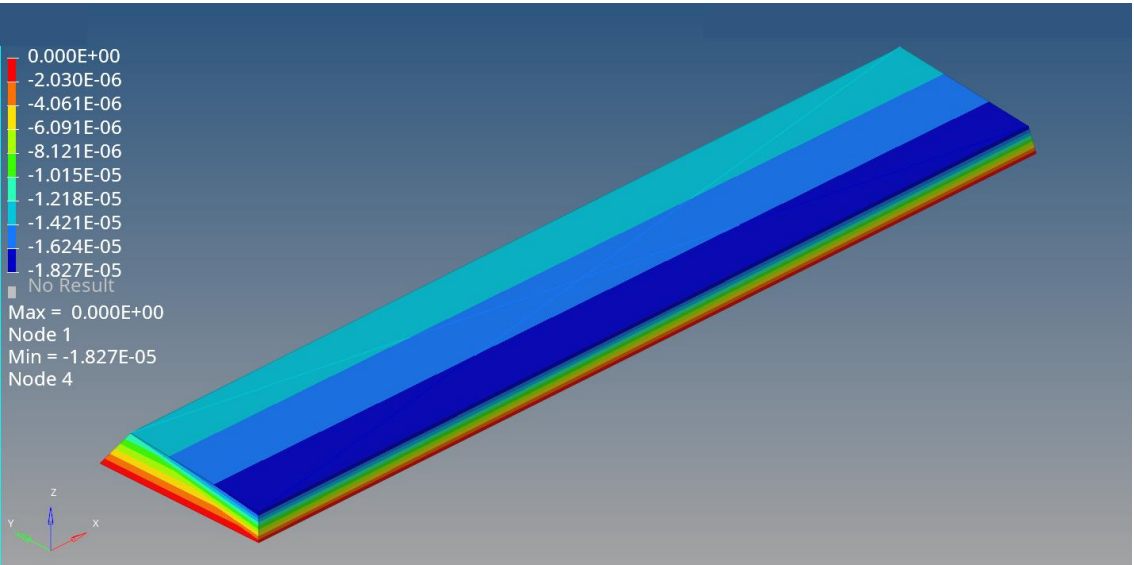
In the pictures are reported volume deformed:
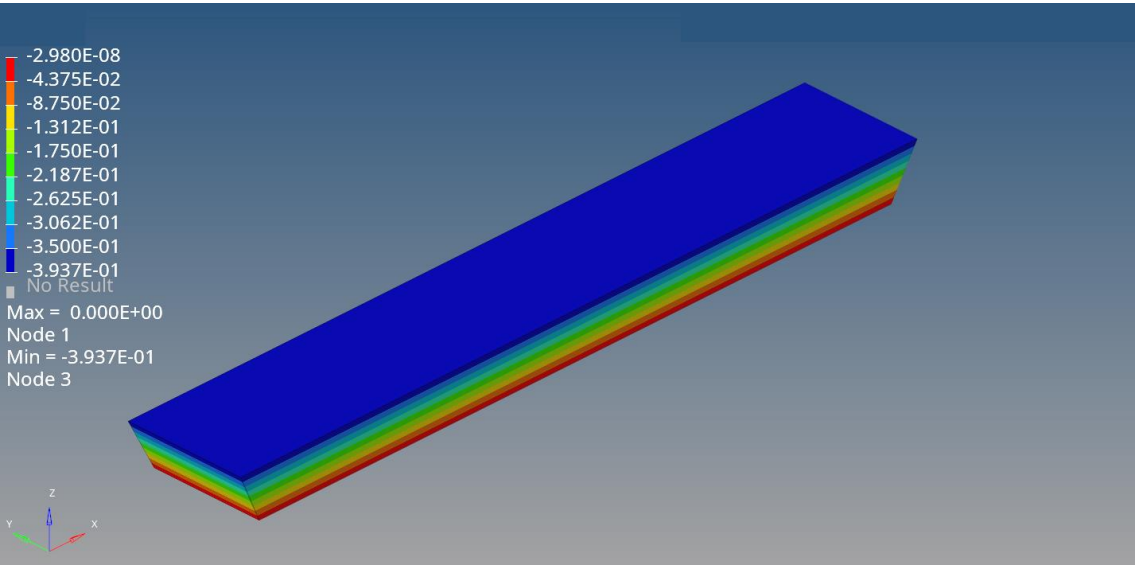
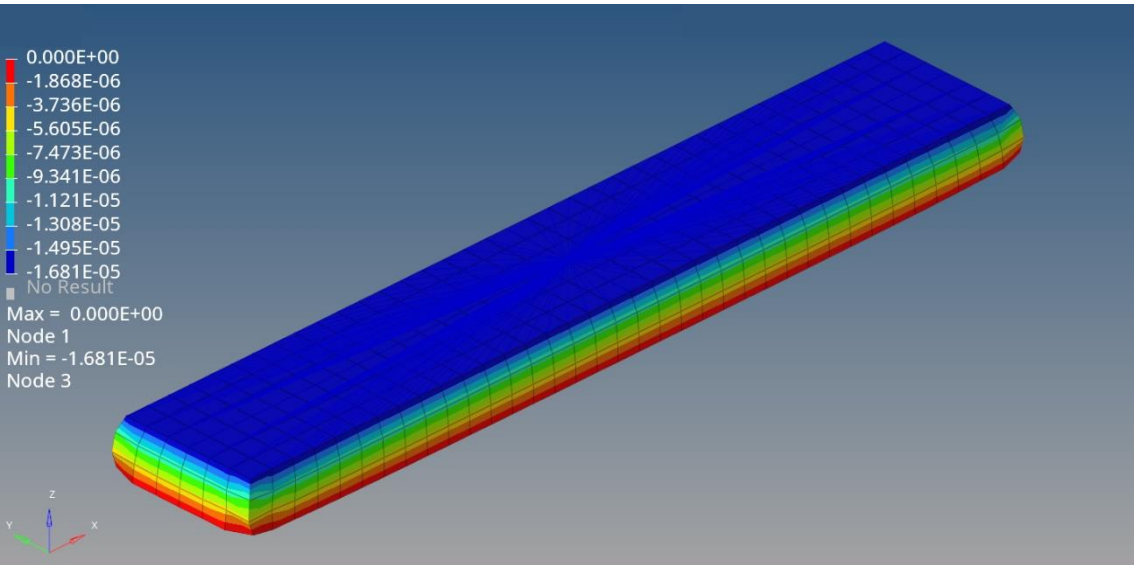*Figure 109 Compression Z: Incorrect deformation (x10) (Eq. Solid (1))*
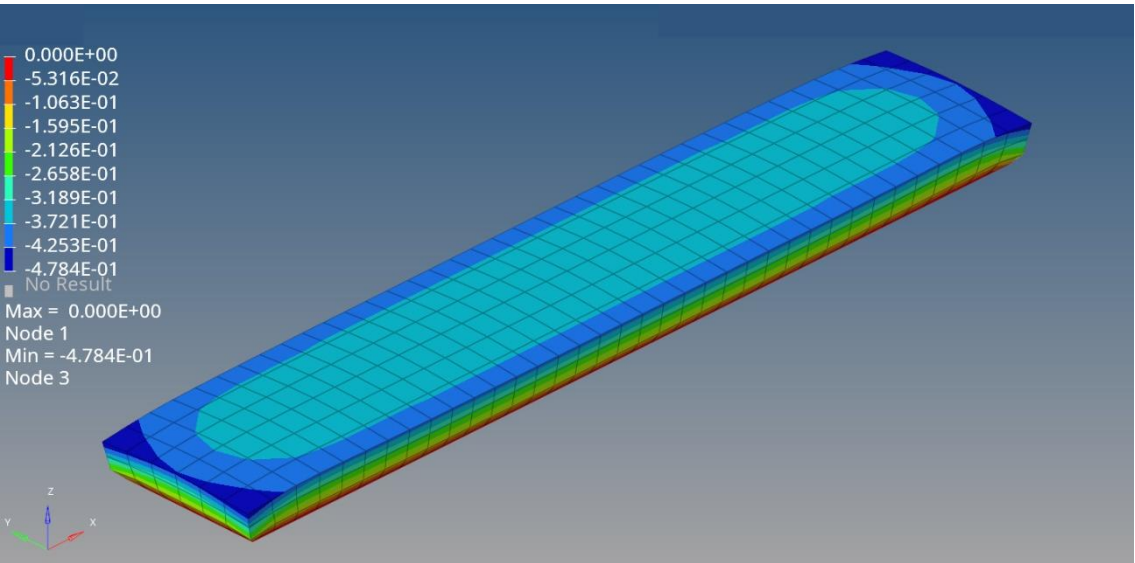
*Figure 110 Compression Z: Incorrect deformation (x30) (Eq. Solid (36x6x3))*
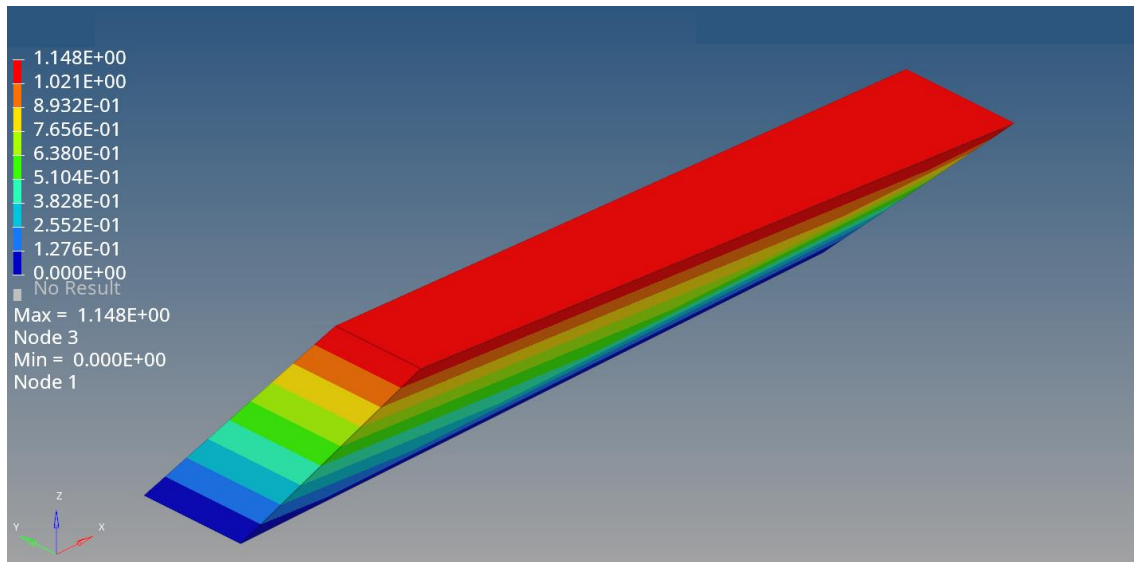
Figure 111 Shear XZ: Incorrect deformation (Eq. Solid (1))

First, consideration must be done about the constraints: they are elastic ones, and all degrees of freedom are locked, so the lower surface cannot be deformed.

This way of applying loads and constraints isn't suitable for the compression of isotropic material because the constraints dominate the deformed structure. Considering a solid meshed with only an element and so high stiffness, the structure's inability to barrel origins a distorted shape that is useless to evaluate the correct value of modulus. Furthermore, thanks to pressure load, the upper surface presents the same displacement all over the area, but the deformed structure isn't coherent with the real one.

Different considerations must be made regarding volume meshed by many elements: it can barrel thanks to high compliance provided by elements along the thickness. Still, the related effect to the constraints remains, forbidding free movement of the lower surface. The deformed structure cannot be used to determine the correct value of Young's modulus.

It is important to underline how shear load applied to both isotropic and anisotropic material meshed by only one element creates a deformed structure that isn't helpful to reaching the goal because it is different from the real one. Indeed, isostatic constraints lock the lower surface in the starting position and shape, but the pressure applied and the presence of a single elements origins a deformation of the upper surface and the bending effect, which isn't desirable because the determination of modulus requests a pure shear as the applied force.

4. Elastic constraints and force load:

Below two pictures show the scheme of loads and constraints application:
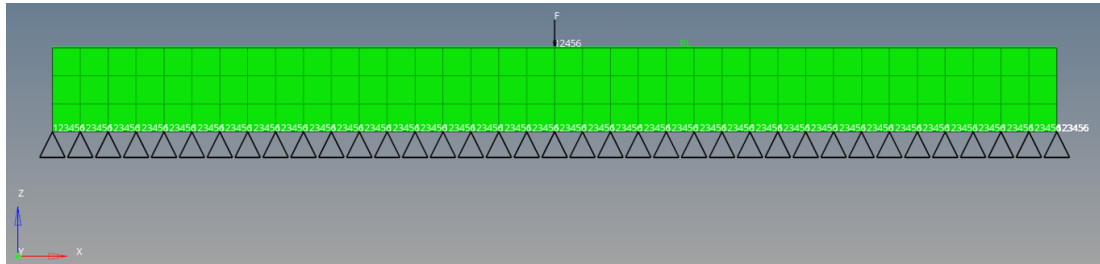
Figure 112 Compression Z: Elastic constraints + Force load
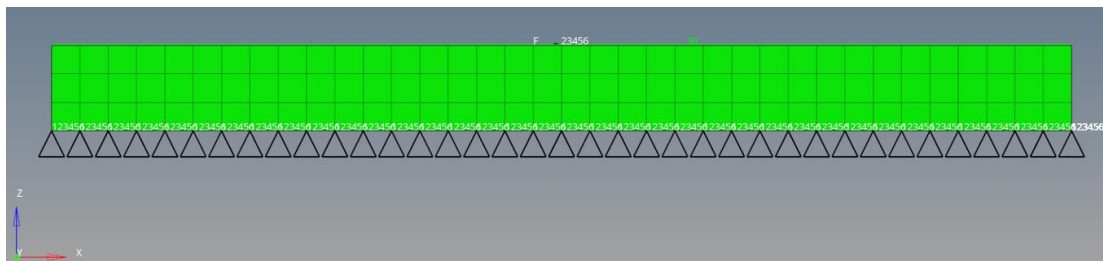
Figure 113 Shear XZ: Elastic constraints + Force load

The table summarizes the results of the simulation considering isotropic and anisotropic material loaded with compression and shear load:

Table 27 Constraints and applied load study

ELASTIC CONSTRAINTS + FORCE	MAT1		MAT9	
COMPRESSION Z	Eq. Solid (1)	Eq. Solid (36x6x3)	Eq. Solid (1)	Eq. Solid (36x6x3)
σ_z [MPa]	0.046	0.046	0.046	0.046
ϵ_z	4.46E-07	5.12E-07	6.61E-07	6.61E-07
E_z [MPa]	103714.99	90461.32	69999.89	69999.89
Discrepancy [%]	-48.16	-29.23	1.52E-04	1.52E-04
SHEAR XZ	Eq. Solid (1)	Eq. Solid (36x6x3)	Eq. Solid (1)	Eq. Solid (36x6x3)
τ_{xz} [MPa]	0.046	0.046	0.046	0.046
γ_{xz} [rad]	1.77E-06	1.80E-06	1.77E-06	1.80E-06
G_{xz} [MPa]	26133.41	25786.40	26111.30	25689.91
Discrepancy [%]	0.69	2.01	0.78	2.38

This way of applying loads and constraints generates coherent deformed structures for isotropic and anisotropic material, considering both compression's and shear's load.

An unexpected result is obtained when compression of an isotropic volume has meshed by a single element. Indeed, it suggests that software cannot correctly determine the module of the structure considering these constraints and the load applied with an isotropic material. The result seems to converge when the number of elements increases. The discrepancy is huge, so this way cannot be followed in determining the modulus.

Instead of anisotropic material, the results are correct and coherent with the real one.

Referring to the shear load, the deformed structure and discrepancy suggest that elastic constraints and force applied with an RBE2 is a possible solution to define the shear's modulus correctly. Indeed, it produces minor differences concerning the real value, but it is negligible and smaller than 5%.

According to the results of four previous parties, the application method is defined. This study permits to state some conclusions:

- Compression → Isostatic constraints and pressure load are selected to evaluate Young's modulus correctly, and the central node's displacement must be considered to calculate the strain
- Shear → Elastic constraints and force load introduced by using RBE2 are selected to estimate the shear's modulus, and the master's node of RBE2 must be considered to define the angle (γ)

3.3.2.2.3.   Plate volume: 36x6x3 unit cell

In the previous paragraphs, all simulation aspects were studied to persecute the goal of the thesis: the definition of a lattice structure's equivalent moduli.

At this point, all information is available to create the sample and test it. In the following they are listed:

- The shape of the lattice structure must be like a plate. Its dimensions are defined: the length side must measure at least 12 times the thickness of the sample to better evaluate the Shear's moduli, and the thickness must have at least 3 unit cells to obtain a reasonable estimation of the Young's moduli
- In the equivalent solid, the number of elements present must be at least the unit cells' number
- To evaluate Young's moduli is necessary to use isostatic constraints and pressure load
- To evaluate Shear's moduli is necessary to utilize elastic constraints and force load (RBE2)

It is realized a sample composed of 36x6x3 unit cells considering these parameters, and it is tested as explained before. This component is formed by 11290752 CTETRA elements and 3200158 nodes, its analysis is starting to become complicated for software possibilities, but it is still possible.

Regarding all considerations, the better tester should be a plate formed by 36x36x3 unit cells because, in this way, shear's moduli in XZ and YZ planes are the same as the real considering geometry and material. An attempt is made to build this lattice structure virtually, but it isn't possible because the number of elements and nodes becomes enormous, and the software collapses.

In the next pictures are reported lattice structure simulations, and their displacement used to determine elastic moduli:
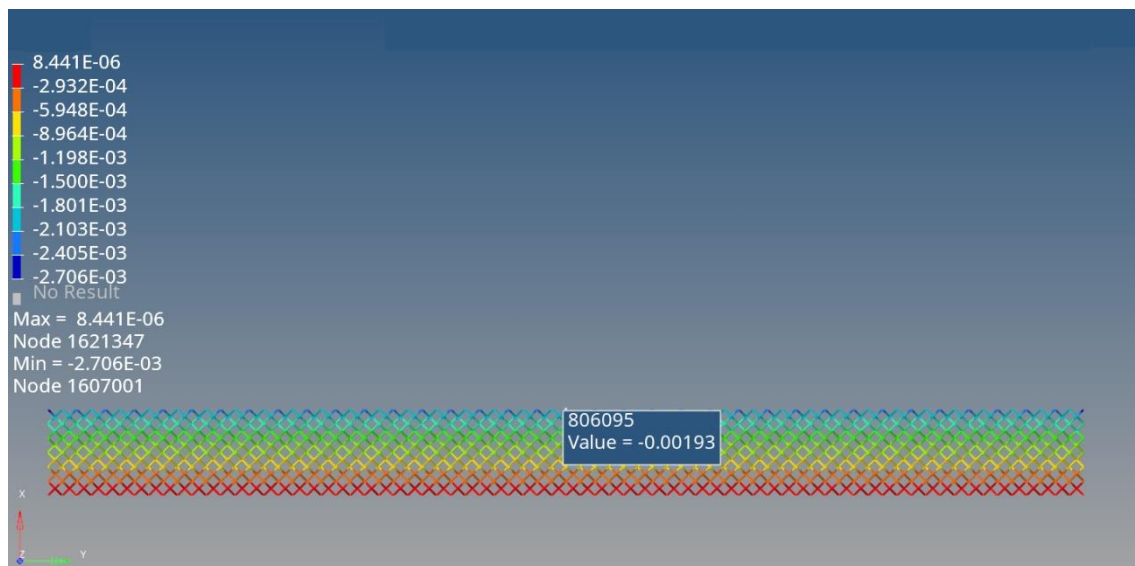
Figure 114 Compression X direction

8.441E-06
-2.932E-04
-5.948E-04
-8.964E-04
-1.198E-03
-1.500E-03
-1.801E-03
-2.103E-03
-2.405E-03
-2.706E-03
No Result
Max = 8.441E-06
Node 1651908
Min = -2.706E-03
Node 1576440

775597
Value = -0.00193
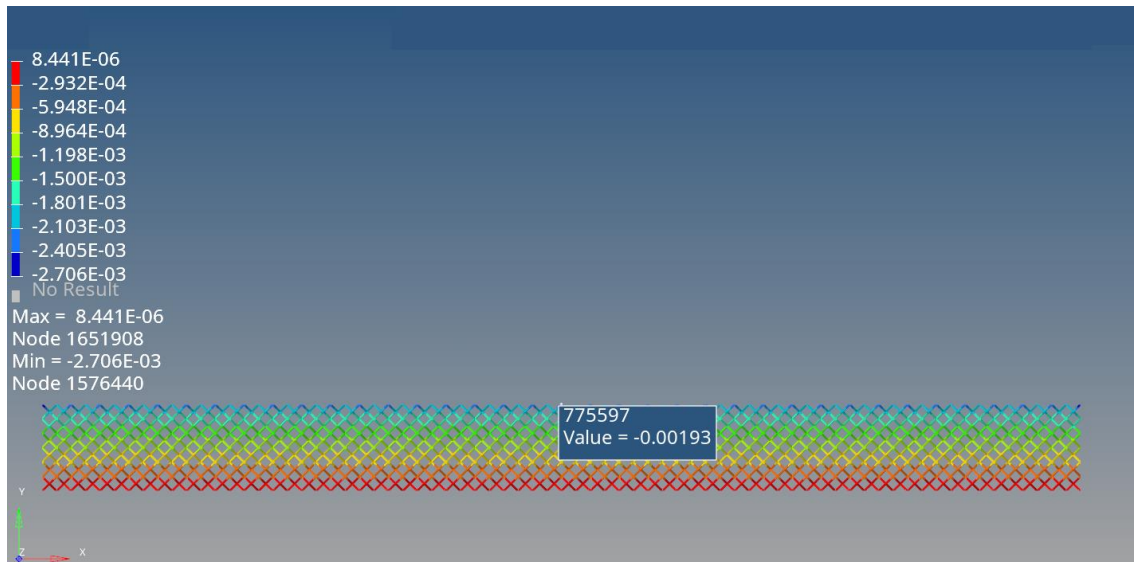
Figure 115 Compression Y direction

1.036E-05
-2.967E-04
-6.038E-04
-9.108E-04
-1.218E-03
-1.525E-03
-1.832E-03
-2.139E-03
-2.446E-03
-2.753E-03
No Result
Max = 1.036E-05
Node 1621347
Min = -2.753E-03
Node 1607001

806095
Value = -0.00196
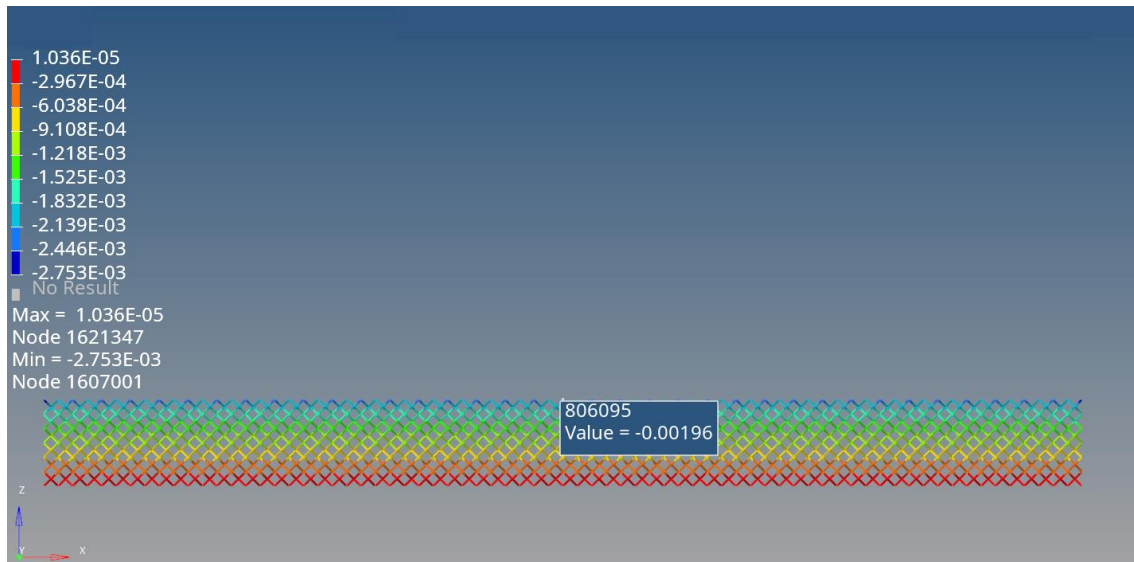
Figure 116 Compression Z direction
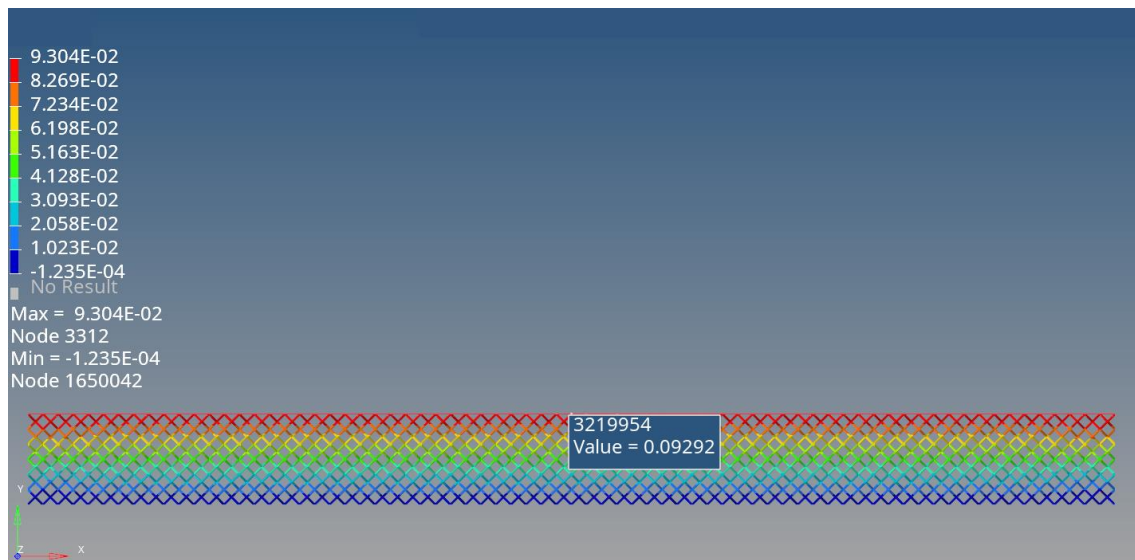
Figure 117 Shear XY plane
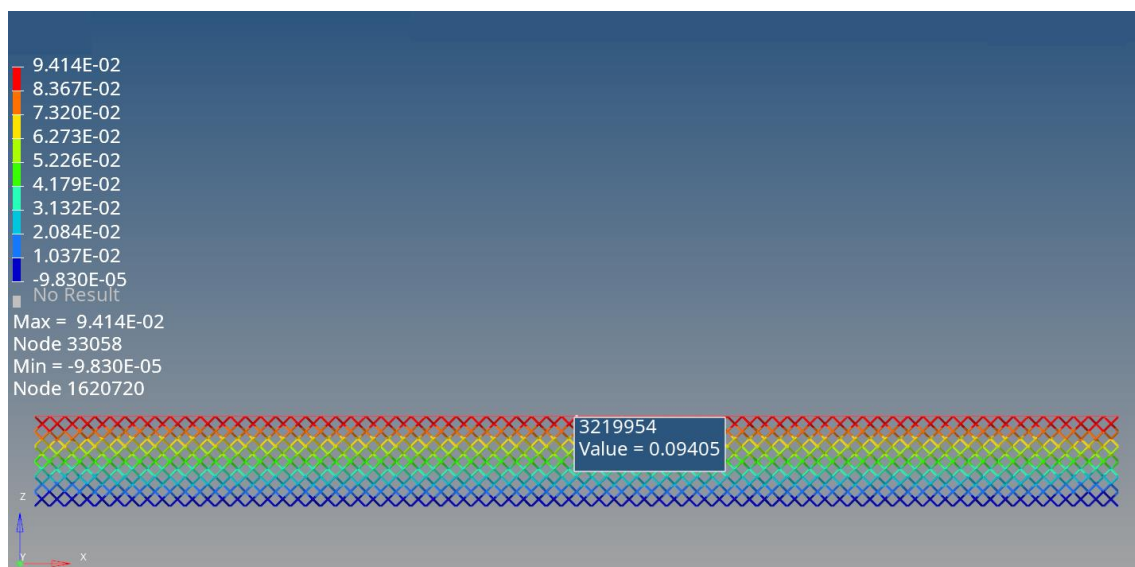
Figure 118 Shear XZ plane
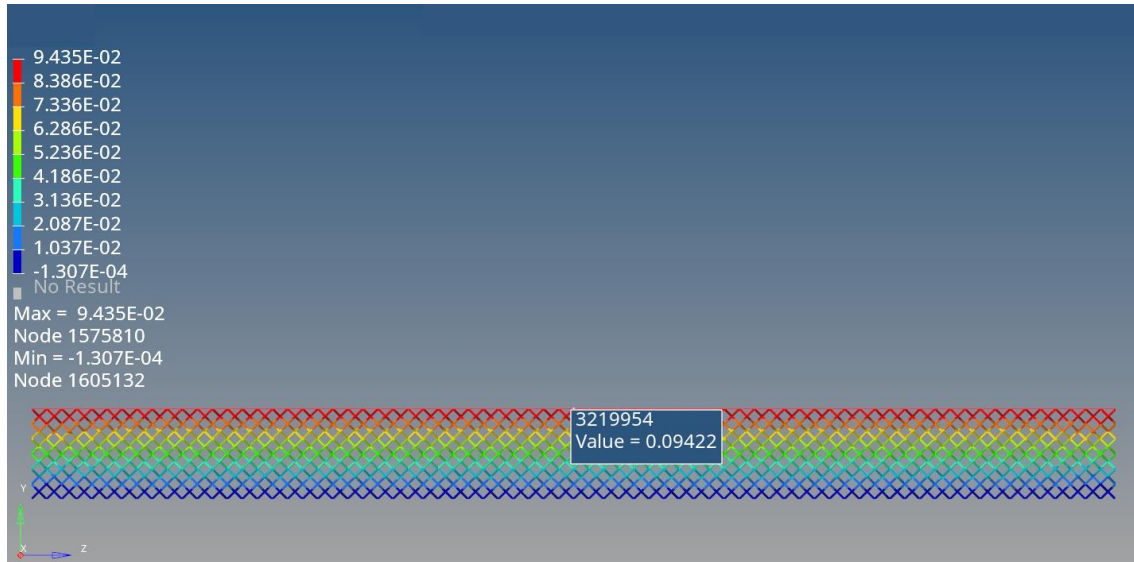
Figure 119 Shear YZ plane

It is possible to determine lattice structure's equivalent moduli using these displacements. The results are shown in the table below:

Table 28 Lattice structure's equivalent moduli

LATTICE		LATTICE		LATTICE	
COMPRESSION X		**COMPRESSION Y**		**COMPRESSION Z**	
σ_x [MPa]	1	σ_y [MPa]	1	σ_z [MPa]	1
Displacement [mm]	1.93E-03	Displacement [mm]	1.93E-03	Displacement [mm]	1.96E-03
ϵ_x	6.44E-05	ϵ_y	6.44E-05	ϵ_z	6.54E-05
E_x [MPa]	15532.89	E_y [MPa]	15532.91	E_z [MPa]	15294.88
LATTICE		LATTICE		LATTICE	
SHEAR XY		**SHEAR XZ**		**SHEAR YZ**	
τ_{xy} [MPa]	1	τ_{xz} [MPa]	1	τ_{yz} [MPa]	1
Displacement [mm]	9.29E-02	Displacement [mm]	9.40E-02	Displacement [mm]	9.42E-02
γ_{xy} [rad]	3.10E-03	γ_{xz} [rad]	3.13E-03	γ_{yz} [MPa]	3.14E-03
G_{xy} [MPa]	322.88	G_{xz} [MPa]	318.99	G_{yz} [MPa]	318.39

Regarding the equivalent moduli, some considerations can be made:
- This type of structure presents high Young's moduli compared to the shear's one, so a lattice structure composed of rhombic dodecahedron lattice structure is more resistant to compression load not to shear one. This result is the same obtained for a sandwich

117

panel; indeed, the lattice is commonly used as filler between skins, and its primary purpose consists of supporting axial loads as compression one

- Considering Young's moduli, they have values very close to each other; this is due to the geometry of the rhombic dodecahedron unit cell that it is symmetrical, and so it resists in the same way along each direction. Young's moduli in the X and Y directions must be the same (powder's properties and cell's geometry), so the equivalent modulus selected is the smallest one because if the strain is the same, the stress is more minor in the structure. In the Z direction, Young's modulus is smaller than the other two directions because powder's characteristics influence the behavior of the structure; indeed, the out-of-plane modulus is equal to 178000 MPa, and the in-plane modulus is 239000 MPa

- Cell's symmetry introduces its effects into the shear's moduli too. Indeed they are very similar to each other. Shear's XY plane is more significant than the others because powder's in-plane Young's modulus is more considerable than out-of-plane one

- According to the theory, shear XZ and shear YZ moduli are the same less than a short discrepancy caused by solver approximation. As equivalent modulus is selected the smallest one because if the strain is the same, the stress is more minor in the structure

3.3.2.3.   Equivalent moduli validation

In the previous paragraph, lattice structure's equivalent moduli are defined, respecting all conditions and conclusions obtained during the thesis work. According to this, the results should be correct and able to describe the behavior of an entire lattice structure composed of rhombic dodecahedron unit cells realized by L-PBF using SS316L powder.

Additional tests are done to confirm that found moduli are equivalent for this type of lattice structure and that sample's dimensions don't influence them.

This way is followed to persecute the goal: two types of new lattice plates are built with different dimensions to evaluate the variability of equivalent determined moduli and the new ones. The first plate presents 36 unit cells along the length, 6 unit cells along the depth, and 6 unit cells along the height. This structure has a double thickness compared to the original one. It is formed by 22581504 CTETRA elements and 6391033 nodes. While the second one has 72 unit cells along the length, 3 unit cells along the depth, and 3 unit cells along the height, this lattice structure presents a double length compared to the original one. It is composed of 11290752 CTETRA elements and 3204481 nodes.

Considering the time and computational cost of the simulation, only compression along the Z direction and shear in the XZ plane are considered in the verification. If these produce positive results, the other moduli are correct.

In the following picture, the comparison between different lattice structures and the original one is reported graphically:
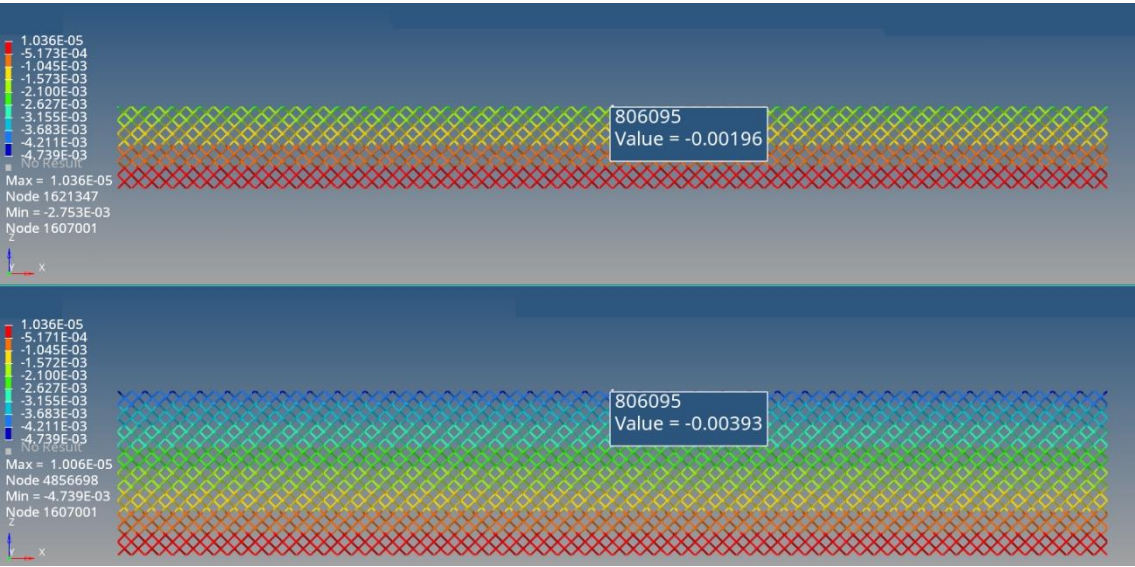
Figure 120 Compression Z: comparison between 36x6x3 plate and 36x6x6 plate
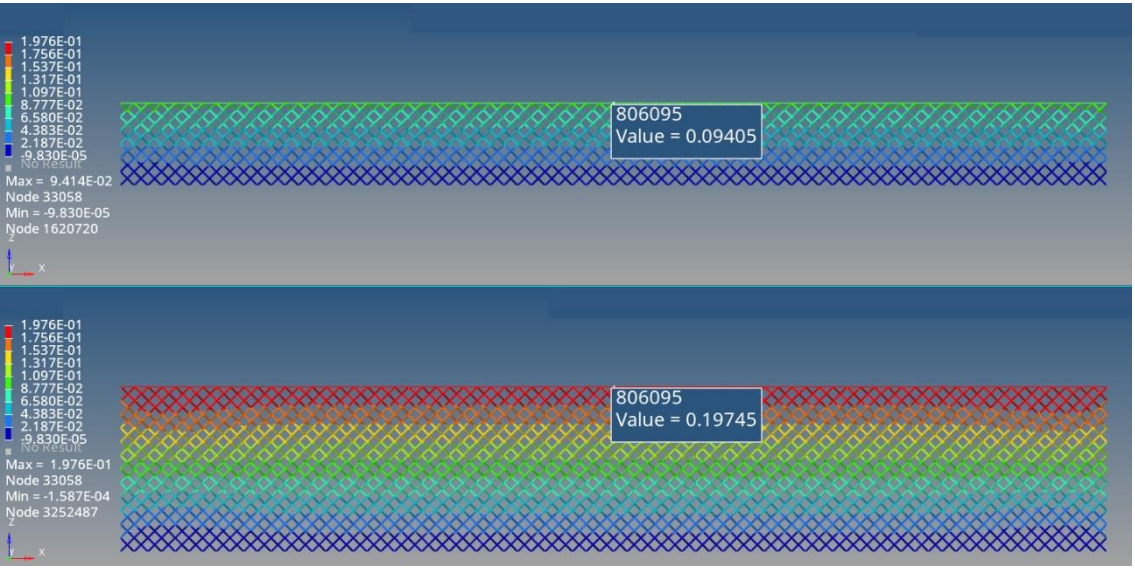
Figure 121 Shear XZ plane: comparison between 36x6x3 plate and 36x6x6 plate
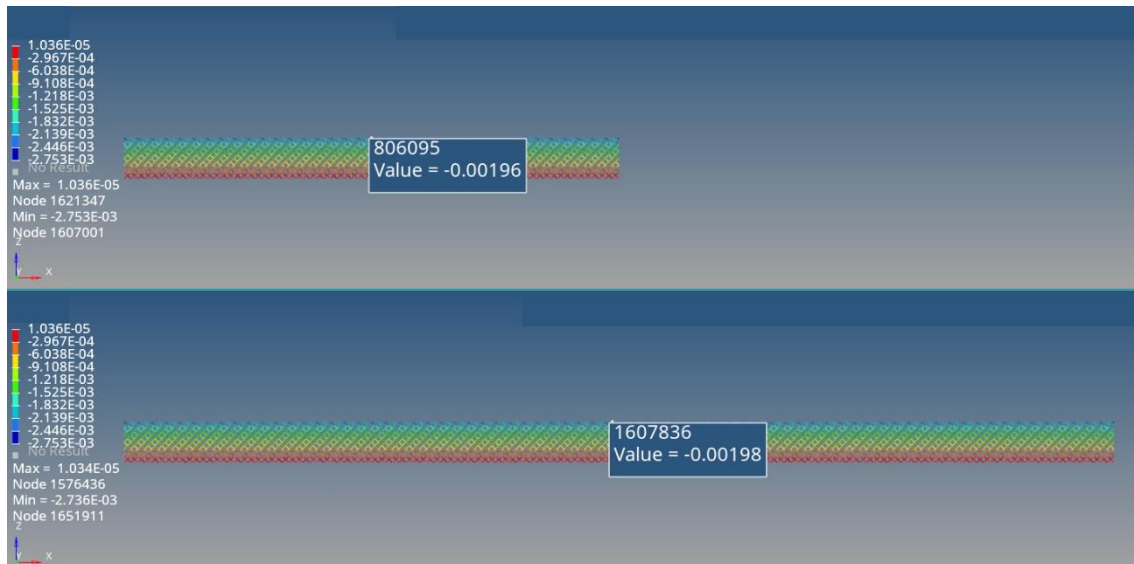
Figure 122 Compression Z: comparison between 36x6x3 plate and 72x3x3 plate
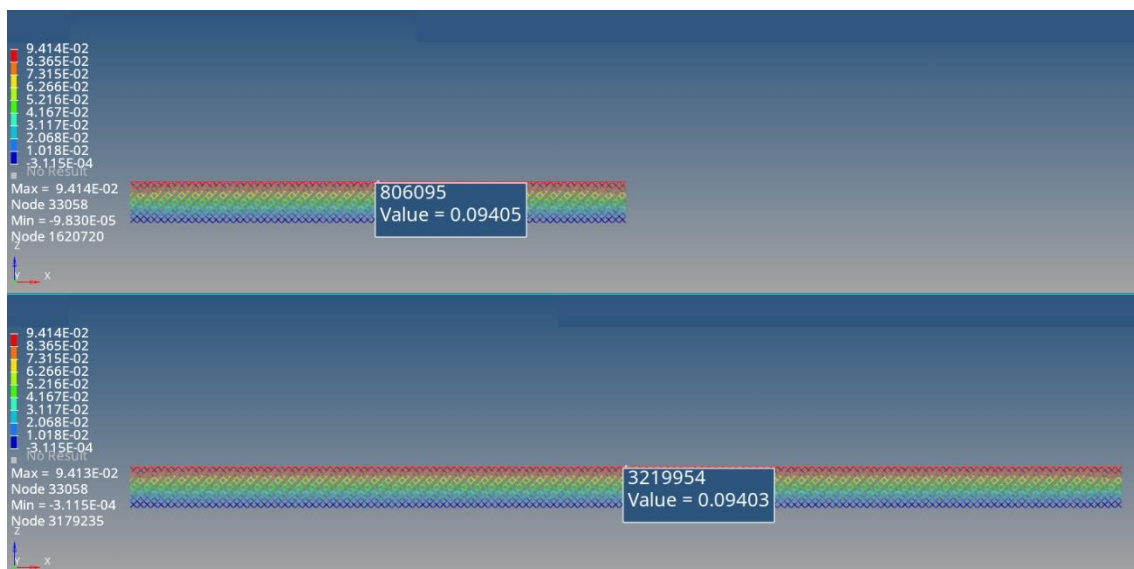
Figure 123 Shear XZ plane: comparison between 36x6x3 plate and 72x3x3 plate

In the below table all results are numerically shown:

Table 29 Comparison between lattice plate dimensions

COMPRESSION Z	Lattice 36x6x3	Lattice 36x6x6	Lattice 72x3x3
σ_z [MPa]	1	1	1
Displacement [mm]	1.96E-03	3.93E-03	1.98E-03
ϵ_z	6.54E-05	6.56E-05	6.61E-05
E_z [MPa]	15294.88	15249.18	15131.40
Discrepancy [%]	0	0.30	1.07
SHEAR XZ	Lattice 36x6x3	Lattice 36x6x6	Lattice 72x3x3
τ_{xz} [MPa]	1	1	1
Displacement [mm]	9.40E-02	1.97E-01	9.40E-02
γ_{xz} [rad]	3.13E-03	3.29E-03	3.13E-03
G_{xz} [MPa]	318.99	303.88	319.04
Discrepancy [%]	0	4.74	-0.02

Some considerations can be stated regarding these results:

- Lattice 36x6x6 → When the sample's thickness doubles, Young's modulus coincides with the original one. The slight discrepancy is due to solver approximation. This result confirms that 3 unit cells in the thickness are the right compromise between computational cost and result accuracy.

  The discrepancy increases considering the shear's modulus because the structure gets away from the plate shape and the ratio between thickness and length decreases. This aspect is relevant considering the real application of the lattice structure because it is commonly used as a filler in the panel, so it has a plate shape, and the ratio condition is ever respected. Anyway, the discrepancy remains smaller than 5%, and so the results can be considered correct

- Lattice 72x3x3 → When the sample's length is doubled, the shear's modulus coincides with the original one. The slight negative difference is due to solver approximation, but it isn't very important. This result confirms the need to use at least a number of unit cells 12 times bigger than the thickness ones. If Young's modulus is evaluated, the discrepancy is very short, and moduli are just coincidence

These simulations' results suggest that these are the correct elastic moduli of a lattice structure with these characteristics. So they can be used to define an equivalent material to substitute the reticular one and determine the reticular structure's behavior saving much time and money.

3.3.2.3.1. Comparison between lattice structure and equivalent plate

The previous paragraph permitted to define and verify the correctness of the lattice structure's elastic moduli. In contrast, this one wants to attribute moduli to an equivalent solid and compare the results with the lattice structure ones.

The procedure followed is the same as in the other paragraphs: equivalent solid is realized as a plate with the exact dimensions and shape of the lattice structure. It is defined with MAT9 (the diagonal matrix parameters are the elastic moduli previously determined, while the extra diagonal ones are zeros). Then it is stimulated by compression and shear loads. Then moduli are calculated and compared to the original one.

In the below pictures are graphically reported all simulations:
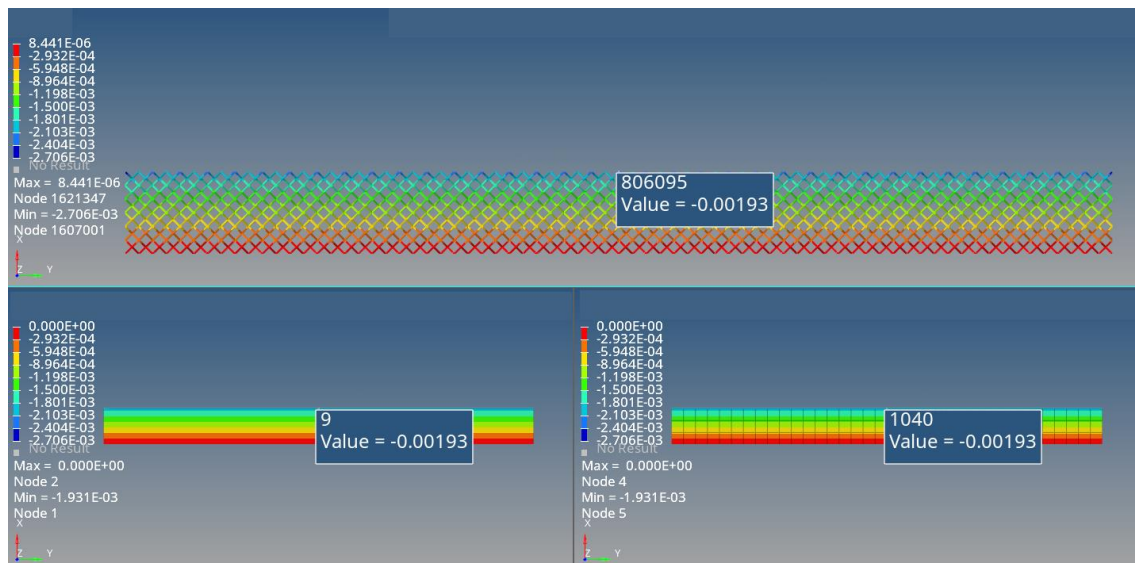
Figure 124 Compression X: Reticular component, Eq. Solid (1), and Eq. Solid (36x6x3)
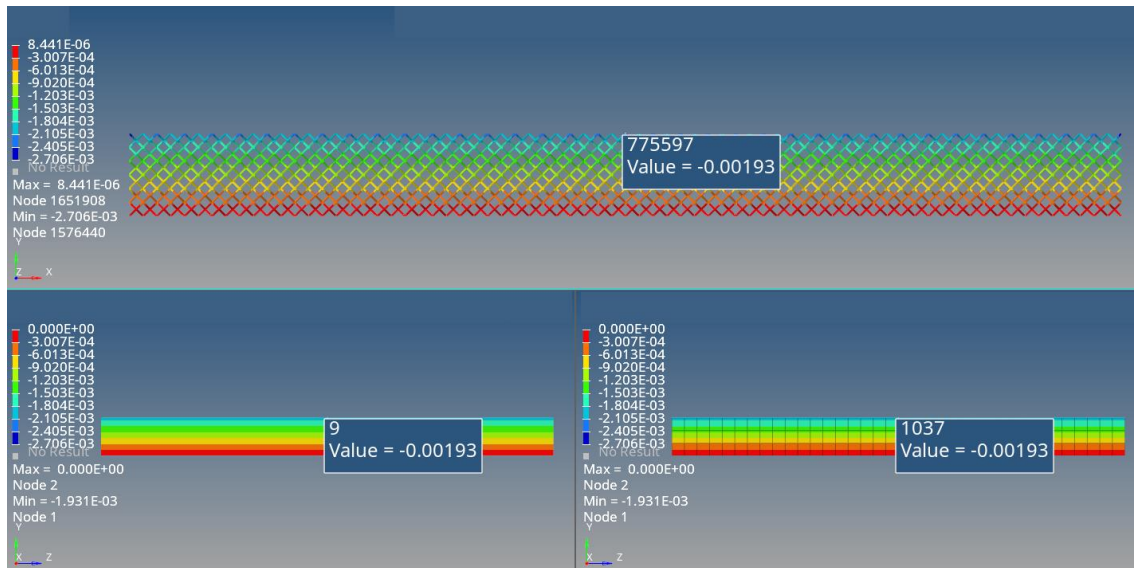
Figure 125 Compression Y: Reticular component, Eq. Solid (1), and Eq. Solid (36x6x3)
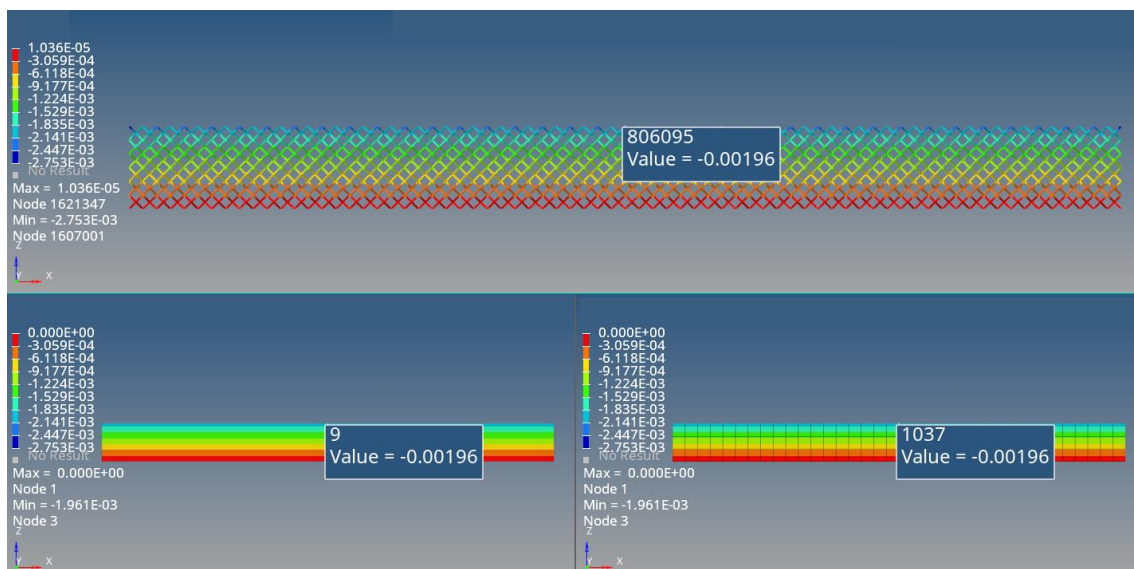
Figure 126 Compression Z: Reticular component, Eq. Solid (1), and Eq. Solid (36x6x3)
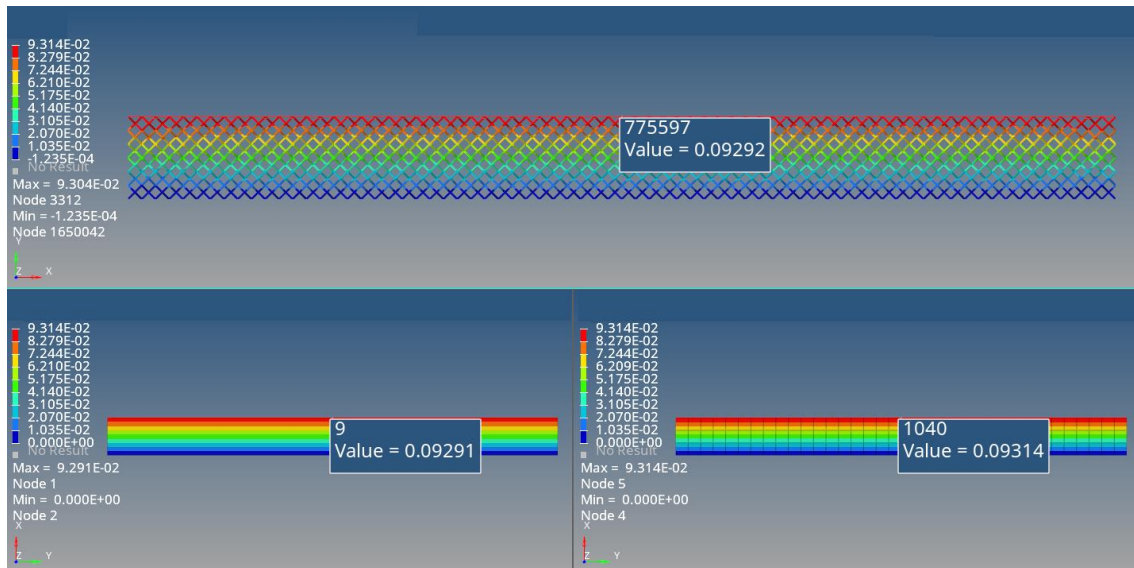
Figure 127 Shear XY: Reticular component, Eq. Solid (1), and Eq. Solid (36x6x3)
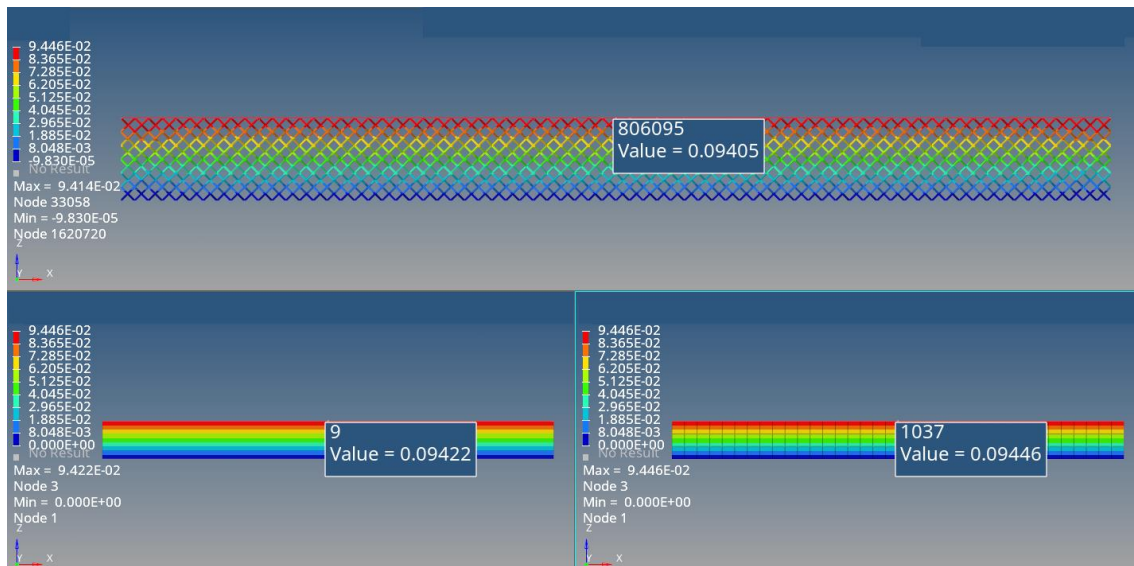
Figure 128 Shear XZ: Reticular component, Eq. Solid (1), and Eq. Solid (36x6x3)
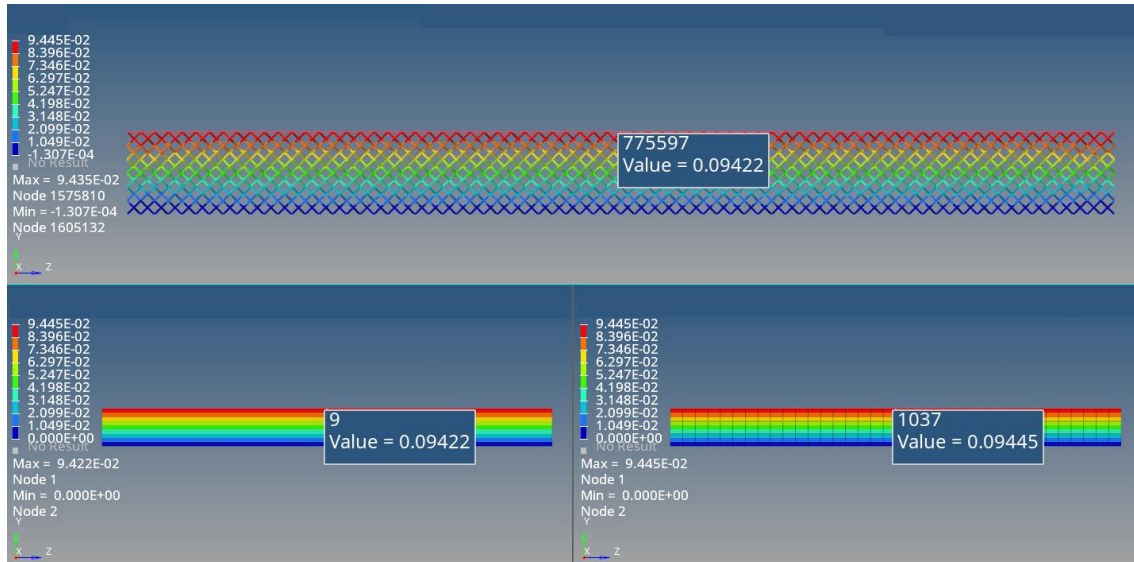
Figure 129 Shear YZ: Reticular component, Eq. Solid (1), and Eq. Solid (36x6x3)

The following table summarizes all simulations results numerically:

Table 30 Comparison between lattice structure and equivalent plate

COMPRESSION X	Ret. Component	Eq. Solid (1)	Eq. Solid (36x6x3)
σ_x [MPa]	1	1	1
Displacement [mm]	1.93E-03	1.93E-03	1.93E-03
ϵ_x	6.44E-05	6.44E-05	6.44E-05
E_x [MPa]	15532.89	15532.89	15532.89
Discrepancy [%]	0	3.11E-05	3.11E-05
COMPRESSION Y	Ret. Component	Eq. Solid (1)	Eq. Solid (36x6x3)
σ_y [MPa]	1	1	1
Displacement [mm]	1.93E-03	1.93E-03	1.93E-03
ϵ_y	6.44E-05	6.44E-05	6.44E-05
E_y [MPa]	15532.89	15532.89	15532.89
Discrepancy [%]	0	2.41E-07	2.41E-07

125

COMPRESSION Z	Ret. Component	Eq. Solid (1)	Eq. Solid (36x6x3)
σ_z [Mpa]	1	1	1
Displacement [mm]	1.96E-03	1.96E-03	1.96E-03
ϵ_z	6.54E-05	6.54E-05	6.54E-05
E_z [MPa]	15294.88	15294.87	15294.87
Discrepancy [%]	0	4.59E-05	4.59E-05
SHEAR XY	Ret. Component	Eq. Solid (1)	Eq. Solid (36x6x3)
τ_{xy} [MPa]	1	1	1
Displacement [mm]	9.29E-02	9.29E-02	9.31E-02
γ_{xy} [rad]	3.10E-03	3.10E-03	3.10E-03
G_{xy} [MPa]	322.88	322.88	322.09
Discrepancy [%]	0	-1.40E-03	2.44E-01
SHEAR XZ	Ret. Component	Eq. Solid (1)	Eq. Solid (36x6x3)
τ_{xz} [MPa]	1	1	1
Displacement [mm]	9.40E-02	9.42E-02	9.45E-02
γ_{xz} [rad]	3.13E-03	3.14E-03	3.15E-03
G_{xz} [MPa]	318.39	318.39	317.16
Discrepancy [%]	0	-3.28E-04	2.45E-01
SHEAR YZ	Ret. Component	Eq. Solid (1)	Eq. Solid (36x6x3)
τ_{yz} [MPa]	1	1	1
Displacement [mm]	9.42E-02	9.42E-02	9.45E-02
γ_{yz} [rad]	3.14E-03	3.14E-03	3.15E-03
G_{yz} [MPa]	318.39	318.39	317.62
Discrepancy [%]	0	0	2.42E-01

Regarding the results, it is possible to declare that these equivalent moduli are mesh independent, further confirming the methodology's quality defined in this thesis.

Considering only compression equivalent moduli, they are precisely coincident with the original one, and the discrepancy remains constant using a single or many elements to mesh the volume. So Young's moduli are defined correctly, and their values represent the entire lattice structure with great accuracy. The discrepancy is about 10^{-5} or 10^{-7}, so it is negligible and attributable to solver approximations.

The situation is different when the shear's moduli are considered: the discrepancy is more considerable and around 10^{-3} and 10^{-4} using a single element to mesh the volume, while if many

elements are used, the discrepancy increases around 10^{-1}. This result is acceptable and coherent with the previous obtained; it is smaller than 5%, so it is good to approximate the behavior of the structure.

Concluding this paragraph, some conclusions are stated:

- Equivalent Young's moduli are exactly and able to describe the behavior of a lattice structure using an equivalent solid with high accuracy
- Equivalent Shear's moduli can be used to predict the lattice's behavior, and the results are acceptable and valuable, but it must be considered that a slight discrepancy is generated compared to the reticular one

3.3.2.3.2. Comparison between lattice structure and equivalent cube

All elastic moduli are correctly evaluated, so they can be used to define an anisotropic material with the same elastic characteristics as a lattice structure.

The definition of an equivalent solid is a solid that presents the same displacements and deformations of the reticular structure but different stresses. According to the previous results, a further test is done: a volume of 30x30x30 mm is filled with 27 unit cells realized with SS316L using the L-PBF technique, and it is compressed in the X direction to evaluate its displacement. An equivalent solid with the exact dimensions and shape is built, and its behavior is defined by the lattice's equivalent moduli calculated using the plate.

The equivalent stiffness matrix is shown below:

$$
\begin{bmatrix}
15532.89 & 0 & 0 & 0 & 0 & 0 \\
0 & 15532.89 & 0 & 0 & 0 & 0 \\
0 & 0 & 15294.88 & 0 & 0 & 0 \\
0 & 0 & 0 & 322.88 & 0 & 0 \\
0 & 0 & 0 & 0 & 318.39 & 0 \\
0 & 0 & 0 & 0 & 0 & 318.39
\end{bmatrix}
$$

In the picture is reported the compression in the X direction:
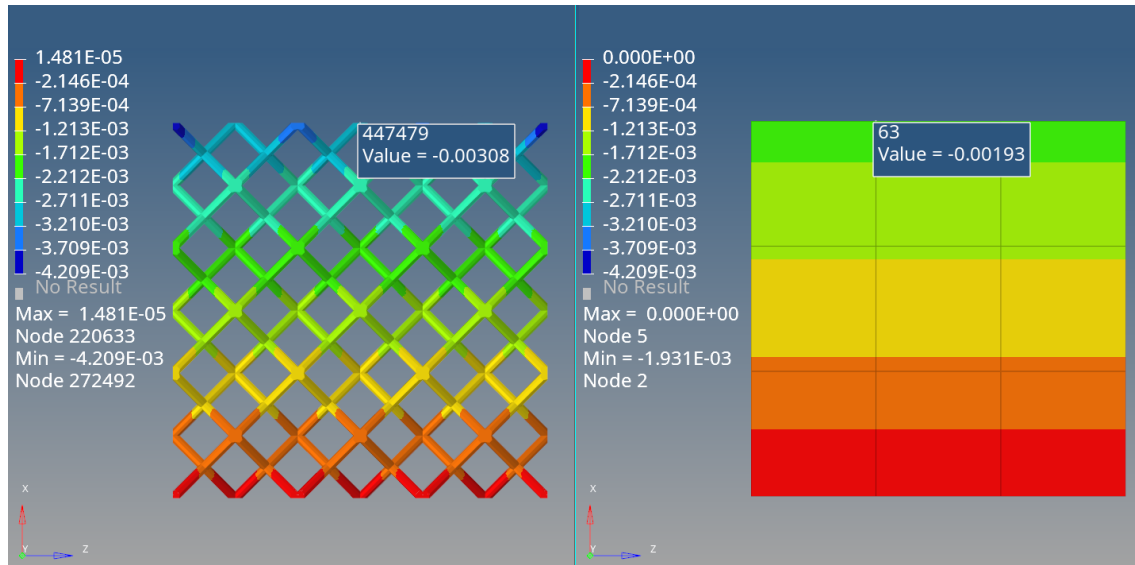
Figure 130 Compression X: comparison between lattice structure and equivalent solid

In the table results are numerically reported:

Table 31 Comparison between lattice structure and equivalent cube

COMPRESSION X	Lattice (27)	Eq. Solid (27)
σ_x [MPa]	1	1
Displacement [mm]	3.08E-03	1.93E-03
ϵ_x	1.03E-04	6.44E-05
E_x [MPa]	9727.11	15532.89
Discrepancy [%]	37.38	0

The discrepancy is referred to plate's equivalent moduli because they are defined as the correct and representative value of the global lattice structure with these characteristics (material, manufacturing process, and unit cell's shape).

This study considers only compression in the X direction because if it is wrong, all the others are too.

This result confirms that all the analysis's chapter considerations are correct and that the initial idea about the equivalent solid must be changed. Indeed, the equivalent solid cannot be a cube, but it must be a plate. This study demonstrated that lattice structure is a kind of component

more sensitive to boundary conditions. So there are dimensional constraints to respect to define an equivalent global behavior.

This problem in real applications doesn't exist because lattice is commonly used as filler in the panel, so the amount of unit cells is closer to a plate than a cube. In this way, the equivalent moduli defined are correct and valid to predict the behavior of a component composed of lattice.

4. CONCLUSIONS

At the end of the thesis is found an equivalent solid able to describe the lattice structure properties correctly. This methodology permits the substitution into the analysis of a complex lattice structure composed of many nodes and elements with a simple component realized with a full material defined as an anisotropy material equivalent to the original formed by several elements and nodes less numerous than the original one. This methodology considerably reduces the analysis's time and costs, so it represents a notable improvement in the FEM study of this type of structure.

The process has two critical aspects of being considered: Non-Linearity and anisotropy.

It consists of different steps, and they are listed below:

1. Material choice and characterization → This step is composed in two ways:

    o   Unknown material: the powder material is used to realize a real sample. It is tested with a compression test to define the true stress-strain curve both in the vertical and horizontal direction, and the relevant points are extracted. Some coordinates are selected from the true curves to introduce them into the software and characterize the virtual material

    o   Known material: the powder material is provided by an external producer who warrants the engineering curve's mechanical characteristics. The entire thesis' study demonstrates that this material has a Non-Linear behavior that is very influential in the mechanical response of the structure, so it must be considered. Using the results provided by the producer, the plastic stress-strain curve is defined by Johnson Cook Law, and it is used to describe the virtual anisotropy material on software

The next step's purpose is to obtain the equivalent moduli of the lattice structure. First, considering the software limitations, the material is treated as Linear and anisotropy, and the Non-Linearity is neglected.

2. The lattice structure component imposes the unit lattice cell, so it is an analysis constraint

3. The virtual lattice sample is built into the software environment respecting the shape and original dimension of the unit lattice cell. The thesis' study underlines how the sample must be built to define the equivalent moduli correctly:

    o   It must have a plate shape

    o   Its dimensions are defined by 3 unit cells in the thickness and at least 12 times unit cells in the length direction. The third dimension is determined following the solver power, machine memory, and referring to this thesis, 6 unit cells are

selected as a good compromise. The shape and dimension of the sample is a plate composed of 36x6x3 unit lattice cells

4. Virtual material definition → The virtual material is defined using a MAT9 card on Hypermesh, exploiting information provided in the first methodology step. It permits to simulate anisotropy behavior of a component realized by L-PBF techniques

5. Test campaign → The sample is stimulated with compression and shear tests to define the diagonal matrix stiffness terms singularly.

   Applied forces and constraints must be imposed correctly to reproduce the lattice's real response exactly:

   o Compression test → Isostatic constraints and pressure load are used to extrapolate the component displacement, and then the equivalent moduli

   o Shear test → Elastic constraints and force load introduced by an RBE2 element is used to extrapolate the component displacement, and then the equivalent moduli

6. The equivalent moduli are calculated, so the stiffness matrix is defined. This result is introduced into a MAT9 card, and it permits to reproduce of the same reticular component response

7. A CAD model of the reticular component is built, and it has meshed with the same element number of the unit lattice cell, and the MAT9 previously defined is used to describe its behavior

8. It is possible to run all types of analysis on this full equivalent component to discover the reticular component response

This thesis and procedure permit studying a lattice structure formed by a rhombic dodecahedron lattice unit cell built by L-PBF using an SS316L powder because the equivalent stiffness matrix is defined, and it represents the entire lattice structure behavior.

In the following it is reported:

$$\begin{bmatrix} 15532.89 & 0 & 0 & 0 & 0 & 0 \\ 0 & 15532.89 & 0 & 0 & 0 & 0 \\ 0 & 0 & 15294.88 & 0 & 0 & 0 \\ 0 & 0 & 0 & 322.88 & 0 & 0 \\ 0 & 0 & 0 & 0 & 318.39 & 0 \\ 0 & 0 & 0 & 0 & 0 & 318.39 \end{bmatrix}$$

To further underline the importance of this result, it just sees to the reduction of time, and consequently in cost, considering the sample necessary to extrapolate the equivalent moduli. Indeed, if the lattice component is made by 11290752 CTETRA elements and 3200158 nodes, it

runs around 00:14:11. In contrast if this methodology is applied to analyze the equivalent component, it is necessary for only 00:00:02, 649 CHEXA elements, and 1037 nodes.

If this result is referred to as the real component, the advantages exponentially increase because the time to run the real part grows significantly. The reason is that many elements are presented in the thickness, so the solver requests much time to evaluate the stiffness matrix and execute the analysis.

5. FUTURE DEVELOPMENTS

The thesis permits a great result and offers a starting point to develop other aspects of the equivalent solid.

First, it should be essential to add experimental tests to verify and reinforce the results obtained during this work. Indeed there is a theoretical method called Gibson Ashby [9,17,18]. It is the most famous and used to predict lattice structure performances. This theory calculates mechanical properties as a fraction of the parental material ones. The relationship depends on the structure's response which is evaluated using Maxwell's criterion. This one relates mechanical properties with a relative density of the structure through a positive power coefficient (C) and exponent (n) with the relative density of the structure [9,11,13,37,47,62].

In the following, the relation is reported:

$$\frac{\sigma^*}{\sigma_s} = C \left(\frac{\rho^*}{\rho_s}\right)^n$$

$$\frac{E^*}{E_s} = C \left(\frac{\rho^*}{\rho_s}\right)^n$$

Where:

E^* is the static modulus of the cellular structure

E_s is the static modulus of the cellular structure's bulk material

C is a Gibson Ashby constant, the value of which is dependent on the unit cell topology and geometry, and it is derived from experimental results

σ^* is the yield stress of the cellular structure's bulk material

Typically metallic open-cell coefficients range between 0.1 and 4 for Young's modulus and around 0.1 and 1 for strength, while the exponent depends on the cell's behavior [13,49].

The coefficient is evaluated forward experimental test considering precisely lattice structure formed by unit cell built-in metal material, so it permits to estimate equivalent moduli and compare it with thesis's results.

Moreover, it is possible to enrich the work by identifying the stiffness matrix's extra diagonal terms to consider the effects that generate deformation in the other directions and not only in the applied load one. This way offers the possibility to evaluate better and predict the structure's behavior, so the equivalent solid becomes more coincident with the reticular one.

In the end, there is another point to deepen, which concerns the equivalent yielding stress determination.

In this thesis work, it is underlined that Hypermesh presents a limit related to the possibility of running a Non-Linear analysis considering an anisotropy material. Initially, the importance of Non-Linearity and anisotropy emerged because these characteristics are fundamental to correctly determining the lattice structure's behavior. A possibility to face the problem is to consider it as a linear problem. Then using superposition, the global effect is evaluated. The thesis analyzed the anisotropy effect as helpful in evaluating the equivalent moduli, and in the future, it should be considered the Non-Linearity to determine the equivalent yielding stress.

The problem can be approached by evaluating the plastic strain development in the lattice sample and defining a limit point where the structure loses its elastic features. So the stress-strain curve enters the plastic segment. This condition is defined as the moment when all joints ultimately reach plasticization. The zones close to the joint are the first to plasticize. This situation occurs because struts are similar to cantilevers, so the maximum stress and deformation are located there.

This type of analysis can be executed considering an isotropy material. So if the metal powder shows anisotropy, in-plane, and out-of-plane features must be regarded as singularly. One of them shows minimum stress, which is considered as the equivalent yielding stress of lattice structure.

This idea must be verified and studied, but it should be considered a starting point to treat this relevant aspect of the problem.

6. APPENDIX

A. Renishaw, AM400 additive manufacturing system, www.tech-labs.com/sites/default/files/H-5800-3137-01-A_EN-07%20-%20AM400%20Data%20Sheet%20-%20Media.pdf

B. SLM Solutions, Material Data Sheet, Fe-Alloy 316L (1.4404), www.slm-solutions.com/fileadmin/Content/Powder/MDS/MDS_Fe-Alloy_316L_0820_V0.91_EN_LS.pdf

7. REFERENCES

1. Nugent J., The History of Additive Manufacturing, www.visibility.com/blog/the-history-of-additive-manufacturing, 21/06/2022

2. Enginsoft, Multiscale.Sim|Multiscale analysis system, A new tool for Ansys that facilitates materials testing and microscopic analysis of composite materials, www.enginsoft.com/solutions/multiscale.html, 30/05/2022

3. SLM Solutions, SLM solutions offers qualified metal powder and material parameters, www.slm-solutions.com/products-and-solutions/powders/, 20/05/22

4. M. Ionni, E. Troiani, V. Massarelli, A. Ceruti, Caratterizzazione meccanica di un pannello sandwich per l'interno di un aeromobile, 2013

5. X. Cao, S. Duan, J. Liang, W. Wen, D. Fang, "Mechanical properties of an improved 3D-printed rhombic dodecahedron stainless steel lattice structure of variable cross section", International Journal of Mechanical Sciences, Elsevier

6. EOS, 3D Printing Metal Materials: Our Portfolio for Additive Manufacturing Metal Parts, https://www.eos.info/en/additive-manufacturing/3d-printing-metal/dmls-metal-materials, 21/05/2022

7. C. Pan, Y. Han, and J. Lu, "Design and Optimization of Lattice Structures: A Review," Appl. Sci., vol. 10, no. 18, 2020, doi: 10.3390/app10186374

8. G. Dong, Y. Tang, and Y. F. Zhao, "A Survey of Modeling of Lattice Structures Fabricated by Additive Manufacturing," J. Mech. Des., vol. 139, no. 10, 2017, doi: 10.1115/1.4037305

9. L. J. Gibson and M. F. Ashby, Cellular Solids: Structure and Properties, 2nd ed. Cambridge University Press, 1997

10. M. F. Ashby, "The properties of foams and lattices.," Philos. Trans. Ser. A, Math. Phys. Eng. Sci., vol. 364, no. 1838, pp. 15–30, Jan. 2006, doi: 10.1098/rsta.2005.1678

11. D. Kang, S. Park, Y. Son, S. Yeon, S. H. Kim, and I. Kim, "Multi-lattice inner structures for high-strength and light-weight in metal selective laser melting process," Mater. Des., vol. 175, p. 107786, 2019, doi: https://doi.org/10.1016/ j.matdes.2019.107786

12. Milan Brandt, Laser Additive Manufacturing Materials, Design, Technologies, and Applications, 2017

13. T. Maconachie et al., "SLM lattice structures: Properties, performance, applications and challenges," Mater. Des., vol. 183, p. 108137, 2019, doi: https://doi.org/10.1016/j.matdes.2019.108137

14. M. Helou and S. Kara, "Design, analysis and manufacturing of lattice structures: an overview," Int. J. Comput. Integr. Manuf., vol. 31, no. 3, pp. 243–261, 2018, doi: 10.1080/0951192X.2017.1407456

15. Kladovasilakis N., Tsongas K., Kostavelis I., Tzovaras D., and Tzetzis D., Effective Mechanical Properties of Additive Manufactured Strut-Lattice Structures: Experimental and Finite Element Study

16. Galati M., Saboori A., Biamino S., Calignano F., Lombardi M., Marchiandi G., Minetola P., Fino P., Iuliano L., Ti-6Al-4V lattice structure produced by EBM: Heat treatment and mechanical properties

17. J. Hutchinson, H. Wadley, L. Gibson, Metal Foams A Design Guide, Elsevier, 2000

18. L.J. Gibson, M.F. Ashby, Cellular Solids, Cambridge University Press, Cambridge, 1997, https://doi.org/10.1017/CBO9781139878326

19. Puzello F., Stampa 3D in metallo, Stampa 3d in metallo - 3D 4Growth, 20/04/2022

20. Van Grunsven W., Hernandez-Nava E., C. Reilly G., and Goodall R., Fabrication and Mechanical Characterisation of Titanium Lattices with Graded Porosity

21. Puzzello F., Materiali stampa 3D: guida completa su come scegliere i migliori, 15/05/2022

22. J. Banhart, J. Baumeister, Production methods for metallic foams, in: D.S. Schwartz, D.S. Shih, A.G. Evans, H.N.G. Wadley (Eds.), Porous and Cellular Materials for Structural Applications, MRS Symposium Proceedings, 521 (1998) p. 121–132

23. H.N.G. Wadley, Proceedings of the International Conference on Cellular Metals and Metal Foaming Technology, Bremen, Germany, 2001, pp. 137–146

24. Pasvanti N., Psarros A., Korbetis G., Vlahinos A., Mihailidis A., Lattice structures modeling: introduction to homogenization

25. L. Hao, et al., Design and additive manufacturing of cellular lattice structures, in: The International Conference on Advanced Research in Virtual and Rapid Prototyping (VRAP), Taylor & Francis Group, Leiria, 2011

26. A.A. Zadpoor, Mechanical performance of additively manufactured metabiomaterials, Acta Biomater. (2018)

27. X.Z. Zhang, et al., Selective electron beam manufactured Ti-6Al-4V lattice structures for orthopedic implant applications: Current status and outstanding challenges, Curr. Opinion Solid State Mater. Sci. 22 (3) (2018) 75-99

28. L. Yuan, S. Ding, C. Wen, Additive manufacturing technology for porous metal implant applications and triple minimal surface structures: A review, Bioactive Mater. 4 (1) (2019) 56-70

29. K.G. Prashanth, et al., Microstructure and mechanical properties of Al12Si produced by selective laser melting: Effect of heat treatment, Mater. Sci. Eng. A 590 (2014) 153-160

30. J.-P. Kruth, et al., Selective laser melting of iron-based powder, J. Mater. Process. Technol. 149 (1-3) (2004) 616-622

31. J.N. Domfang Ngnekou, et al., Influence of defect size on the fatigue resistance of AlSi10Mg alloy elaborated by selective laser melting (SLM), Procedia Struct. Integrity 7 (2017) 75-83

32. M. Hirsch, et al., Meso-scale defect evaluation of selective laser melting using spatially resolved acoustic spectroscopy, Proc. R. Soc. A Math. Phys. Eng. Sci. 473 (2205) (2017), 20170194

33. E. Liverani, et al., Effect of selective laser melting (SLM) process parameters on microstructure and mechanical properties of 316L austenitic stainless steel, J. Mater. Process. Technol. 249 (2017) 255-263

34. A. Armillotta, R. Baraggi, S. Fasoli, SLM tooling for die casting with conformal cooling channels, Int. J. Adv. Manuf. Technol. 71 (1) (2014) 573-583

35. H. Alsalla, L. Hao, C. Smith, Fracture toughness and tensile strength of 316L stainless steel cellular lattice structures manufactured using the selective laser melting technique, Mater. Sci. Eng. A 669 (2016) 1-6

36. I. Maskery, et al., Compressive failure modes and energy absorption in additively manufactured double gyroid lattices, Addit. Manuf. 16 (2017) 24-29

37. M. Leary, et al., Selective laser melting (SLM) of AlSi12Mg lattice structures, Mater. Des. 98 (2016) 344-357

38. P. Hanzl, et al., The Influence of Processing Parameters on the Mechanical Properties of SLM Parts, Procedia Eng. 100 (2015) 1405-1413

39. Kempen, K., et al. Process optimization and microstructural analysis for selective laser melting of AlSi10Mg

40. E. Brandl, et al., Additive manufactured AlSi10Mg samples using Selective Laser Melting (SLM): Microstructure, high cycle fatigue, and fracture behavior, Mater. Des. 34 (2012) 159-169

41. T. Niendorf, F. Brenne, M. Schaper, Lattice Structures Manufactured by SLM: On the Effect of Geometrical Dimensions on Microstructure Evolution During Processing, Metall. Mater. Trans. B 45 (4) (2014) 1181-1185

42. L. Thijs, et al., A study of the microstructural evolution during selective laser melting of Tie6Ale4V, Acta Mater. 58 (9) (2010) 3303-3312

43. A. Ataee, et al., Ultrahigh-strength titanium gyroid scaffolds manufactured by selective laser melting (SLM) for bone implant applications, Acta Mater. 158 (2018) 354-368

44. L. Thijs, et al., A study of the microstructural evolution during selective laser melting of Tie6Ale4V, Acta Mater. 58 (9) (2010) 3303-3312

45. S. Li, G. Cui, Dependence of strength, elongation, and toughness on grain size in metallic structural materials, J. Appl. Phys. 101 (8) (2007), 083525

46. H. Gong, et al., Influence of defects on mechanical properties of Tie6Ale4 V components produced by selective laser melting and electron beam melting, Mater. Des. 86 (2015) 545-554

47. M. Leary, et al., Inconel 625 lattice structures manufactured by selective laser melting (SLM): Mechanical properties, deformation and failure modes, Mater. Des. 157 (2018) 179-199

48. M. Dallago, et al., Effect of the geometrical defectiveness on the mechanical properties of SLM biomedical Ti6Al4V lattices, Procedia Struct. Integrity 13 (2018) 161-167

49. Iuliano L., Saboori A., Iannuzzo U., Mechanical characterization of lattice structured by Selective Laser Melting process (SLM), 2021

50. B. Vandenbroucke, J.-P. Kruth, Selective laser melting of biocompatible metals for rapid manufacturing of medical parts, Rapid Prototyp. J. 13 (4) (2007) 196-203

51. A. Sarker, et al., Angle defines attachment: Switching the biological response to titanium interfaces by modifying the inclination angle during selective laser melting, Mater. Des. 154 (2018) 326-339

52. D.K. Pattanayak, et al., Bioactive Ti metal analogous to human cancellous bone: fabrication by selective laser melting and chemical treatments, Acta Biomater. 7 (3) (2011) 1398-1406

53. C. Yan, et al., Advanced lightweight 316L stainless steel cellular lattice structures fabricated via selective laser melting, Mater. Des. 55 (2014) 533-541

54. S. Van Bael, et al., Micro-CT-based improvement of geometrical and mechanical controllability of selective laser melted Ti6Al4V porous structures, Mater. Sci. Eng. A 528 (24) (2011) 7423-7431

55. M. Ashby, The properties of foams and lattices, Philos. Trans. R. Soc. A Math. Phys. Eng. Sci. 364 (1838) (2005) 15-30

56. M.F. Ashby, et al., Metal foams: a design guide, Elsevier, 2000

57. ISO/ASTM, Additive manufacturing — General principles — Terminology, in 52900, ISO/ASTM: Switzerland, 2015

58. E. Atzeni, A. Salmi, Economics of additive manufacturing for end-usable metal parts, Int. J. Adv. Manuf. Technol. 62 (9–12) (2012) 1147–1155

59. V. Deshpande, M. Ashby, N. Fleck, Foam topology: bending versus stretching dominated architectures, Acta Mater. 49 (6) (2001) 1035–1040

60. X. Ren, et al., Design and characterisation of a tuneable 3D buckling-induced auxetic metamaterial, Mater. Des. 139 (2018) 336–342

61. X. Ren, et al., Auxetic nail: design and experimental study, Compos. Struct. 184 (2018) 288–298

62. N. Pasvanti, A. Psarros, G. Korbetis, A. Vlahinos, A.Mihailidis, Lattice structures modelling: introduction to homogenization

63. M. Mazur, M. leary, M. McMillan, S. Sun, D. Shidid, M. Brandt, Mechanical properties of Ti6Al4V and AlSi12Mg lattice structures manufactured by selective laser melting (SLM), (2017) 119–161

64. D.-W. Lee, K.A. Khan, R.K. Abu Al-Rub, Stiffness and yield strength of architectured foams based on the Schwarz Primitive triply periodic minimal surface, Int. J. Plast. 95 (2017) 1–20

65. D.W. Abueidda, R.K. Abu Al-Rub, A.S. Dalaq, D.-W. Lee, K.A. Khan, I. Jasiuk, Effective conductivities and elastic moduli of novel foams with triply periodic minimal surfaces, Mech. Mater. 95 (2016) 102–115

66. L. Zhang, S. Feih, S. Daynes, S. Chang, M.Y. Wang, J. Wei, W.F. Lu, Energy absorption characteristics of metallic triply periodic minimal surface sheet structures under compressive loading, Addit. Manuf. 23 (2018) 505–515

67. O. Al-Ketan, R. Rowshan, R.K. Abu Al-Rub, Topology-mechanical property relationship of 3D printed strut, skeletal, and sheet based periodic metallic cellular materials, Addit. Manuf. 19 (2018) 167–183

68. O. Rehme, C. Emmelmann, Rapid manufacturing of lattice structures with selective laser melting, Proceedings of SPIE The International Society for Optical Engineering 6107 (2006) 192–203

69. K. Osakada, M. Shiomi, Flexible manufacturing of metallic products by selective laser melting of powder, International Journal of Machine Tools & Manufacture 46 (2006) 1188–1193

70. Cybernet, About Multiscale.Sim, www.cybernet.co.jp/ansys/product/lineup/multiscale/en/multiscale/

71. Scheffler, M., Colombo, P.. Cellular Ceramics: Structure, Manufacturing, Properties and Applications. Wiley; 2006. ISBN 9783527606702

72. M. Falcone, F. Barpi, G. Iabichino, C. Fidelibus, Stima dei moduli pseudo-elastici in un mezzo trasversalmente isotropo, 2018

73. Loughborough University, Additive Manufacturing Research Group, About Additive Manufacturing, www.lboro.ac.uk/research/amrg/about/the7categoriesofadditivemanufacturing/direct edenergydeposition/

74. Biamino S., Slide del corso di Materiali per applicazioni aerospaziali, Additive Manufacturing, 2021

75. Enginsoft, Our Expertise|Composites, Numerical applications of an Ansys-based tool to analyze hybrid metal/composite lattice structures, Computationally efficient method enables design and optimization processes of axial-symmetric lattice structures to be conducted simply and quickly, www.enginsoft.com/expertise/numerical-applications-of-an-ansys-based-tool-to-analyze-hybrid-metal/composite-lattice-structures.html

76. Enteknograte, Additive Manufacturing process FEA simulation, Additive Manufacturing: FEA Based Design and Optimization with SImufact, Abaqus, Ansys and MSC Apex, www.enteknograte.com/additive-manufacturing-process-simulation/

77. Flow-3D, www.flow3d.com/products/flow3d-am/

78. Simulia, Simulia Community News, How simulation Can Help Advance Additive Manufacturing Technology, www.3ds.com/products-services/simulia/resources/how-simulation-can-help-advance-additive-manufacturing-technology/, 2015

79. Digital Engineering, Automatic Lattice Generation and Optimization with Autodesk Within, www.digitalengineering247.com/article/automatic-lattice-generation-and-optimization-with-autodesk-within, 2015

80. Hexagon, Simufact Additive, Uno strumento di simulazione per la stima della distorsione dei pezzi durante il processo di additive manufacturing a letto di polvere, www.mscsoftware.com/it/product/simufact-additive

81. Hexagon, Simulating Additive Manufacturing with Simufact Additive, www.simufact.com/simufact-additive.html

82. C. Zambonini, Netfabb, prezioso alleato della produzione additiva, www.making.oneteam.it/2020/05/18/netfabb-alleato-della-produzione-additiva/, 2020

83. Hexagon, Digimat, The Non-Linear Multi-scale Material and Structure Modeling Platform, www.mscsoftware.com/product/digimat

84. Hexagon, New Generative Design Solution Cuts Additive Manufacturing Design Processes by up to 80 Percent, MSC Apex Generative Design produces stress-optimised,

3D printable designs automatically to reduce design cycles from days to hours, www.hexagonmi.com/it-it/about-us/news/media-releases/2019/november-2019/new-generative-design-solution-cuts-additive-manufacturing-design-processes-by-up-to-80-percent, 2019

85. Hexagon, Additive Manufacturing, 3D printing: First Time Right, MSC and Hexagon are leading the additive manufacturing market with our unique combined simulation and test solution, www.mscsoftware.com/application/additive-manufacturing

86. Hexagon, Digimat-AM, Your next Innovative solution to optimize and control process quality, www.e-xstream.com/product/digimat-am

87. P. Keane, Simulation of Metal Additive Manufacturing Now Available on HyperWorks, Amphyon brings optimization of part orientation and simulation of 3DPrinting to the APA, www.engineering.com/story/simulation-of-metal-additive-manufacturing-now-available-on-hyperworks, 2017

88. Siemens Digital Industries Software, Simcenter 3D for composites simulation, Enhancing the development of robust, lightweight structures, www.cardsplmsolutions.com/nl/wp-content/uploads/sites/2/2020/11/Siemens-SW-Simcenter-3D-for-composites-simulation-SG_compressed-1.pdf, 2019